

UC Berkeley

UC Berkeley Electronic Theses and Dissertations

Title

The effect of ubiquitin on protein energy landscapes and consequences for proteasomal degradation

Permalink

<https://escholarship.org/uc/item/87r54746>

Author

Carroll, Emma C

Publication Date

2020

Peer reviewed|Thesis/dissertation

The effect of ubiquitin on protein energy landscapes and consequences for
proteasomal degradation

By
Emma C Carroll

A dissertation submitted in partial satisfaction of the
requirements for the degree of
Doctor of Philosophy
in
Molecular and Cell Biology
in the
Graduate Division
of the
University of California, Berkeley

Committee in Charge:

Professor Susan Marqusee, Chair
Professor Andreas Martin
Professor Gloria Brar
Professor Matthew Francis

Summer 2020

Abstract

The effect of ubiquitin on protein energy landscapes and consequences for proteasomal degradation

By Emma C Carroll

Doctor of Philosophy in Molecular and Cell Biology

University of California, Berkeley

Professor Susan Marqusee, Chair

Changes in the cellular environment, such as the hundreds of possible posttranslational modifications, modulate protein energy landscapes to drive important biology, with consequences for signaling, allostery, and other vital processes. The effects of ubiquitination are particularly important because of their potential influence on degradation by the 26S proteasome. Specifically, proteasomal engagement requires unstructured initiation regions that many known proteasome substrates lack. This paradox raises the intriguing possibility that ubiquitin modification itself may induce local or global destabilization, thus revealing the requisite unstructured region for proteasome engagement. However, experimental determination has been hampered by difficulty in producing biophysical quantities of pure, native isopeptide-conjugated ubiquitinated samples. Further, any measured signal must be decoupled between ubiquitin and the substrate protein.

To assess the energetic effects of ubiquitination and how these manifest at the proteasome, we developed a generalizable strategy to create isopeptide-linked ubiquitin within structured regions of a protein. The effects on the energy landscape vary from negligible to dramatic, depending on the protein and site of ubiquitination. Ubiquitination at sensitive sites destabilizes the native structure and increases the rate of proteasomal degradation. Importantly, in well-folded proteins, ubiquitination can even induce the requisite unstructured regions needed for proteasomal engagement. Our results indicate a biophysical role of site-specific ubiquitination as a potential regulatory strategy for energy-dependent substrate degradation. We further characterize the biophysical mechanism of site-specific destabilization and discover distinct modes of destabilization and stabilizing interactions between ubiquitin and the substrate at different sites.

Table of Contents

1. Introduction.....	1
1.1 Protein energy landscapes drive functional and pathological biological processes.....	1
1.2 Overview of the ubiquitin-proteasome system.....	2
1.2.1 Overview of ubiquitin modification.....	2
1.2.2 Ubiquitin attachment can have many functional consequences.....	3
1.2.3 Overview of proteasomal degradation and its regulation by protein conformational properties.....	4
1.3 Challenges and solutions to experimentally determining the effect of ubiquitin.....	6
2. Ubiquitination modulates a protein energy landscape site-specifically with consequences for proteasomal degradation.....	8
2.1 Identification, purification, and characterization of candidate single-lysine proteins.....	8
2.1.1 Single-lysine variants of model protein barstar.....	8
2.1.2 <i>src</i> SH3 single-lysine variant.....	9
2.1.3 wild-type <i>M. smegmatis</i> single-lysine DHFR.....	9
2.2 Developing a generalizable <i>in vitro</i> ubiquitination system for targeted modification of lysines in structured domains.....	10
2.3 Purification of homogenously mono-ubiquitinated single-lysine proteins.....	13
2.4 Ubiquitin modulates a protein's energy landscape in a site-specific and protein-specific manner.....	14
2.4.1 Effect of mono-ubiquitin on the energetics of global unfolding.....	14
2.4.2 Effect of mono- and poly-ubiquitin on the energetics of partial unfolding.....	16
2.5 Ubiquitin-induced energetic changes tune proteasomal degradation rate.....	21
2.5.1 <i>ssrA</i> / <i>SspB</i> ubiquitin-independent proteasome delivery system to directly measure effect of ubiquitin on proteasomal unfolding.....	21
2.5.2 Effect of topology and deubiquitination timing on degradation.....	26
2.6 Ubiquitin-induced destabilization can reveal the unstructured initiation region in otherwise well-folded proteins.....	27
2.6.1 Kinetics of proteasomal degradation of poly-ubiquitinated barstar variants.....	27
2.6.2 <i>o</i> -phenanthroline inhibition of Rpn11 suggests C-terminal barstar initiation.....	31
2.6.3 Engagement is the rate-limiting step in the absence of an intrinsic unstructured region.....	33

2.7	Conclusions.....	34
2.8	Materials and Methods.....	37
2.8.1	MATLAB script.....	37
2.8.2	Expression and purification of single-lysine substrate proteins.....	38
2.8.3	Purification of ubiquitination enzymes.....	38
2.8.4	Preparation of homogenous mono-ubiquitinated substrate proteins.....	39
2.8.5	Preparation of mono-ubiquitinated substrate proteins with C-terminal ssrA tag/engageable tail.....	40
2.8.6	Equilibrium urea denaturation to measure global stability.....	40
2.8.7	Native state proteolysis to measure the energetics of partial unfolding.....	41
2.8.8	Purification of proteasome lid, base, and core.....	42
2.8.9	Preparation of polyubiquitinated barstar variants.....	43
2.8.10	Gel-based and fluorescence polarization-based ssrA/sspB ubiquitin-independent proteasomal degradations.....	44
2.8.11	Fluorescence polarization-based WT proteasomal degradations...	45
3.	Site-specific mechanisms for ubiquitin modulation of the protein energy landscape.....	46
3.1	Introduction.....	46
3.2	Mono-ubiquitinated and unmodified barstar adopt a similar native state conformation.....	47
3.2.1	¹ H/ ¹⁵ N HSQC barstar spectra reveal native-like chemical shifts with some subtle changes.....	47
3.3	Hydrogen-deuterium exchange/mass spectrometry studies: the effect of ubiquitination.....	48
3.3.1	Uptake plots for non-C-terminal peptides.....	49
3.3.2	Uptake plots for C-terminal peptides.....	51
3.3.3	NMR-HDX protection factors for unmodified barstarK60.....	52
3.4	Destabilizing sites occur in regions of high backbone conformational flexibility but destabilize barstar through distinct mechanisms.....	54
3.4.1	MD simulation native contacts and C α RMSF plots.....	54
3.4.2	Disruption of β -strand hydrogen bonds in monoUb-barstarK2, decrease in configurational space in monoUb-barstarK60.....	55
3.5	Direct, stabilizing ubiquitin-barstar interactions at the non-destabilizing site.....	58
3.5.1	Stabilizing hydrogen bonds between flexible ubiquitin C-terminus and barstarK78.....	58
3.6	Conclusions.....	60
3.7	Materials and Methods.....	66
3.7.1	¹³ C/ ¹⁵ N-labeled protein purification for NMR.....	66
3.7.2	NMR data acquisition and analysis.....	66

3.7.3 Preparation of deuterated buffers and mass spectrometry samples.....	65
3.7.4 Hydrogen-deuterium exchange mass spectrometry experiments...	65
3.7.5 All-atom molecular dynamics simulations.....	66
4. References.....	67

Table of Figures

Figure 1.1 Population of high-energy, partially-folded states on a protein energy landscape.....	1
Figure 1.2 General overview of the ubiquitination enzymatic cascade.....	3
Figure 1.3 Overview of how substrate conformational properties influence and regulate proteasomal degradation.....	5
Figure 2.1 Single-lysine substrates used in these studies.....	10
Figure 2.2 Generation of single-K substrates with isopeptide-linked ubiquitin in structured regions.....	11
Figure 2.3 Purification of mono-ubiquitinated proteins.....	11
Figure 2.4 Reconstituted <i>in vitro</i> ubiquitination system for diverse single-lysine substrates.....	12
Figure 2.5 SDS-PAGE gels showing size exclusion chromatography fractions for purified monoUb-substrates.....	13
Figure 2.6 Equilibrium unfolding studies of unmodified and mono-ubiquitinated barstar variants.....	15
Figure 2.7 Comparison of non-methylated monoUb and methylated monoUb modifications on barstar.....	17
Figure 2.8 Native-state proteolysis demonstrates the effects of mono-ubiquitination on the energetics of partial unfolding.....	18
Figure 2.9 Explanation of native-state proteolysis for investigating the energetics of partial unfolding and validation of native-state proteolysis with these systems.....	19
Figure 2.10 Methotrexate effect on monoUb-DHFR.....	21
Figure 2.11 Schematic of ubiquitin-independent substrate delivery system...	22
Figure 2.12 Schematic showing substrate design and confirmation of single-turnover conditions for ubiquitin-independent delivery.....	22
Figure 2.13 Ubiquitin-induced energetic effects tune proteasomal degradation rate.....	24
Figure 2.14 Ubiquitin-independent substrate delivery allows comparison of unmodified and mono-ubiquitinated barstar variants.....	25
Figure 2.15 Proteolysis kinetics for ssrA-tagged barstar substrates by the 20S core particle.....	26
Figure 2.16 Topology favoring early deubiquitination affects observed degradation kinetics.....	27
Figure 2.17 Ubiquitin-mediated destabilization of barstar is sufficient to expose a proteasome-engageable unstructured region.....	29
Figure 2.18 Native state proteolysis experiments for polyUb-barstar variants.....	30
Figure 2.19 Observed polyUb-barstar degradation is 26S proteasome-dependent.....	31

Figure 2.20 The proteasome engages polyUb-barstarK2 C-terminal to the ubiquitin modification.....	32
Figure 2.21 Proteasome engagement can be the rate limiting step for degradation.....	33
Figure 2.22 Model for the consequences of site-specific, ubiquitin-induced substrate energy landscape modulation on proteasomal degradation.....	34
Figure 3.1 BarstarK60 and BarstarK78 NMR HSQCs show subtle changes to native conformational ensemble upon ubiquitination.....	48
Figure 3.2 HDX-MS supports hypothesis of subtle structural changes upon ubiquitination at destabilizing sites.....	49
Figure 3.3 HDX-MS supports hypothesis of subtle structural changes upon ubiquitination at destabilizing sites.....	50
Figure 3.4 HDX-MS provides evidence for C-terminus as proteasome-engagable region.....	51
Figure 3.5 Destabilizing sites form fewer contacts with nearby residues compared to the non-destabilizing site.....	53
Figure 3.6 Ubiquitination sites that energetically destabilize barstar are predicted to occur within regions of high backbone conformational flexibility.....	54
Figure 3.7 Ubiquitination sites that energetically destabilize barstar exist within regions of high intrinsic conformational flexibility.....	55
Figure 3.8 Ubiquitin-mediated destabilization arises through distinct mechanisms at different modification sites, which depend upon the local biophysical context of each site.....	57
Figure 3.9 Predicted stabilizing H-bonding networks between ubiquitin and barstarK78.....	59

Acknowledgements

I have a great deal of gratitude for my family, friends, and coworkers who have been there for me through the course of my PhD. The work described in this thesis would not have been possible without their constant and unwavering support.

First, I thank all of my labmates and colleagues over the years who have provided immeasurable help, advice, and support (scientific and otherwise). A special thanks goes to Dr. Charlotte Nixon and Dr. Helen Hobbs, who embarked on this journey together with me. I will never forget going through the ups and downs of grad school together, from studying together for quals in our hotel in Los Angeles during BPS, to navigating our virtual “graduations” in the middle of a global pandemic. I also thank our lab manager, Dr. Brendan Maguire, for his scientific insights, reagent prepping, and commentary, without which my thesis work would have progressed much more slowly. I also thank my wonderful scientific collaborators in the lab, Dr. Naomi Latorraca and Dr. Johanna Lindner, without whom the work contained in Chapter 3 would not exist.

Next, I thank my advisor, Dr. Susan Marqusee, for supporting every aspect of my work in the lab over the past six years. Thank you especially to Susan for allowing me to venture into a new scientific direction for the lab, and for helping me to troubleshoot all of the expected and unexpected roadblocks along the way. I really cannot adequately express how much this has helped me develop my scientific instincts and creativity, and I am so grateful that she was willing to take a chance on me and a chance on this project. Thank you also to Susan for tirelessly supporting my career development over the years, from sending me to numerous conferences with opportunities to publicize my work to helping me navigate the postdoc application and selection process. I also thank all members of my thesis committee for providing advice and support along the way. A special thanks goes to Dr. Andreas Martin for facilitating such an exciting joint project/collaboration with his lab for the work presented in Chapter 2 and for his scientific guidance and mentorship at all stages of the work.

Third, I thank all of my friends and family, both near and far. I am so grateful for my college best friend Dr. Molly Kupfer, who even though she was all the way working on her PhD all the way in Minnesota, was always there for me and always understood exactly what I was going through. Sometimes it feels beyond coincidence that we were both struggling to write our first big papers at the same time and that they were accepted and published in the same journal family within a month of one another. I also thank both my Molecular and Cell Biology and Chemical Biology Program cohorts, who created a wonderful community of researchers and friends.

I thank my mom, Janice Carroll, who has believed in me and supported me in working towards my goals since day one. I especially must thank my mom for not talking me out of it when, after asking if my PhD program was a two year program or a three year program, I informed her it was actually a six year program. I thank my dad, David Carroll, who passed away during my second year. My dad was always my biggest fan and advocate, and was especially determined that I would get to fulfill the dream of going to graduate school since he never did. I owe my determination and perseverance through this thesis work to them. I also thank my sister, Anna Carroll, for supporting me as only a sister can. It has been so nice having you nearby for lots of visits and Ethiopian food dinners. I also thank my cats, Stella and Alvin, who always remind me of what is truly important in life and sat on my lap a lot to prevent me from typing while trying to write this thesis.

Finally, I thank my best friend and partner, Dr. Eric Greene. Thank you for always being right by my side in adventure, life, and science. You have lifted me up in the hardest and most difficult moments and are the first to celebrate every triumph. I so enjoy our conversations about science, the universe, and everything. From learning to mountain bike, to going backpacking, to traveling to Mexico, to adopting a special needs cat, to running a half-marathon, to buying our Prius, I have cherished every moment of the last six years together. I am also grateful that we had the opportunity to collaborate scientifically on the work presented in Chapter 2. I look forward to continuing this journey together, and I cannot wait to see where our paths lead next.

1. Introduction

1.1 Protein energy landscapes drive functional and pathological biological processes

Proteins are the executors of most cellular functions and must fold to their native structures to perform their roles faithfully. Towards this goal, proteins navigate their conformational energy landscapes, which are frequently depicted as “folding funnels” (Figure 1.1). These folding funnels are graphical depictions of all of the conformations a protein can adopt, from the heterogeneous unfolded ensemble to the compact native state, and the associated energies of each state. These landscapes also contain the barriers and rates (kinetics), mechanisms, and trajectories between states (Dill et al., 2012).

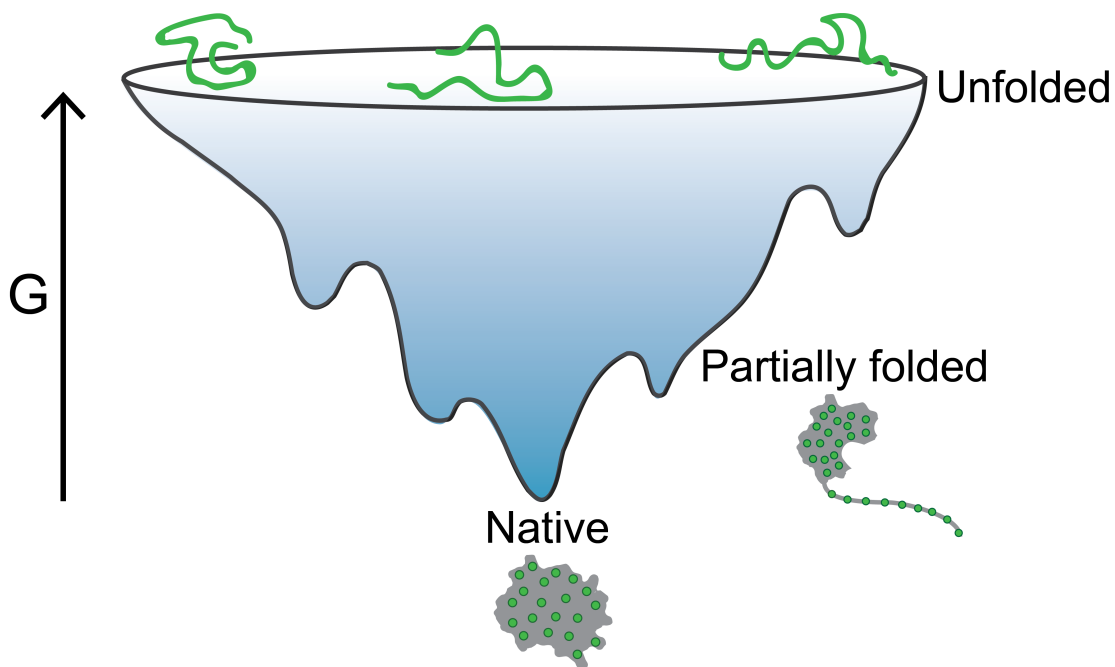


Figure 1.1 | Population of high-energy, partially-folded states on a protein energy landscape. This graphical depiction of a protein conformational energy landscape illustrates all of the possible conformations that a polypeptide can adopt and the associated energies of these conformations (G). The landscape is frequently described as a funnel, with the heterogeneous unfolded ensemble at the top (typically higher energy) and the relatively compact native ensemble at the bottom (typically lower energy). Depending on the landscape, partially-folded states may be populated between these extremes. While the landscape is fully encoded by the amino acid sequence of a polypeptide, it is not fixed. Rather, the shape of the landscape is sensitive to changes in sequence and environment. Population of partially-folded, high-energy states on the landscape drives important processes in biology.

Protein conformational energy landscapes are fully encoded by a protein's amino acid sequence, but they are not fixed. Rather, they are readily modulated by cellular and environmental factors. Additionally, only relatively few states are populated under native conditions (i.e. the native ensemble). However, changes in conditions that allow population of high-energy, partially folded, states on the landscape can drive important biological processes, both functional and pathological (Kenniston et al., 2004; Liu et al., 2006; Martin et al., 2008; Raschke et al., 1999). For example, transient excursions to partially unfolded states could allow for proteolysis events that are crucial for cellular signaling like recruitment of an E3 ligase (Ravalin et al., 2019) Conversely, populating a partially unfolded state that exposes buried hydrophobic residues could seed aggregation (Balchin et al., 2016; Park, 2014).

Posttranslational modifications (PTMs) are a key factor with the potential to modulate protein energy landscapes. There are hundreds of known PTMs, and nearly every eukaryotic protein will experience PTMs during their lifetimes. However, the effect of PTMs on protein energy landscapes and the subsequent biological consequences remain poorly characterized for all but a few modifications, such as some glycosylation and phosphorylation events (Hagai et al., 2011; Xin and Radivojac, 2012). This thesis focuses on the PTM of ubiquitination, although many of the techniques developed here are generally applicable.

1.2 Overview of the ubiquitin-proteasome system

1.2.1 Overview of ubiquitin modification

Ubiquitin is a small 8.5 kDa protein that is typically attached via an isopeptide bond from its C-terminus to the ϵ -primary amine of lysine residues of target proteins (Figure 1.2). Attachment proceeds via a complex and highly regulated enzymatic cascade in which an E1 activating enzyme activates ubiquitin's C-terminus using ATP. The activated ubiquitin protein is then passed to an E2 ubiquitin conjugating enzyme cysteine residue via a transthioesterification reaction with ubiquitin's C-terminus, forming a thioester bond. Finally, an E3 ubiquitin ligase facilitates ubiquitin transfer to the substrate, either by serving as a scaffold between the E2 and the substrate (RING E3s) or transferring the ubiquitin to an E3 cysteine and then to the substrate (HECT and RING-between-RING E3s) (Komander and Rape, 2012; Swatek and Komander, 2016). Ubiquitin itself has seven lysines, so the enzymatic machinery can build ubiquitin chains of diverse lengths, linkages, and topologies.

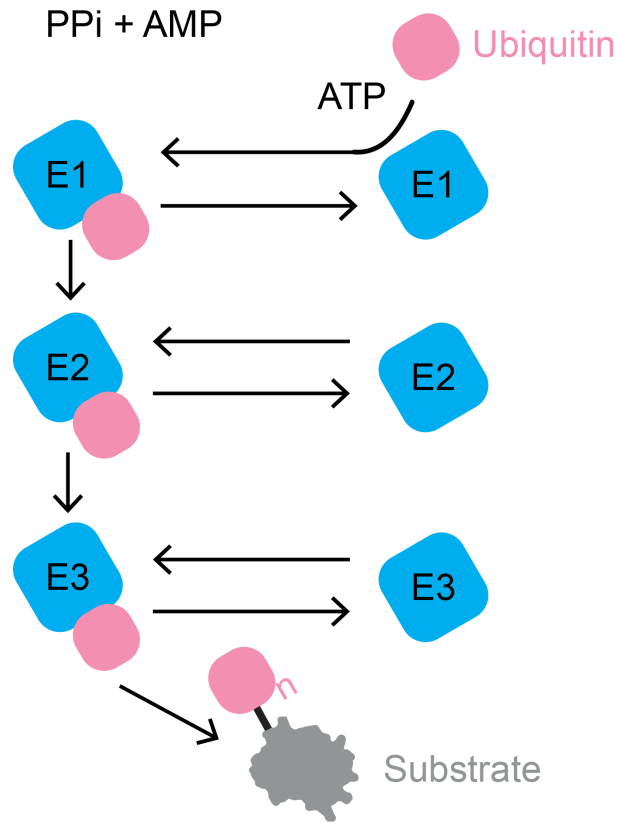


Figure 1.2 | General overview of the ubiquitination enzymatic cascade. The E1 ubiquitin activating enzyme uses ATP to activate ubiquitin’s C terminus. Activated ubiquitin is then transferred to a cysteine residue on the E2 ubiquitin conjugating enzyme. The E3 ubiquitin ligase then serves as a ‘matchmaker’, facilitating interaction between the charged E2 and the intended substrate. Ubiquitin is typically attached to the substrate by an isopeptide bond between ubiquitin’s C terminus and the ϵ -amino group of substrate lysine residues. In some cases (HECT and RING-between-RING E3s), there is a covalent ubiquitin-E3 intermediate, while in others (RING E3s), the E3 serves only as a molecular scaffold. This enzymatic cascade is complex and highly-regulated, and the consequences of misregulation are severe.

1.2.2 Ubiquitin attachment can have many functional consequences

As the name suggests, ubiquitin is an abundant protein and has a large and ever-expanding number of roles in important cellular processes. The ‘ubiquitin code’ hypothesis posits that the pattern of ubiquitin modifications on substrate lysines, ubiquitin chain lengths thereon, and differential topologies of chain linkages between individual ubiquitin molecules encode vital signaling information (Komander and Rape, 2012; Yau and Rape, 2016). The position and identity of a given ubiquitin modification is determined by the E1, E2, E3 enzymatic cascade (the ‘writers’ of the ubiquitin code). Substrate selection is controlled principally by

E3 identity, while chain length and linkage type can be determined by interplay between the E2 and E3 (Komander and Rape, 2012). The enzymatic ubiquitin conjugation machinery compete with a host of cellular deubiquitinases that remove ubiquitin from substrate proteins (the ‘erasers’ of the ubiquitin code) (Komander and Rape, 2012).

The presence of ubiquitin modification on a given protein at a given site is read out by downstream cellular players (the ‘readers’ of the ubiquitin code’) (Grice and Nathan, 2016). Additionally, structural features of ubiquitin, including surface exposed hydrophobic and acidic patches are believed to mediate interactions with downstream binding/signaling partners, allowing propagation and amplification of ubiquitin signals (Debelouchina et al., 2017; Mortensen et al., 2015). Ubiquitin modification has been shown to play a key signaling role in a large and ever-growing list of crucial regulatory, non-degradative cellular processes. These include endocytosis, vesicle trafficking, DNA repair, and enzymatic function (Komander and Rape, 2012; Oh et al., 2018; Werner et al., 2015; Yau and Rape, 2016). However, the canonical and best-characterized role for ubiquitin modification is to target condemned substrate proteins to the 26S proteasome for degradation (Coll-Martinez, Bernat; Crosas, 2019; Grice and Nathan, 2016).

1.2.3 Overview of proteasomal degradation and its regulation by protein conformational properties

The ubiquitin-proteasome system (UPS) is responsible for the majority of protein turnover in eukaryotic cells. The 26S proteasome is the executor of the UPS, using ubiquitin receptors to selectively bind ubiquitinated substrates and degrade them in an ATP-dependent manner. The degradation activity resides in the proteasome’s 20S core particle, whose proteolytic sites are sequestered inside a central cavity. Substrates are delivered to the 20S core particle through the 19S regulatory particle (RP), which caps one or both sides of the barrel-shaped 20S core. RP recruits ubiquitinated substrates, mechanically unfolds them with its AAA+ (ATPase Associated with diverse cellular Activities) motor, and translocates the unstructured polypeptides into the core particle for proteolysis (Bard et al., 2018; Greene et al., 2020).

Ubiquitin modification is an especially interesting PTM from the perspective of protein energetics because the 26S proteasome requires an unstructured region to initiate degradation – in a step known as proteasomal “engagement” (Lee et al., 2001; Prakash et al., 2004; Tomita and Matouschek, 2019; Yu and Matouschek, 2017). Typically, this region occurs on either the N- or C-terminus, and directionality has been shown to affect processing efficiency and peptide production (Berko et al., 2012). Interestingly, meta-analysis of known proteasome clients suggests that at least 30% lack such a region (Hagai et al., 2011). This has led to the interesting hypothesis that ubiquitin itself could destabilize substrate proteins,

perhaps in turn allowing population of partially-unfolded, high-energy states that feature the requisite unstructured region for proteasome engagement (Figure 1.3). Indeed, computational molecular dynamics simulations have predicted that this could in fact be the case (Gavrilov et al., 2015; Hagai and Levy, 2010), but challenges in purifying homogeneously ubiquitinated substrates conjugated to ubiquitin with native isopeptide bonds has prevented experimental testing of this hypothesis. The experimental characterization of ubiquitin-mediated changes in protein energetics has therefore been limited to artificial, non-physiological ubiquitin-attachment strategies (Morimoto et al., 2016) or heterogeneous samples (Cundiff et al., 2019).

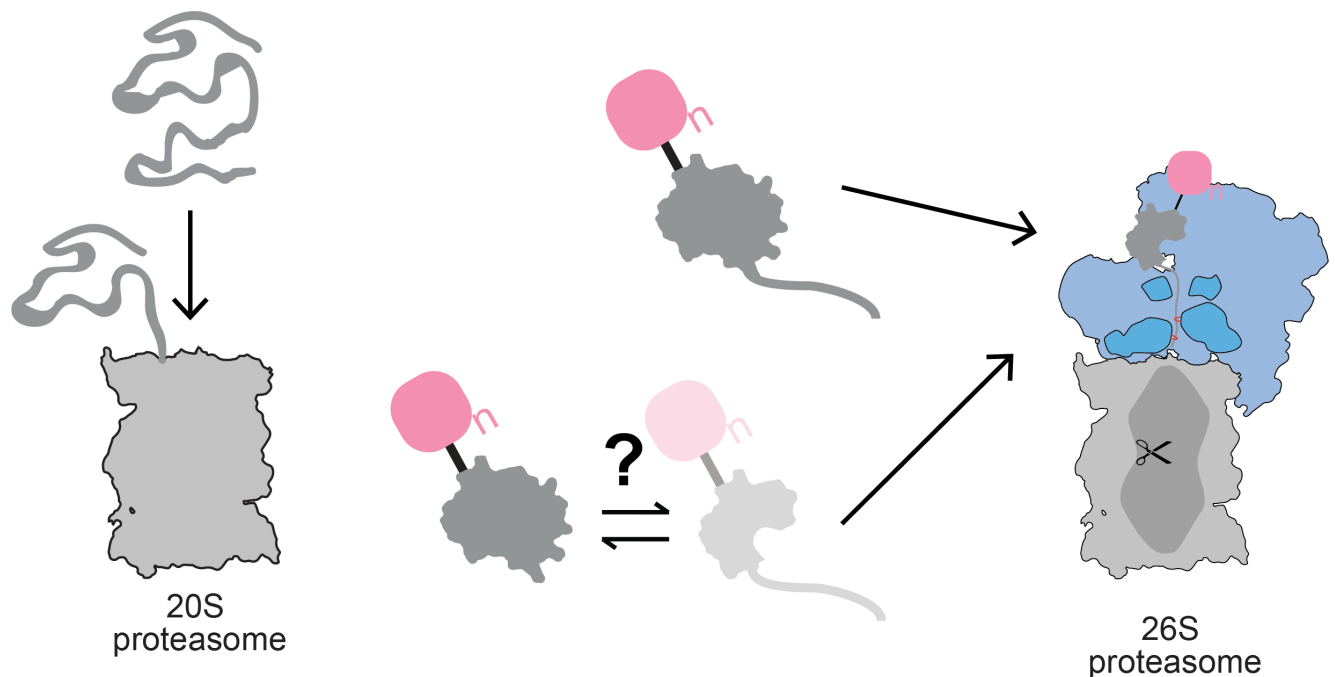


Figure 1.3 | Overview of how substrate conformational properties influence and regulate proteasomal degradation. Certain classes of proteins, when unfolded, will be degraded by the 20S proteasome core particle in the absence of ubiquitin modification. In the canonical model for proteasomal degradation, ubiquitinated substrates contain an obligate unstructured region through which the 26S proteasome engages the condemned substrate for degradation (right, top). However, a substantial fraction of bona-fide proteasome clients contain known ubiquitination sites but lack an unstructured region through which the 26S proteasome could initiate degradation. An exciting possibility is that ubiquitination itself can modulate the energy landscape of these substrates and expose an unstructured region for initiation of proteasomal degradation.

1.3 Challenges and solutions to experimentally determining the effect of ubiquitin

It is reasonable to expect that the addition of a protein domain, such as ubiquitin, can alter the energetics and dynamics of a target protein. Biophysical studies of multidomain proteins have demonstrated that the stability of one domain can be modulated by covalent linkage to another (Batey et al., 2008). In differentially-linked polyubiquitin chains, the ubiquitin monomers themselves can have different thermodynamic and mechanical stabilities (Carrion-Vazquez et al., 2003; Morimoto et al., 2015). Studies on N-terminal ubiquitin fusions and disulfide-linked ubiquitin attachments have reported small changes in the midpoints for thermally-induced unfolding depending on the modification (Morimoto et al., 2016).

A number of inherent challenges have hampered previous experimental measurements of the effect of ubiquitin on a protein energy landscape. First, ubiquitin itself is a protein, so there must be a way to differentiate between the signal from ubiquitin and the signal from the substrate. At the outset of this thesis work, we could foresee several potential solutions to this obstacle, including analysis by proteolysis/gel-based techniques (Na and Park, 2009; Park, 2014; Park and Marqusee, 2004, 2005, 2006) and investigation using intrinsic tryptophan fluorescence since ubiquitin is tryptophan-free.

Second, no characterized single-lysine model substrates existed that could be used to test this hypothesis. Substrates need to be single-lysine for homogeneity of ubiquitin modification at a single site. Additionally, model substrates need to meet other stringent criteria to ensure interpretability of results, including adopting a folded native state (i.e. not an intrinsically disordered protein), existing as a monomer, not containing disulfide bonds, and ideally possessing kinetics of full or partial unfolding on the timescales suitable for characterization by proteolysis. Towards this goal, I wrote a MATLAB script to search the PDB for proteins with low lysine content (see Materials and Methods section 2.8.1), which identified several candidates used in this thesis. I adapted an existing single-lysine SH3 domain, created single-lysine variants of barstar, a protein with a well-studied energy landscape, and characterized a variant of the protein dihydrofolate reductase from *Mycobacterium smegmatis* that naturally only contains one lysine.

Third, and most significantly, no methods existed for purifying biophysical quantities of native isopeptide-modified ubiquitinated substrates, and this has historically been a challenging endeavor (challenging enough to merit its own review article about how challenging it is) (Faggiano and Pastore, 2014). Due to the unique nature of the isopeptide bond, we felt it was quite important to pursue a strategy that resulted in a native isopeptide bond rather than utilizing the many chemical strategies developed for artificial ubiquitin ligation to substrates (Pham and Strieter, 2015; Pham et al., 2016). The isopeptide bond is particularly flexible

and affords a large amount of space between the substrate and ubiquitin, which is difficult to recapitulate with harsh chemical conjugation strategies. Further, it would be impossible to study the downstream biological outcomes of the effect of ubiquitin on protein energetics without using an isopeptide bond.

Here, I adapted an existing set of *in vitro* purified and biochemically-reconstituted ubiquitination enzymatic machinery (Saeki et al., 2005) previously used in Andreas Martin's lab (UC Berkeley) to target lysines on long, unstructured tails. Using recent discoveries in the mechanistic biology of the *S. cerevisiae* HECT E3 ubiquitin ligase used in this reconstituted system (Kamadurai et al., 2013; Kim et al., 2011a), I modified this substrate design to optimize substrate architecture for ubiquitination of lysines on structured domains. This new ubiquitination system works robustly and appears to be generalizable across diverse single-lysine substrates.

Herein, I present the work completed for my PhD, towards the goal of answering the following questions: Does ubiquitin affect a protein energy landscape and, if so, are these effects general or site-specific? Do energetic changes due to ubiquitination affect proteasomal degradation? I developed a suite of single-lysine substrates and adapted an *in vitro* ubiquitination system to show that the effects of ubiquitin on the energy landscape vary from negligible to dramatic, depending on the protein and site of ubiquitination. Ubiquitination at sensitive sites destabilizes the native structure and increases the rate of proteasomal degradation. Importantly, in well-folded proteins, ubiquitination can even induce the requisite unstructured regions needed for proteasomal engagement. Finally, I will describe our dual experimental and computational approaches to understand the molecular mechanisms driving the site-specificity of ubiquitin's energetic effects. Destabilizing sites arise in local regions of high conformational flexibility, but the molecular mechanism of destabilization at each site is unique. In contrast, ubiquitination at a non-destabilizing site creates a stabilizing interaction between ubiquitin and the substrate, suggesting that the energetic effects of ubiquitination are highly dependent on each site's local biophysical context.

2. Ubiquitination modulates a protein energy landscape site-specifically with consequences for proteasomal degradation

A portion of the work presented in this chapter has been previously published as part of the following paper: Carroll, E.C., Greene, E.R., Martin, A., and Marqusee, S. Site-specific ubiquitination affects protein energetics and proteasomal degradation. *Nat Chem Biol* (2020). <https://doi.org/10.1038/s41589-020-0556-3>

All experiments involving the proteasome were performed in collaboration with graduate student Eric Greene in Andreas Martin's lab (University of California, Berkeley).

2.1 Identification, purification, and characterization of candidate single-lysine proteins

Lysine is a highly abundant amino acid, constituting 6% of residues in the human proteome (Hacker et al., 2017). Many proteins, particularly well-characterized model proteins in the protein folding field, contain many lysines. Thus, identifying candidate proteins that were either naturally single-lysine or low enough lysine content to be amenable to single-lysine mutations proved a significant hurdle to establishing the project. In addition, candidate single-lysine proteins need to meet several other stringent criteria as detailed above, including adopting a folded native state (i.e. not an intrinsically disordered protein), existing as a monomer, not containing disulfide bonds, and ideally possessing kinetics of full or partial unfolding on the timescales suitable for characterization by proteolysis. All single-lysine substrates studied in this chapter are depicted in Figure 2.1.

2.1.1 Single-lysine variants of model protein barstar

Barstar is a small 89-residue protein from *Bacillus amyloliquefaciens* that serves as the intracellular inhibitor of a toxic secreted RNase, barnase (Bacillus RNase). Wild-type barstar is monomeric and contains two reduced cysteines (Khurana et al., 1995). Barstar's energy landscape has been well-characterized by the Jayant Udgaonkar and Alan Fersht groups, due to the prediction of intermediates on the unfolding trajectory (Nolting et al., 1997; Zaidi et al., 1997). Additionally, barstar possesses a surface acidic patch that drives its femtomolar barnase binding affinity (Schreiber et al., 1994). Interestingly, this surface acidic patch leads to a tradeoff between binding affinity and barstar stability, and single mutations of the acidic residues can add as much as 2 kcal/mol stability (Schreiber et al., 1994). We chose to attempt making single-lysine variants of barstar because barstar has relatively

low lysine-content – only six lysines out of 89 residues – and all six lysines are surface-exposed.

Wild-type barstar’s thermodynamic stability has been previously measured ($\Delta G_{\text{unfolding}} = 5.0 \pm 0.5$ kcal/mol and $C_m = 4.7 \pm 0.2$ M urea) (Khurana et al., 1995). The six lysines in wild-type barstar are at positions 1, 2, 21, 22, 60, and 78. We created single-lysine versions by mutating the other five lysines to arginine residues. The single remaining lysine is denoted after the name (i.e. barstarK60 refers to barstar that contains a single lysine at position 60). All six single-lysine variants initially expressed poorly in *E. coli* with only an N-terminal His₆ tag but expressed well with an N-terminal His-MBP tag that could them be further processed to remove the tags. Single-lysine variants were only marginally destabilized compared to wild-type barstar (Table 2.1).

2.1.2 *srcSH3* single-lysine variant

As part of his postdoctoral work in the Marqusee lab, Bharat Jagannathan cloned a large number of single point mutations of the *srcSH3* domain (Guinn et al., 2015; Jagannathan et al., 2012). *srcSH3* is a 64 amino acid protein domain that naturally contains two lysines at positions 21 and 22. Bharat’s variant K22M was thus single lysine. Because it was a convenient, easily-available candidate single-lysine substrate, we also chose to test *srcSH3* as a ubiquitin target. Additionally, even though this particular variant had not been characterized, *srcSH3* had well-established expression and purification protocols, making it an attractive option for our studies. However, *srcSH3* also had the caveat that its unfolding kinetics would be too fast for proteolysis-based measurements of equilibrium unfolding (pulse proteolysis) (Park and Marqusee, 2005).

2.1.3 wild-type *M. smegmatis* single-lysine DHFR

We wanted to identify additional potential substrate proteins that naturally contained a single lysine or possessed low lysine content and thus might be amenable to mutation to single-lysine proteins. Towards this goal, I wrote a MATLAB script to search all available sequences in the PDB for proteins that may fit these criteria. Searching the PDB had the additional advantage that all structures in the PDB are proteins that have been successfully expressed and purified in sufficient quantities for structural determination. The script is a simple FASTA parse that reads through downloaded FASTA sequence files of all structures in the PDB and assigns a score based on the number of lysines in each sequence. Then, results that contain at least 100 total residues and two or fewer lysines are returned (though of course these parameters can be set as desired).

This search returned a number of interesting hits, including several mycobacterial proteins that have perhaps evolved low lysine content as part of the host-pathogen

‘arms race’ to evade host degradation machinery (Wang et al., 2020a). The most promising hit was a dihydrofolate reductase (DHFR) homolog from *Mycobacterium tuberculosis* (the bacterium that causes tuberculosis in humans) that was naturally single-lysine. A BLAST search revealed that the homolog from *Mycobacterium smegmatis* was also naturally single-lysine (although at a different position), and we chose to move forward with this variant to avoid regulatory issues of working with a protein from a pathogen.

M. smegmatis DHFR was ordered as a gblock and cloned into a His-MBP expression construct. Although it expresses well, it is prone to aggregation upon cleavage from this His-MBP expression tag, making it more difficult to work with than the other single-lysine substrates.

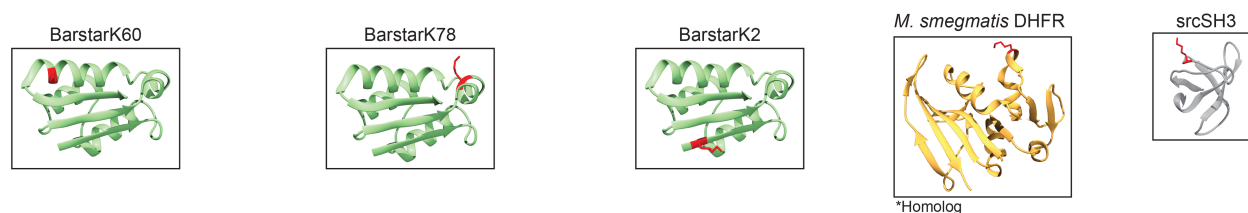


Figure 2.1 | Single-lysine substrates used in these studies. Ribbon diagrams of barstar (green: PDB: 1BTA) showing the position of ubiquitinated lysines in red. Ribbon diagram of *M. smegmatis* DHFR homolog from *M. tuberculosis* (orange: PDB: 1DG8) and srcSH3 (grey: PDB: 1SRL) showing ubiquitinated lysine positions in red.

2.2 Developing a generalizable *in vitro* ubiquitination system for targeted modification of lysines in structured domains

We used a biochemically reconstituted enzymatic ligation and deubiquitination strategy to overcome technical obstacles and produce ubiquitin-substrate conjugates with native isopeptide bonds. This system had been previously used in the Martin lab to append long polyubiquitin chains to proteins that contained a single lysine in a long, disordered tail. However, it was not capable of appending ubiquitin to lysines within structured domains. I realized that a better understanding of the mechanistic biochemistry of the HECT E3 ubiquitin ligase used in this system, yeast Rsp5, could inform the design of better substrates to achieve this goal. Previous Rsp5 structural work from the Huibregtse and Schulman labs (Kamadurai et al., 2013; Kim and Huibregtse, 2009; Kim et al., 2011a) had indicated the relatively large E3 enzyme requires a “scaffold” for docking to productively interact with small substrates like those in our study. Kamadurai et al also found that Rsp5 lysine prioritization for ubiquitination was highly dependant on linker length between Rsp5 docking sites and the substrate lysine position. We hypothesized that we could design substrates with these criteria in mind to facilitate ubiquitination of our single-lysine substrates.

Toward this goal, substrate proteins were expressed as C-terminal fusions to maltose binding protein (MBP) with a connecting linker containing a PPPY recognition sequence for Rsp5 binding. We hoped that MBP would act as a scaffold to promote productive E3-substrate interaction, as previously described (Kamadurai et al., 2013; Kim et al., 2011a). Substrates also contain a single cysteine for fluorescein-maleimide labeling.

Efficient *in vitro* poly-ubiquitination was achieved using a reconstituted system with mouse Uba1 ubiquitin-activating enzyme (E1), yeast Ubc4 ubiquitin conjugase (E2), and yeast Rsp5 ubiquitin ligase (E3) (Figure 2.2). Treatment with the K63-specific deubiquitinase AMSH (Associated Molecule with the SH3 domain of STAM) collapses the heterogeneously poly-ubiquitinated substrates into lower molecular weight conjugates (Figure 2.2). AMSH efficiently trims the Rsp5-generated, K63-linked ubiquitin chains, but is much slower in removing the proximal, substrate-attached ubiquitin moiety. Optimizing the AMSH amount and the duration of deubiquitination before quenching with EDTA allowed accumulation of the mono-ubiquitinated species. For experiments requiring large quantities, we generated mono-ubiquitinated substrates using methylated ubiquitin, which prevents chain formation and results in higher yield of modified protein (Figure 2.3).

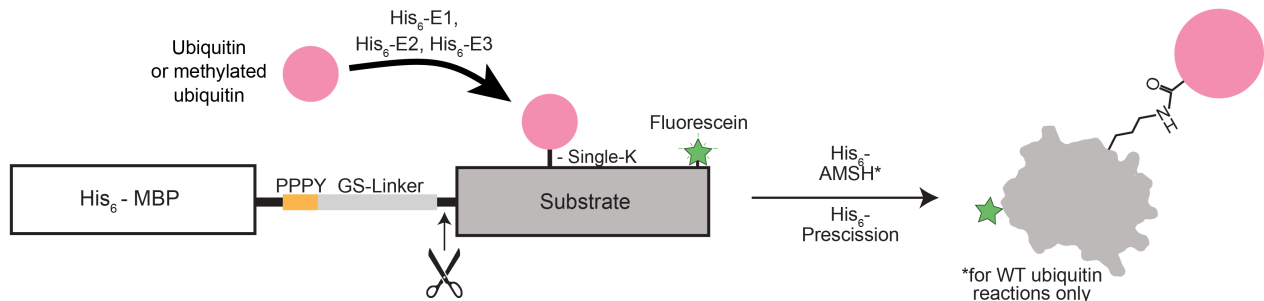


Figure 2.2 | Generation of single-K substrates with isopeptide-linked ubiquitin in structured regions. Schematic of ubiquitination machinery and substrate design. A His₆-MBP scaffold with PPPY Rsp5-binding motif for enzymatic ubiquitination is fused to the N-terminus of a single-lysine substrate.

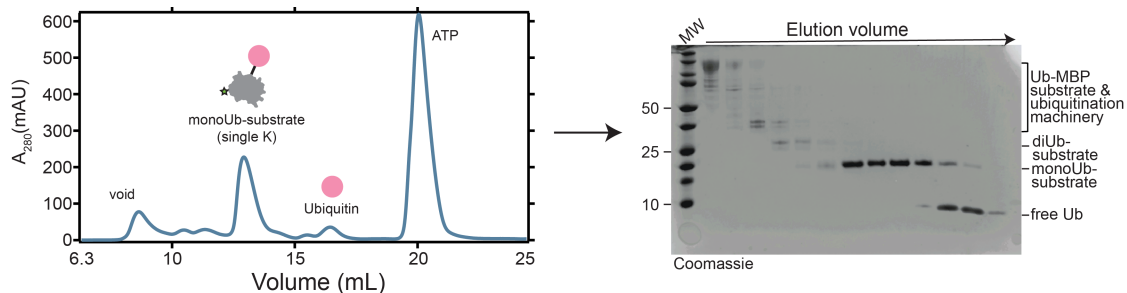


Figure 2.3 | Purification of mono-ubiquitinated proteins. Representative size exclusion chromatography trace for methylated monoUb-barstar and Coomassie-stained gel of selected size exclusion fractions.

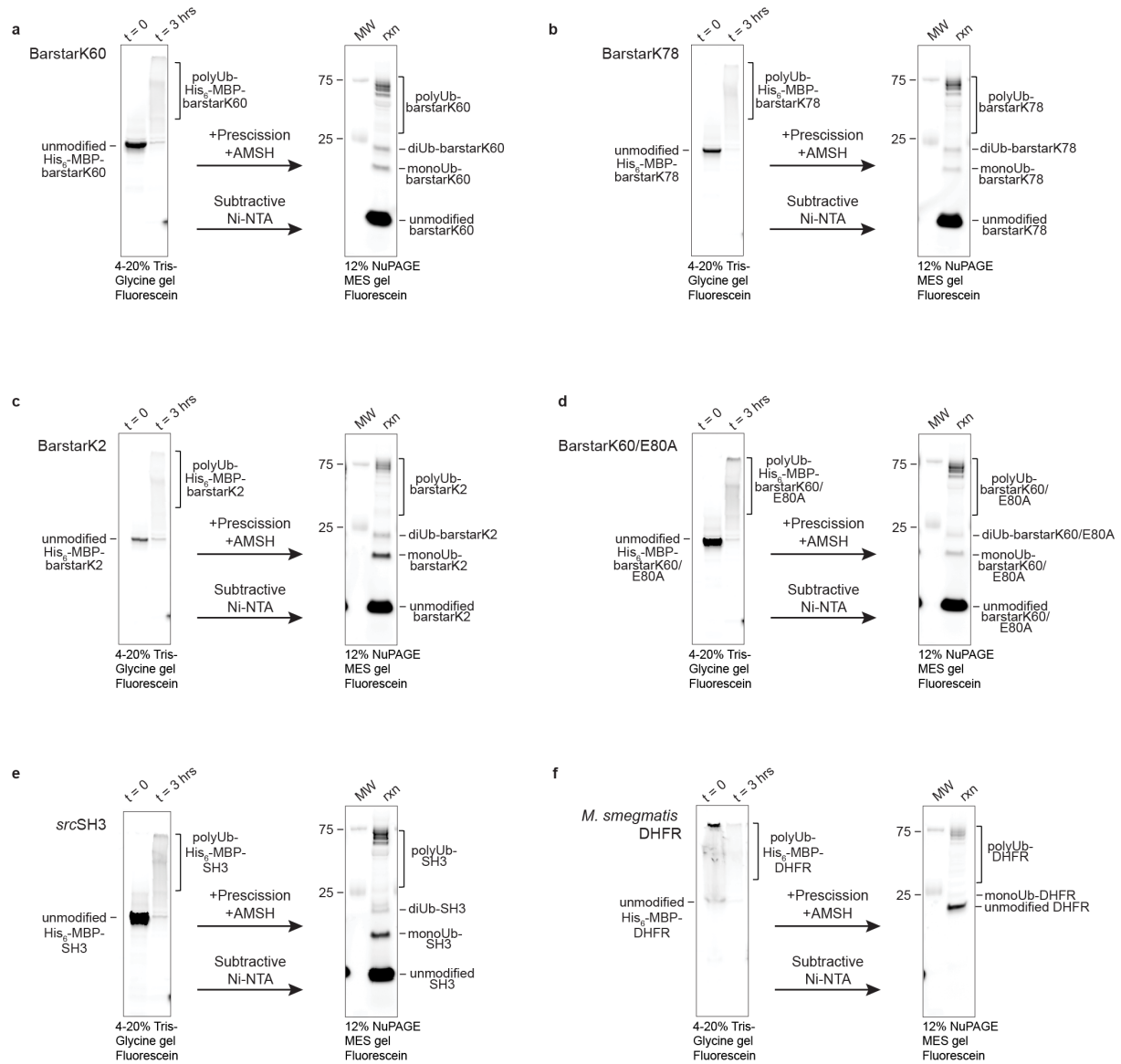


Figure 2.4 | Reconstituted *in vitro* ubiquitination system for diverse single-lysine substrates. (a-f) Representative fluorescence scans of SDS-PAGE gels showing the full-length substrates immediately after reaction initiation and after 3 hours of ubiquitination. Reactions were treated with Precision (HRV3C) protease and AMSH deubiquitinase prior to subtractive Ni²⁺-NTA chromatography to reveal clearly defined mono- and di-ubiquitinated substrate with native isopeptide linkages. All experiments were repeated at least five times with similar results.

2.3 Purification of homogenously mono-ubiquitinated single-lysine proteins

After *in vitro* ubiquitination, a two-step subtractive Ni²⁺-NTA purification followed by size-exclusion chromatography was sufficient to purify the mono-ubiquitinated substrate to homogeneity (Figure 2.3). Using this generalizable method, we attached ubiquitin to the suite of single-lysine substrates and scaled up to produce spectroscopic quantities (Figure 2.4 and Figure 2.5).

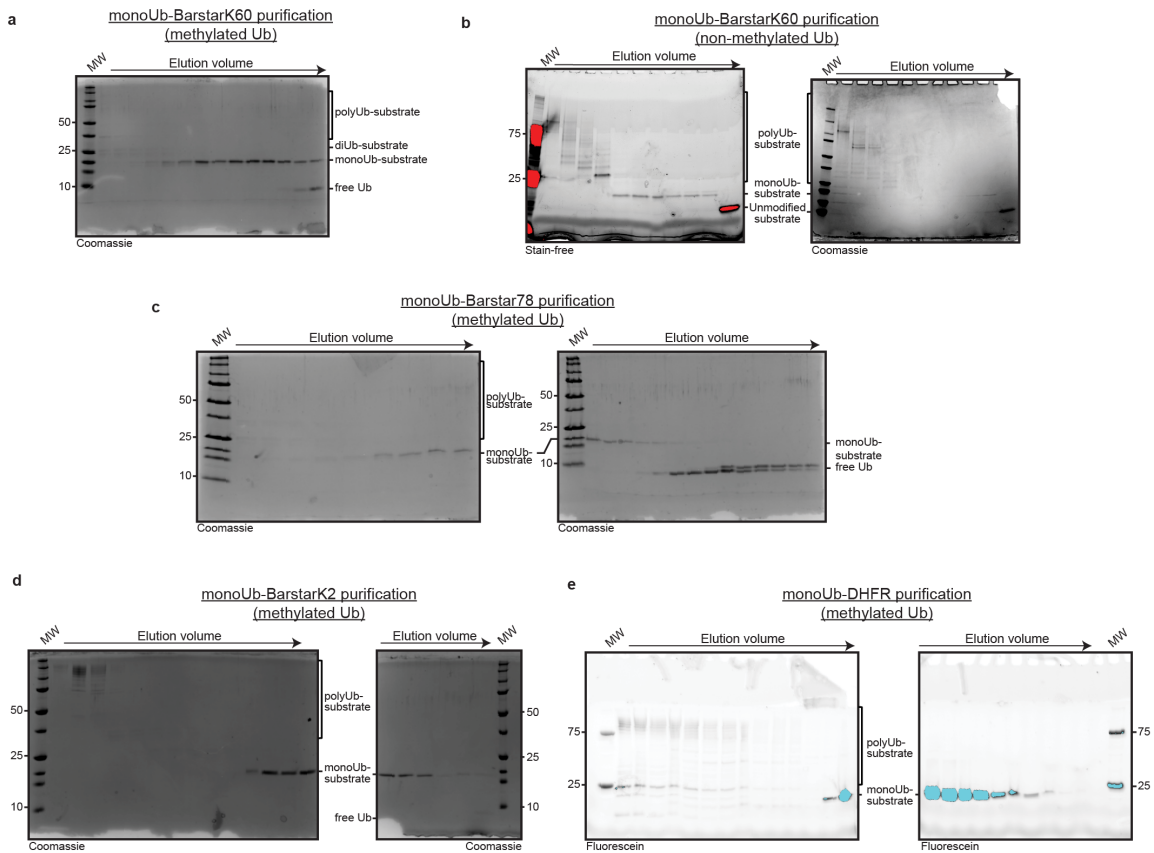


Figure 2.5 | SDS-PAGE gels showing size exclusion chromatography fractions for purified monoUb-substrates. Representative gels (with indicated imaging modalities) of selected S75 size exclusion chromatography fractions from purification of monoUb-barstarK60 proteins with methyl-ubiquitin (a) or non-methylated ubiquitin (b) conjugation. Representative gels (with indicated imaging modalities) of selected S75 size exclusion chromatography fractions from purifications of methyl-ubiquitinated monoUb-barstarK78 (c) monoUb-barstarK2 (d) or monoUb-DHFR (e). Experiments a-d were repeated at least once with similar results.

2.4 Ubiquitin modulates a protein's energy landscape in a site-specific and protein-specific manner

2.4.1 Effect of mono-ubiquitin on the energetics of global unfolding

The ability to purify milligram quantities of homogeneously mono-ubiquitinated proteins enabled us to determine global stability changes using traditional chemically-induced equilibrium unfolding monitored by intrinsic fluorescence. The fluorescence signal arises exclusively from tryptophan residues in our substrates, as ubiquitin is tryptophan-free. For these studies, we used a well-established model protein, barstar from *Bacillus amyloliquefaciens*, in which all except one lysine were replaced by arginine to generate different single-lysine variants for site-specific ubiquitination.

Four single-lysine barstar variants were characterized: barstarK2, barstarK60, barstarK78, and barstarK60/E80A (where the position of the remaining lysine is denoted after barstar). We determined their global stabilities in both unmodified and purified mono-ubiquitinated forms by urea-induced chemical denaturation and fit the data using a two-state assumption and linear extrapolation (see Methods). The non-ubiquitinated versions of all single-lysine variants display only minor destabilization compared to wild-type barstar ($\Delta G_{\text{unfolding}} = 5.0 \pm 0.5$ kcal/mol and $C_m = 4.7 \pm 0.2$ M urea (Khurana et al., 1995) (Table 2.1). In contrast, we observed dramatically different stabilities upon modification with mono-ubiquitin, indicating site-specific effects (Figure 2.6 and Table 2.1).

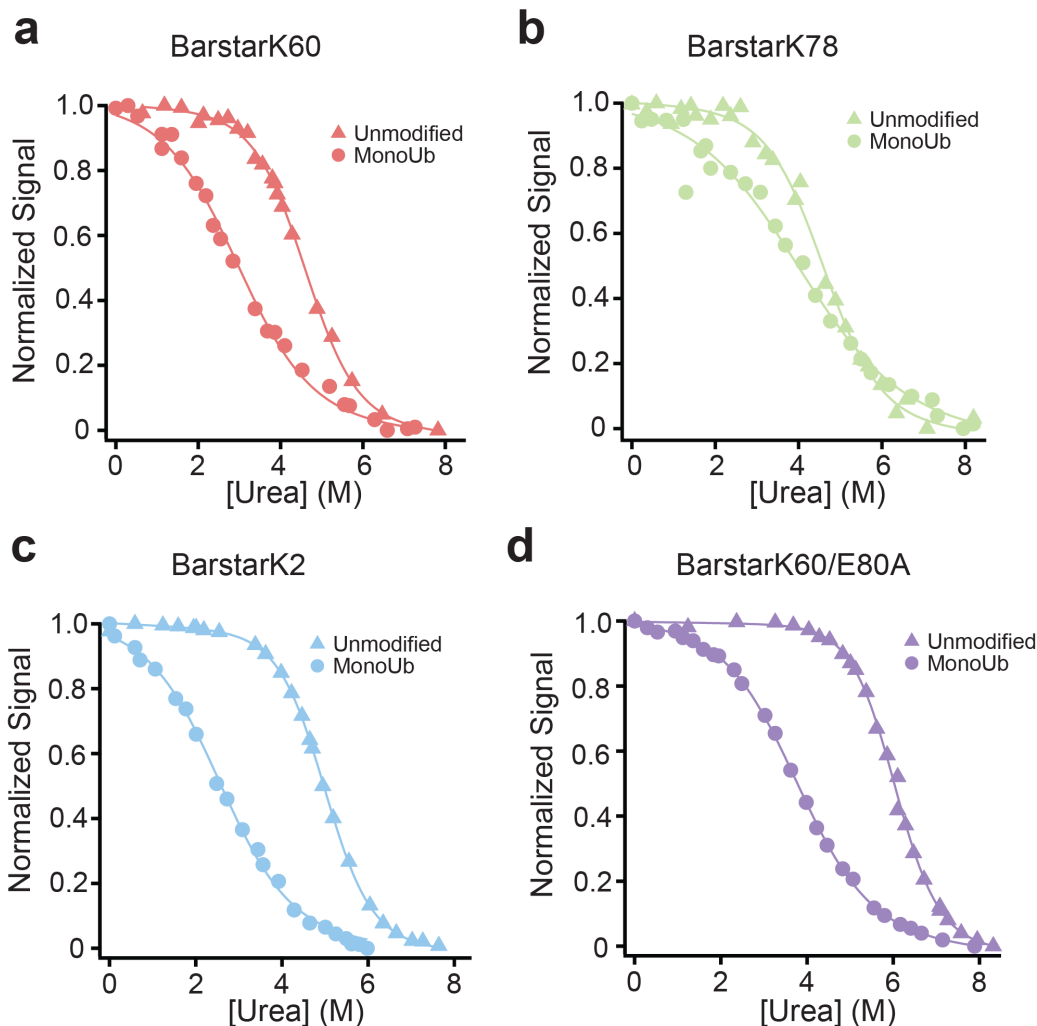


Figure 2.6 | Equilibrium unfolding studies of unmodified and mono-ubiquitinated barstar variants. (a) Urea-induced unfolding transition ($n=1$) of unmodified (triangles) and methylated monoUb-barstarK60 (circles). (b) Unmodified (triangles) and methylated monoUb-barstarK78 (c) unmodified (triangles) and methylated monoUb-barstarK2 and (d) unmodified (triangles) and methylated monoUb-barstarK60/E80A.

Interestingly, all mono-ubiquitinated constructs show a small but notable decrease in m -value (the denaturant dependence of stability) compared to their unmodified counterparts (Table 2.1). m -values are known to correlate with the size of a protein or the non-polar surface area exposed during unfolding (Myers et al., 1995), which may slightly change with the various ubiquitin attachments. Alternatively, these decreased m -values may indicate direct surface interactions with ubiquitin or a loss of two-state unfolding behavior, with the population of an unfolding intermediate (Zaidi et al., 1997; Nolting et al., 1997). Because this questions the validity of the two-state assumption used to calculate $\Delta G_{\text{unfolding}}$, we report the midpoints of the denaturation curves (C_m) for the unmodified and mono-ubiquitinated variants.

BarstarK2 and barstarK60 were destabilized upon mono-ubiquitination (ΔC_m of 2.5 M and 1.9 M urea, respectively, Figure 2.6). A stabilized mutant of barstarK60, barstarK60/E80A, exhibited nearly identical net destabilization upon mono-ubiquitination (ΔC_m of 2.3 M urea, Figure 2.6). Conversely, mono-ubiquitination of barstarK78 caused only marginal destabilization (ΔC_m of 0.42 M urea, Figure 2.6). To provide a sense for the thermodynamic changes associated with ubiquitination, we used the average m -value of the fits for unmodified and mono-ubiquitinated barstar variants to approximate $\Delta G_{\text{unfolding}}$ (Table 2.1). Taken together, these results establish that the energetic effects of ubiquitin on a particular substrate can be highly site-specific, rather than broadly destabilizing. Importantly, although ubiquitin methylation has been observed to have various effects on the behavior and recognition of ubiquitin, we observed no difference compared to non-methylated ubiquitin in our biophysical measurements (Figure 2.7).

2.4.2 Effect of mono- and poly-ubiquitin on the energetics of partial unfolding

While the above results demonstrate that mono-ubiquitin attached via a native isopeptide bond can site-specifically alter a substrate's global stability, the globally unfolded state is unlikely to be the most relevant fluctuation for proteasomal degradation. Under cellular conditions, proteins sample partially-unfolded conformations more frequently than the globally-unfolded state. Furthermore, the proteasome does not require global unfolding for successful substrate engagement.

To assess the population of partially-unfolded states, we utilized a quantitative analysis of susceptibility to a soluble protease, thermolysin (Park, 2014; Park and Marqusee, 2004). Because cleavage by soluble proteases requires regions of ~ 10 - 12 unstructured amino acids, proteolysis of well-folded proteins under native conditions occurs via transient excursions to partially-unfolded, high-energy states (Figure 2.8). Typically, the lowest energy conformation that is competent for proteolytic cleavage (the "cleavable state") predominates. Because thermolysin has low affinity for its substrates ($K_d \sim 0.1$ - 10 mM), proteolysis of the native state typically proceeds via an EX2-like kinetic regime, in which the proteolysis step itself, rather than the conformational change to the cleavable state, is rate-limiting (Park and Marqusee, 2004). As such, observed proteolysis rates are directly related to the free-energy difference between the native state and this cleavable state ($\Delta G_{\text{proteolysis}}$, Figure 2.9). The $\Delta \Delta G_{\text{proteolysis}}$ for the same protein in two different states (i.e. unmodified and mono-ubiquitinated) can be reliably determined (Park, 2014; Park and Marqusee, 2004).

We measured the $\Delta G_{\text{proteolysis}}$ for unmodified and mono-ubiquitinated (non-methylated) versions of all single-lysine barstar variants described above, as well as single-lysine *srcSH3* and *M. smegmatis* DHFR (wildtype is single-lysine) (Figure 2.8). AMSH concentration and reaction length were adjusted to yield a mixture of

both unmodified and mono-ubiquitinated protein, which allowed their direct comparison within the same experiment.

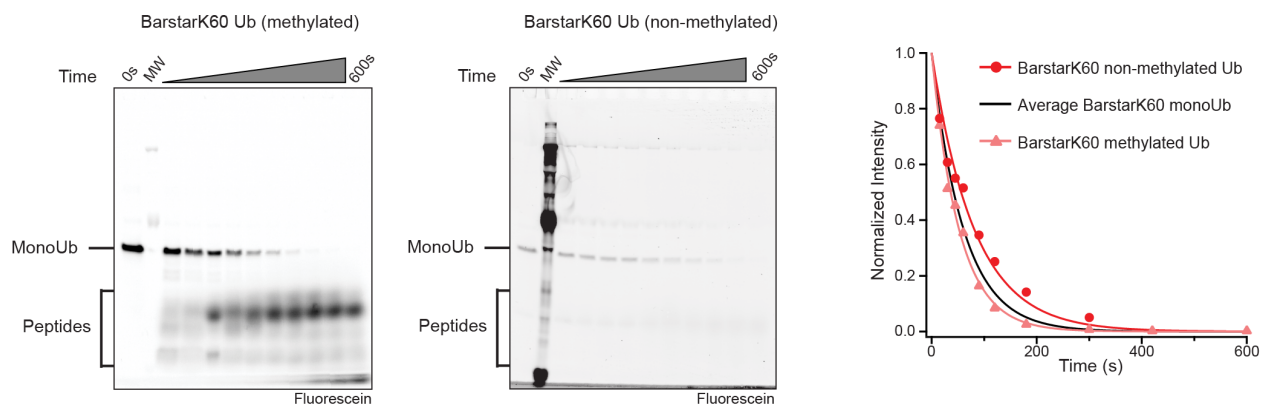


Figure 2.7 | Comparison of non-methylated monoUb and methylated monoUb modifications on barstar. Fluorescein imaged gels and quantified band intensities for native-state proteolysis of barstarK60 substrate proteins at 0.2 mg/mL thermolysin with either methylated monoUb or non-methylated monoUb modification. Quantified band intensities were fit to Equation 3 ($n=1$) and overlaid with the calculated model from the data presented in Figure 2.8.

Unmodified barstarK2, barstarK60, and barstarK78 exhibit nearly identical proteolysis kinetics and are proteolyzed through sub-global unfolding ($\Delta G_{\text{proteolysis}} < \Delta G_{\text{unfolding}}$, Table 2.1, Figure 2.9). We observed a similar trend in the $\Delta\Delta G_{\text{proteolysis}}$ values as for the global stabilities, with barstarK2 and barstarK60 showing significant changes in the population of the cleavable state ($\Delta\Delta G_{\text{proteolysis}} = -1.1$ kcal/mol, Table 2.1). BarstarK60/E80A exhibited a similar $\Delta\Delta G_{\text{proteolysis}}$ (-0.96 kcal/mol, Figure 2.8, Table 2.1). Conversely, negligible $\Delta\Delta G_{\text{proteolysis}}$ was detected for barstarK78, indicating no change in the energetics of partial unfolding upon mono-ubiquitination (Figure 2.8).

These variable effects on $\Delta G_{\text{proteolysis}}$ were recapitulated with other proteins. A single-lysine *srcSH3* domain variant showed little $\Delta\Delta G_{\text{proteolysis}}$ (-0.32 kcal/mol, Figure 2.8, Table 2.1), which is particularly interesting because the *srcSH3* domain is smaller than ubiquitin (64 aa vs 76 aa). In contrast, the naturally single-lysine *M. smegmatis* DHFR (159 aa) shows the most drastic changes upon mono-ubiquitination (Figure 2.8, Table 2.1) and is completely proteolyzed within the dead time of the experiment (15 seconds), despite very little cleavage on this timescale for unmodified DHFR. Interestingly, monoUb-DHFR is still capable of binding methotrexate, albeit with greatly reduced affinity, suggesting that the native state is populated (Figure 2.9). Nevertheless, even in the presence of 500 μM methotrexate, the mono-ubiquitinated variant is completely proteolyzed within the dead time of the experiment (Figure 2.10).

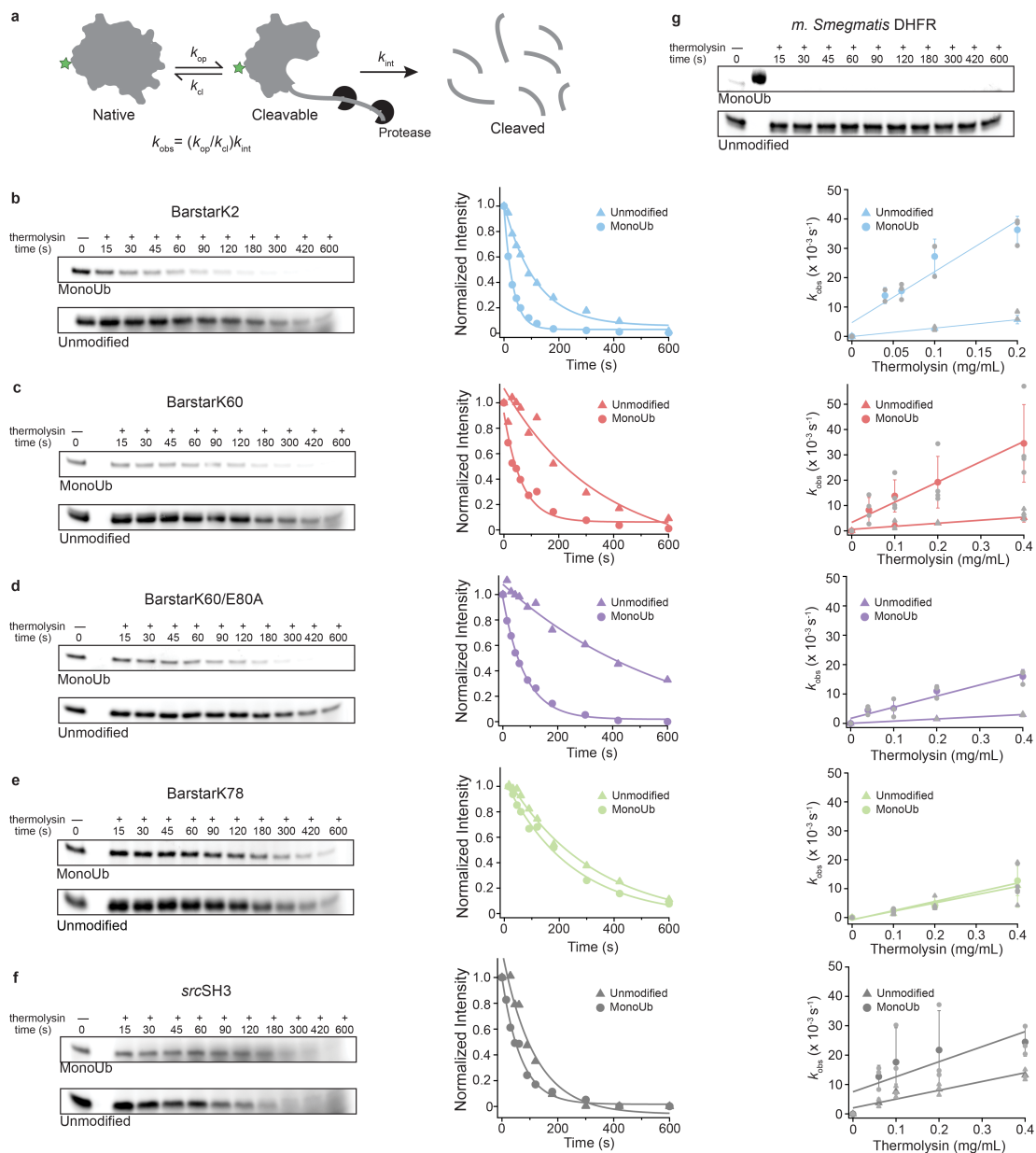


Figure 2.8 | Native-state proteolysis demonstrates the effects of mono-ubiquitination on the energetics of partial unfolding. (a) Under native conditions, well-folded proteins are proteolyzed via transient excursions to partially-unfolded states. The observed rate of proteolysis, k_{obs} , is proportional to the free energy of the conformational change from the native to partially-unfolded state ($\Delta G_{proteolysis}$). (b-f) Representative gels for native-state proteolysis and quantified band intensities for indicated substrate proteins at 0.2 mg/mL thermolysin. $\Delta\Delta G_{proteolysis}$ upon mono-ubiquitination with non-methylated ubiquitin is calculated from the ratio of slopes of the mean k_{obs} ($n=3$ for barstarK2, barstarK78, and barstarK60/E80A; or $n=4$ for barstarK60) against thermolysin concentration ranging from 0.04 to 0.4 mg/mL. Individual trial data are represented in light grey. Error bars represent the standard deviation of replicates. (g) Representative gels for native-state proteolysis of *M. smegmatis* DHFR at 0.2 mg/mL thermolysin ($n=2$).

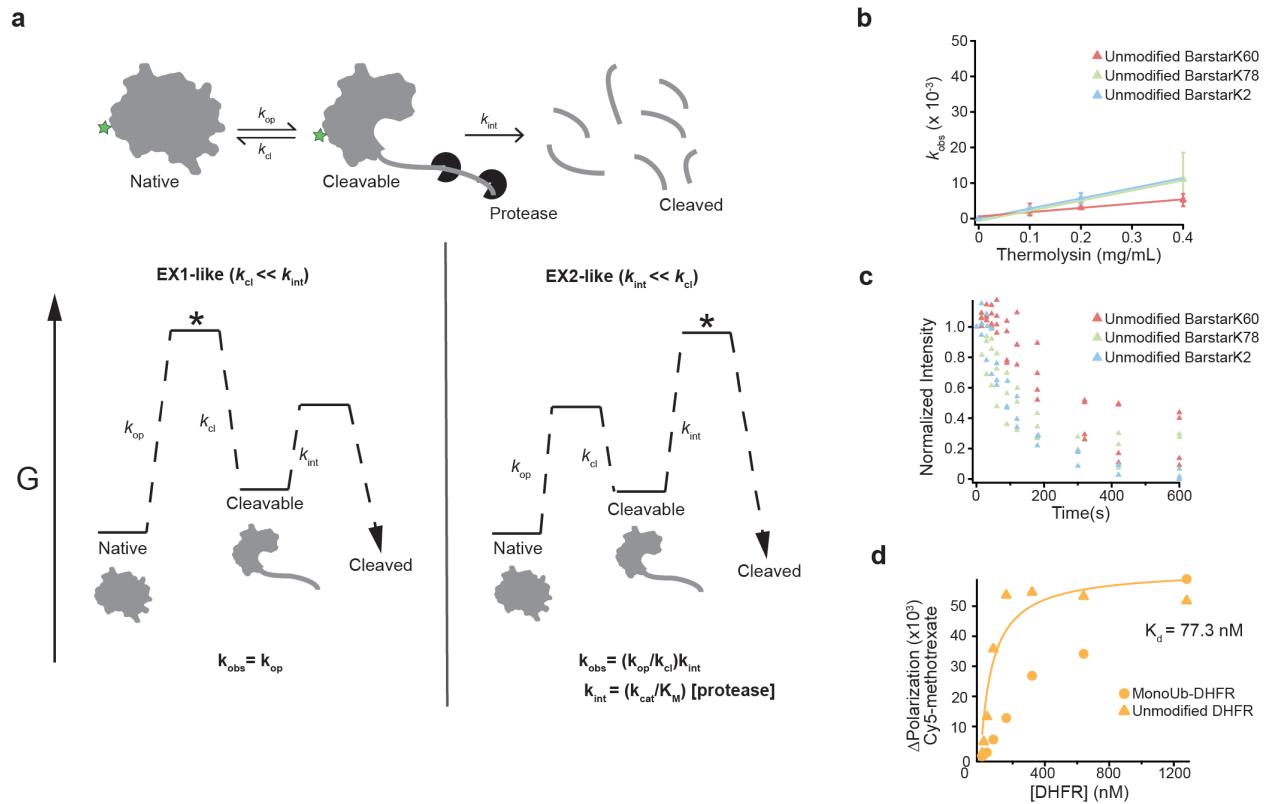


Figure 2.9 | Explanation of native-state proteolysis for investigating the energetics of partial unfolding and validation of native-state proteolysis with these systems. (a) EX1 and EX2-like kinetic regimes for native-state proteolysis. In EX1-like experiments, the conformational change between the native and cleavable states is the rate-limiting step, and $k_{obs} = k_{op}$. In EX2-like experiments, as shown in Fig. 2, the proteolysis of the cleavable state is the rate-limiting step, and $k_{obs} = K_{op}(k_{cat}/K_M)[\text{protease}]$. (b) Fits of thermolysin concentration vs. mean k_{obs} for unmodified barstarK2 ($n=3$), barstarK60 ($n=4$), and barstarK78 ($n=3$) show a linear dependence within error (standard deviation). (c) Example individual data points for time courses of unmodified barstarK2 ($n=3$), barstarK60 ($n=4$), and barstarK78 ($n=3$) at 0.2 mg/mL thermolysin showing the similarity of k_{obs} for the three unmodified barstar variants. (d) Binding curve for unmodified *M. smegmatis* DHFR and monoUb-*M. smegmatis* DHFR to Cy5-methotrexate measured by Cy5 fluorescence polarization ($n=1$).

	BarstarK2	BarstarK60	BarstarK78	BarstarK60/E80A	SH3
C_m unmodified (M urea)	4.97 +/- 0.28	4.41 +/- 0.55	4.65 +/- 1.19	6.02 +/- 0.38	n.d.
C_m monoUb (M urea)	2.52 +/- 0.16	2.51 +/- 0.34	4.24 +/- 1.05	3.72 +/- 0.26	n.d.
ΔC_m (unmodified-monoUb) (M urea)	2.45 +/- 0.32	1.90 +/- 0.65	0.42 +/- 1.59	2.30 +/- 0.46	n.d.
m-value_{global} unmodified (kcal/mol M)	1.06 +/- 0.04	0.96 +/- 0.08	0.89 +/- 0.17	1.16 +/- 0.05	n.d.
m-value_{global} monoUb (kcal/mol M)	0.59 +/- 0.02	0.68 +/- 0.07	0.48 +/- 0.09	0.70 +/- 0.04	n.d.
Δm-value_{global} unmodified-monoUb (kcal/mol M)	-0.47 +/- 0.05	-0.28 +/- 0.11	-0.41 +/- 0.19	-0.47 +/- 0.06	n.d.
ΔG_{unfolding} unmodified[#] (kcal/mol)	5.27 +/- 0.20	4.25 +/- 0.38	4.16 +/- 0.74	6.99 +/- 0.31	n.d.
ΔΔG_{unfolding} unmodified-monoUb* (kcal/mol)	-2.02 +/- 0.10	-1.56 +/- 0.22	-0.29 +/- 0.45	-2.14 +/- 0.11	n.d.
ΔG_{proteolysis} unmodified (kcal/mol)	2.72 +/- 0.02	3.24 +/- 0.11	2.72 +/- 0.06	3.52 +/- 0.01	2.70 +/- 0.12
ΔG_{proteolysis} monoUb (kcal/mol)	1.66 +/- 0.10	2.12 +/- 0.06	2.66 +/- 0.09	2.56 +/- 0.08	2.38 +/- 0.23
ΔΔG_{proteolysis} unmodified-monoUb (kcal/mol)	-1.06 +/- 0.11	-1.12 +/- 0.13	-0.06 +/- 0.15	-0.96 +/- 0.12	-0.32 +/- 0.10

Table 2.1 | Summary of thermodynamic values determined for all barstar variants and srcSH3 in this study. Equilibrium denaturant-induced unfolding transitions were performed in a single trial (n=1), and values reported represent fit parameters. Native-state proteolysis experiments were performed in triplicate (n=3; barstarK2, barstarK78, and barstarK60/E80A) or quadruplicate (n=4; barstarK60), and values represent the mean. All reported errors represent S.E.M derived from curve fitting and propagated through all calculations. [#] indicates that ΔG_{unfolding} values were calculated using a two-state model with linear extrapolation. * indicates that ΔΔG_{unfolding} values were calculated by multiplying the C_m from the denaturation curves by the average m-value for the unmodified and mono-ubiquitinated proteins.

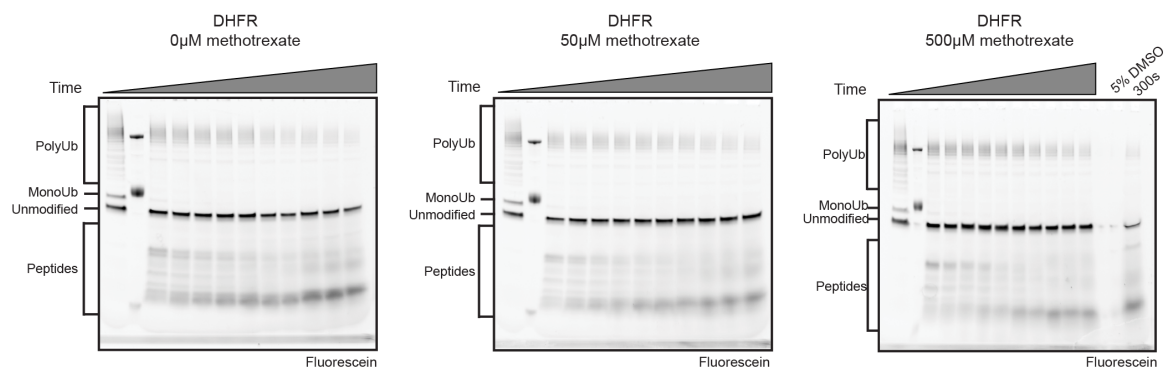


Figure 2.10 | Methotrexate effect on monoUb-DHFR. Full fluorescein imaged gels for native-state proteolysis of monoUb-DHFR (0.2 mg/mL thermolysin) in the presence or absence of saturating concentrations of methotrexate (n=1).

2.5 Ubiquitin-induced energetic changes tune proteasomal degradation rate

2.5.1 *ssrA*/SspB ubiquitin-independent proteasome delivery system to directly measure effect of ubiquitin on proteasomal unfolding

The ability of the proteasome's AAA⁺ motor to unfold proteins is paramount to successful clearance of substrates and has been proposed as the rate-limiting step for degradation (Bard et al., 2019). Therefore, we asked whether ubiquitin-mediated substrate destabilization conferred an increase to the proteasomal degradation rate. In order to compare directly mono-ubiquitinated substrates to their non-ubiquitinated counterparts, we used a system for ubiquitin-independent substrate delivery to the proteasome. In this system, a permutant of the bacterial SspB₂ adaptor protein fused to the N-terminus of the Rpt2 ATPase in the proteasomal AAA⁺ motor recruits substrates that contain an *ssrA* sequence on a sufficiently long unstructured tail region for engagement (Bashore et al., 2015) (Figure 2.11 and Figure 2.12). All substrates delivered in this manner are engaged equally, and thus, observed changes in degradation rate can be attributed to differences in substrate energetics. These experiments were performed at substrate concentrations saturating for SspB₂ binding, but well below the K_d of mono-ubiquitin for proteasomal ubiquitin receptors (Chojnacki et al., 2017) to rule out contributions of ubiquitin to substrate recruitment and engagement. Proteasome-mediated degradation under single-turnover conditions (Figure 2.12) was monitored by SDS-PAGE, and rates were determined based on both the disappearance of full-length substrate and the appearance of peptide products (Figure 2.13).

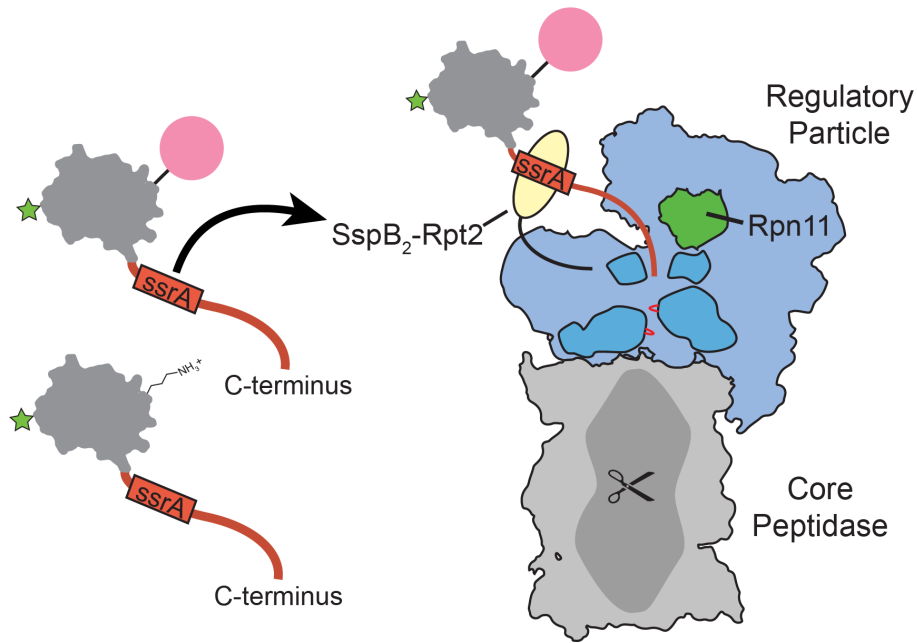


Figure 2.11 | Schematic of ubiquitin-independent substrate delivery system. In this system, substrates contain a flexible C-terminal tail with an ssrA-recognition motif that binds an SspB₂-dimer (yellow) fused to the base AAA+ ATPase. Core particle is represented in gray, regulatory particle in blue, Rpn11 in green, the AAA+ ATPase motor in dark blue, pore loops in red, substrate in gray, with a green star representing fluorescein, red representing the unstructured tail, and ubiquitin in pink.

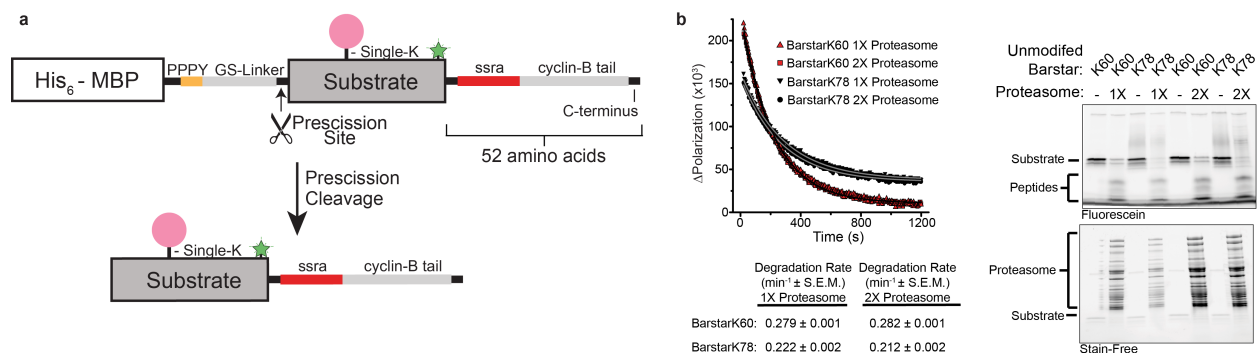


Figure 2.12 | Schematic showing substrate design and confirmation of single-turnover conditions for ubiquitin-independent delivery. (a) An *in vitro* ubiquitination system as in Figure 2.2 and Figure 2.3 is used for enzymatic ligation of methylated ubiquitin to a single lysine on barstar, which contained a C-terminal unstructured region with an ssrA tag, zero-lysine cyclin-B tail, and C-terminal zero-lysine Strep(II) tag for selection. Scaffolding was removed by Prescission (HRV3C) protease and a subtractive Ni²⁺-NTA affinity step. (b) Confirmation of single-turnover degradation conditions through doubling of proteasome concentration. BarstarK60 and barstarK78 degradation by proteasome at the indicated concentrations were monitored by fluorescence polarization (n=2). Observed rates are reported with S.E.M. Right, end-point SDS-PAGE gel of degradation showing conversion of barstarK60 and barstarK78 to peptides (fluorescein channel) and total protein (Stain-Free imaging, Bio-Rad).

All ubiquitinated and non-ubiquitinated barstar variants were processed by the proteasome. As expected, all showed anti-correlated substrate depletion and peptide formation with fast kinetics that were dependent on the presence of RP and ATP (Figure 2.13, Figure 2.14, and Figure 2.15). Degradation rates thereby correlated with the stability changes described above. All non-ubiquitinated barstar variants displayed similar degradation kinetics, with an observed rate (k_{obs}) of 0.1 - 0.3 min^{-1} (Figure 2.13). As previously documented, full-length, unmodified substrate bands appeared as doublets (Bard et al., 2019). MonoUb-barstarK78 showed comparable kinetics, consistent with the negligible stability change upon ubiquitination for this variant (Figure 2.13). However, for the highly destabilized monoUb-barstar variants, degradation kinetics were substantially increased ($k_{\text{obs}} = 1.04 \text{ min}^{-1}$ for monoUb-barstarK60 and 0.93 min^{-1} for monoUb-barstarK2), suggesting that ubiquitin-mediated substrate destabilization increases the rate of unfolding by the proteasome.

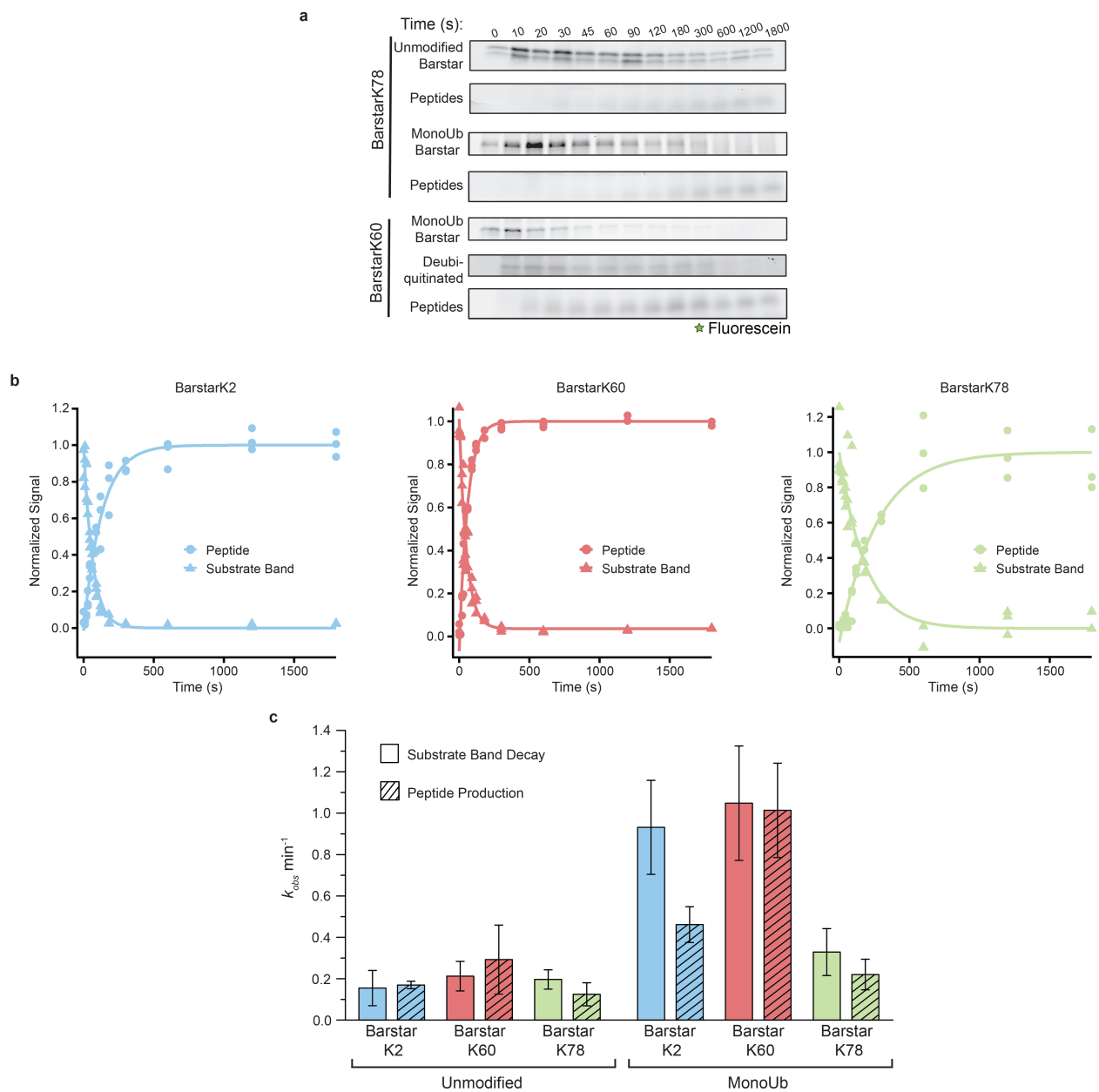


Figure 2.13 | Ubiquitin-induced energetic effects tune proteasomal degradation rate. (a) Representative fluorescein-scanned SDS-PAGE gels showing disappearance of unmodified barstarK78 or mono-ubiquitinated (monoUb) barstarK78 and K60 with concomitant peptide production during proteasomal degradation upon ubiquitin-independent delivery. (b) Normalized fractional signal plotted as individual points ($n=3$) of mono-ubiquitinated substrate band decay and peptide production. Lines represent fit of mean values ($n=3$) to Equation 3. (c) Calculated rates for proteasomal degradation derived by curve fitting to the mean ($n=3$) and associated fitting errors (S.E.M.) from a and b.

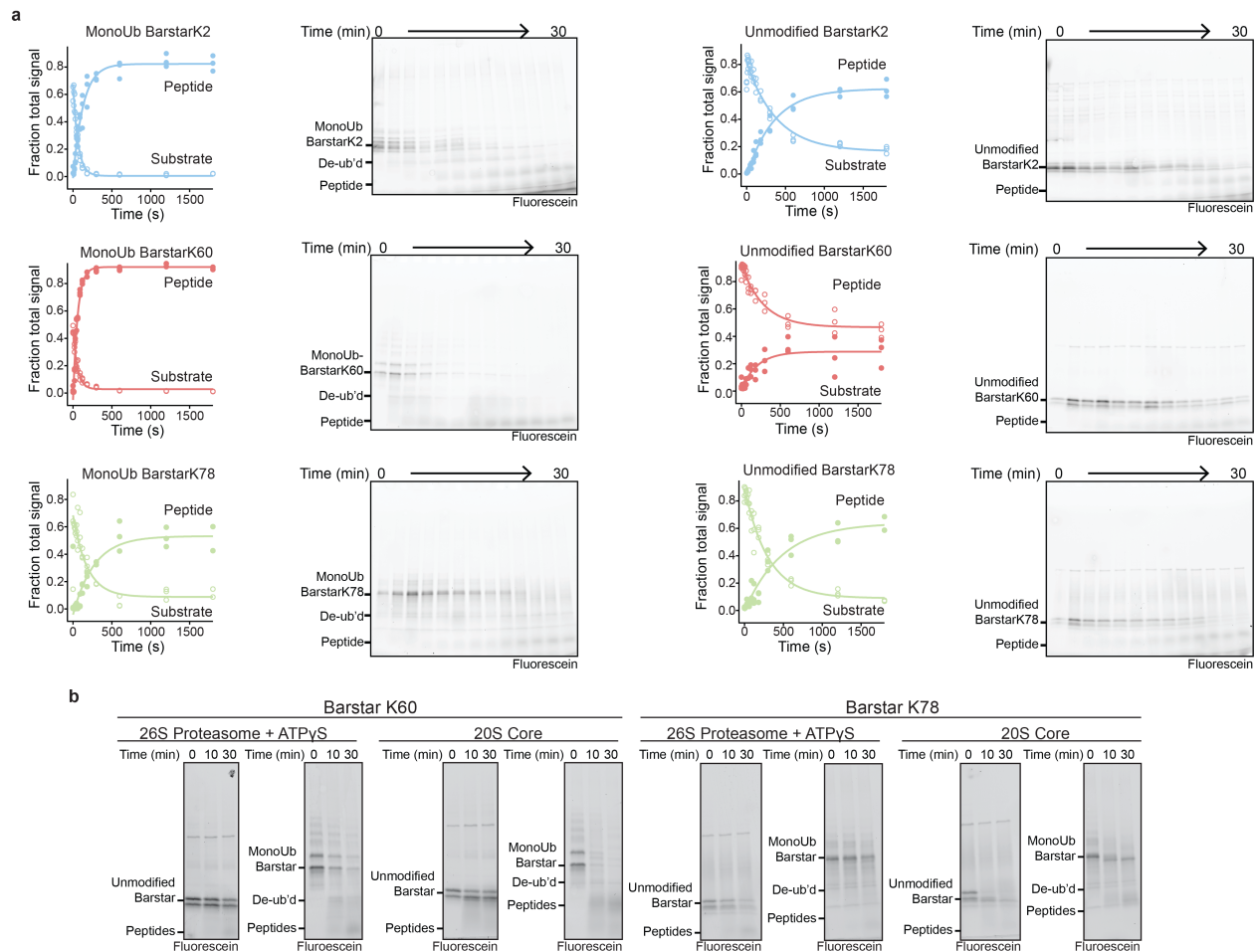


Figure 2.14 | Ubiquitin-independent substrate delivery allows comparison of unmodified and mono-ubiquitinated barstar variants. (a) Representative SDS-PAGE gels of ubiquitin-independent degradations with identified bands indicated at left for each variant. Quantifications and fits of substrate bands are shown left of the representative gels. “Substrate” and “Peptide” bands as a fraction of total lane intensity are presented ($n=3$). **(b)** Fluorescence scans of SDS-PAGE gels from time courses of unmodified or monoUb-barstarK60 and barstarK78 degradations with proteasome in the presence of ATP γ S ($n=1$) or with isolated core particle ($n=2$). Core particle replicate is presented in Figure 2.15. Identified bands are indicated.

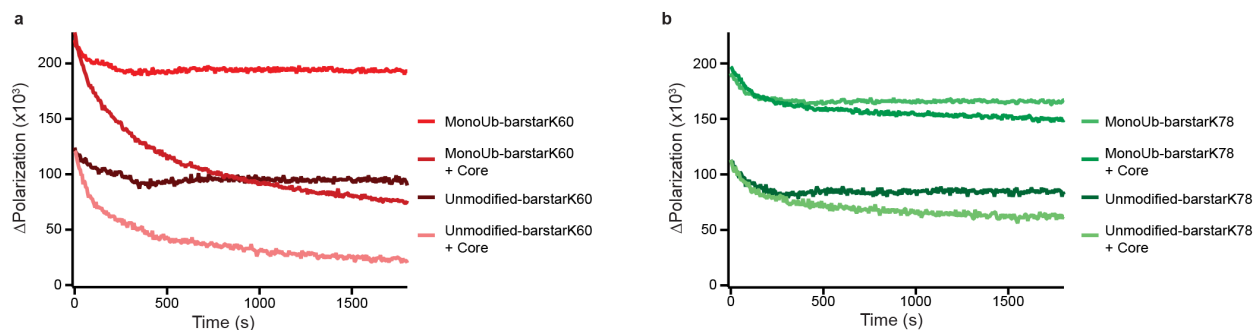


Figure 2.15 | Proteolysis kinetics for ssrA-tagged barstar substrates by the 20S core particle. Fluorescence polarization measurements of (a) ssrA-tagged, tailed barstarK60 or (b) ssrA-tagged, tailed barstarK78 with or without monoUb modification (300 nM) in the presence of excess core particle (2.5 μ M) displays slow, non-exponential kinetics and lower extent of proteolysis.

2.5.2 Effect of topology and deubiquitination timing on degradation

For monoUb-barstarK60, we obtained similar results when following the substrate decay versus peptide production (Figure 2.13 and Figure 2.14). For the monoUb-barstarK2 variant, however, these two processes were decoupled, with the mono-ubiquitinated species disappearing two times faster than the appearance of peptide products (Figure 2.14). This apparent decoupling may originate from differences in the temporal order of deubiquitination and unfolding. All variants showed a transient appearance of deubiquitinated species (Figure 2.16), accounting for $\sim 10\%$ of the total substrate intensity for barstarK2 and barstarK60 at their peak. However, the deubiquitinated barstarK60 species was short-lived (peaked at 30 s, negligible at 3 mins), while the barstarK2 species persisted for ~ 5 mins. Differences in the placement of ubiquitin relative to the substrate-engagement site (the C-terminal appended tail) may alter the timing of deubiquitination relative to crossing the unfolding barrier. In the native barstar structure, the N- and C-termini are located in close proximity (Figure 2.1, PDB: 1BTA). Engagement via the fused C-terminal tail may therefore place the K2-ubiquitin in close proximity to the proteasome's deubiquitinase (Rpn11), allowing deubiquitination immediately after engagement and before unfolding. If deubiquitination occurs prior to substrate unfolding, the destabilizing effect conferred by ubiquitin is lost, resulting in a lower rate of peptide production compared to the disappearance of the ubiquitinated substrate. Other ubiquitination sites (such as K60 or K78) might require substrate unfolding and translocation to occur first to position the ubiquitin-modified lysine for deubiquitination. These data therefore support the correlation between a substrate's thermodynamic stability and its rate of proteasomal degradation, and extend this hypothesis to include ubiquitin attachment as a mode of site-specific destabilization of substrate proteins.

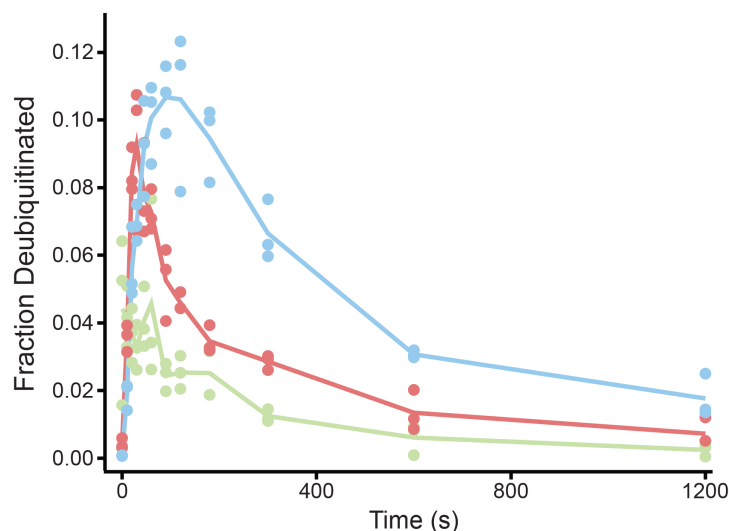


Figure 2.16 | Topology favoring early deubiquitination affects observed degradation kinetics. Fraction of total signal of deubiquitinated species plotted against time as mean (line) and individual data points (dots; $n=3$). BarstarK2 is shown in blue, barstarK60 is shown in red, and barstarK78 is shown in green. Unlike barstarK60 and barstarK78, barstarK2 populates a long-lived deubiquitinated species, which could explain the uncoupling between the disappearance of the monoUb-barstarK2 band and the appearance of degradation peptides.

2.6 Ubiquitin-induced destabilization can reveal the unstructured initiation region in otherwise well-folded proteins

2.6.1 Kinetics of proteasomal degradation of poly-ubiquitinated barstar variants

We next investigated the effect of ubiquitin-induced energetic changes on substrate engagement by the proteasomal AAA+ motor. Numerous studies have demonstrated the role of an unstructured initiation or engagement region (Lee et al., 2001; Prakash et al., 2004; Tomita and Matouschek, 2019; Yu and Matouschek, 2017), yet a substantial fraction of cellular proteasomal substrates appear to lack such flexible segments (Hagai et al., 2011), begging the question of how their degradation is initiated. While other unfoldases, like Cdc48/p97 likely generate disordered regions (Godderz et al., 2015; Olszewski et al., 2019; Twomey et al., 2019), it is also possible that for some proteins ubiquitin-mediated conformational changes are sufficient to expose the obligate unstructured segments. To test this hypothesis, we poly-ubiquitinated our panel of single-lysine barstar variants (Ub_n -barstar) and assayed the proteasome's ability to recognize these substrates via its endogenous ubiquitin receptors and degrade them in an ATP-dependent manner (Figure 2.17). Native-state proteolysis experiments showed that these poly-ubiquitinated barstar variants have similar energetic profiles as the mono-ubiquitinated variants (Figure 2.18).

Surprisingly, despite not harboring any obvious proteasome-engageable unstructured region, some poly-ubiquitinated single-lysine barstar variants were fully degraded by the 26S proteasome, whereas others were only slowly deubiquitinated (Figure 2.17 and Figure 2.19). Importantly, the degradation kinetics depend on the ubiquitination site and correlate with the thermodynamics reported above. To gain a quantitative understanding of the degradation kinetics, we utilized the fluorescein label on Ub_n-barstar and monitored degradation through the decrease in fluorescence polarization (Figure 2.17a). Under single-turnover conditions (confirmed by varying the proteasome concentration, Supplementary Fig. 9c), Ub_n-barstarK60 and Ub_n-barstarK2 showed exponential degradation kinetics, with time constants of approximately 310 s and 432 s, respectively (Figure 2.17b-c). In contrast, Ub_n-barstarK78 did not show measurable degradation, consistent with the hypothesis that site-specific, ubiquitin-mediated substrate destabilization determines whether an unstructured region for proteasome engagement is sufficiently populated (Figure 2.17 d). Furthermore, introducing the stabilizing mutation E80A to Ub_n-barstarK60 substantially increased the degradation time constant to 1018 s (Figure 2.17b).

To further support our hypothesis that the ubiquitin-mediated modulation of barstar's energy landscape is the principal determinant for its degradability, we added saturating concentrations of barnase, the high-affinity ligand of barstar, to these reactions (Figure 2.19). In all cases, barnase ablated substrate degradation. The remaining minimal decrease in fluorescence polarization could be attributed to minor degradation-independent deubiquitination (Figure 2.18b-d). Addition of barnase has no effect on the degradation of a ubiquitinated titin substrate with a flexible initiation region (FAM-Titin-I27^{V13P,V15P}-35mer-tail) (Bard et al., 2019), confirming that the inhibition observed for the barstar variants was due to specific binding and stabilization of barstar's folded state, rather than inhibitory interactions with the proteasome (Figure 2.19c).

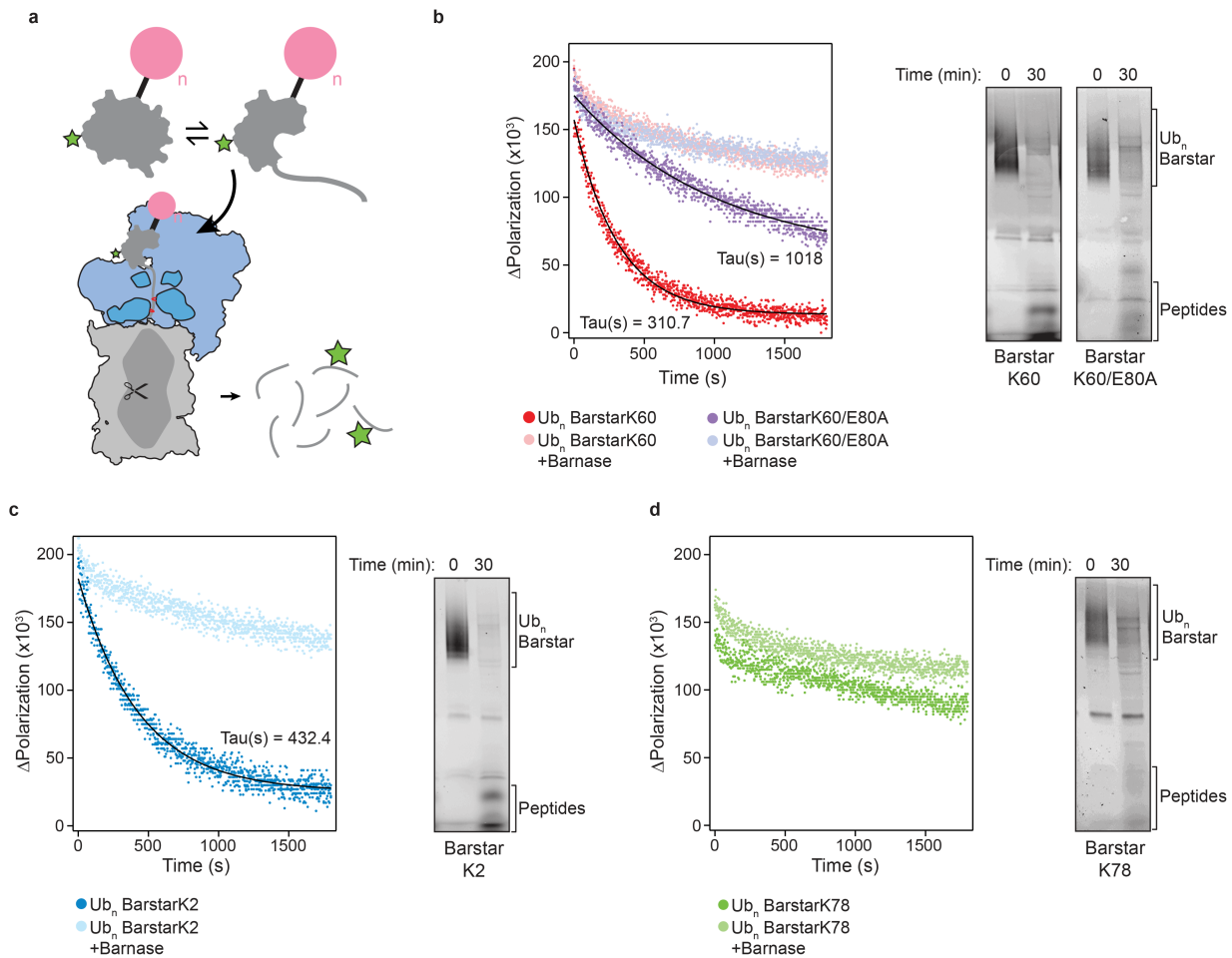


Figure 2.17 | Ubiquitin-mediated destabilization of barstar is sufficient to expose a proteasome-engageable unstructured region. (a) Schematic of degradation reaction, showing Ub_n-substrate lacking an unstructured region at equilibrium with a partially-unfolded state, whereby the partially-unfolded state is competent for proteasome engagement, unfolding, and proteolysis. Core particle is represented in gray, regulatory particle in blue, the AAA+ ATPase motor in dark blue with pore loops in red, substrate in gray with a green star representing fluorescein, and ubiquitin in pink. Degradation can be monitored through the decrease in fluorescence polarization upon transition from a large poly-ubiquitinated substrate to peptides. (b-d) Left: fluorescence polarization kinetic measurements for single-turnover degradations of Ub_n-barstar in absence or presence of saturating barnase, presented as individual data points (n=3), with lines representing fitting to Equation 3 and calculated time constants (Tau) shown. Right: fluorescein scan of SDS-PAGE gel with 30-minute endpoint samples for single-turnover Ub_n-barstar degradations, showing conversion of substrate to peptides and/or deubiquitinated species.

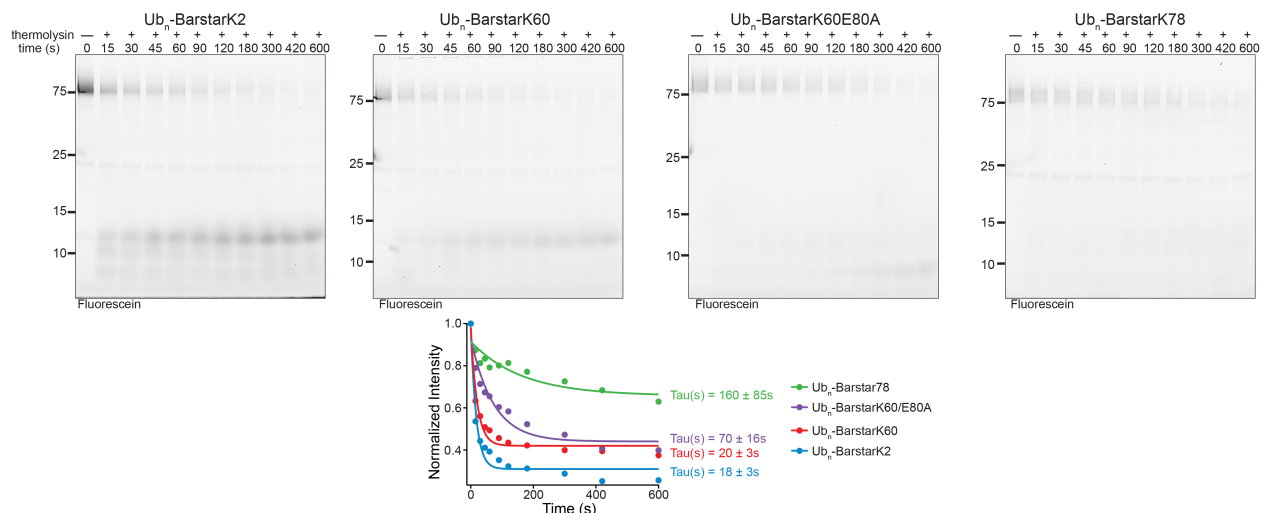


Figure 2.18 | Native state proteolysis experiments for polyUb-barstar variants. Fluorescein scans of 12% Bis-Tris Nu-PAGE (Invitrogen) SDS-PAGE gels of thermolysin proteolysis of Ub_n-barstar variants, with molecular weight standards and time points indicated (Top; n=1). Quantified gel bands were normalized and plotted against time, and time constants were calculated by fitting to Equation 3 with error representing S.E.M. for the fit.

In addition, we monitored degradation of the Ub_n-barstar variants by the isolated core particle to verify that robust degradation requires the entire 26S proteasome and includes ubiquitin recognition, ATP-driven unfolding and translocation. The core particle can only hydrolyze unstructured polypeptides that diffuse into its central chamber to access the proteolysis sites. Indeed, the core particle only minimally cleaved the Ub_n-barstarK2 and Ub_n-barstarK60 species with low rates compared to the 26S holoenzyme (Figure 2.19b,d). Similar to the differences seen for the ATP-dependent degradation by the 26S proteasome, Ub_n-barstarK78 displayed no core-particle mediated degradation, and Ub_n-barstarK60/E80A was cleaved by the core much more slowly than Ub_n-barstarK60.

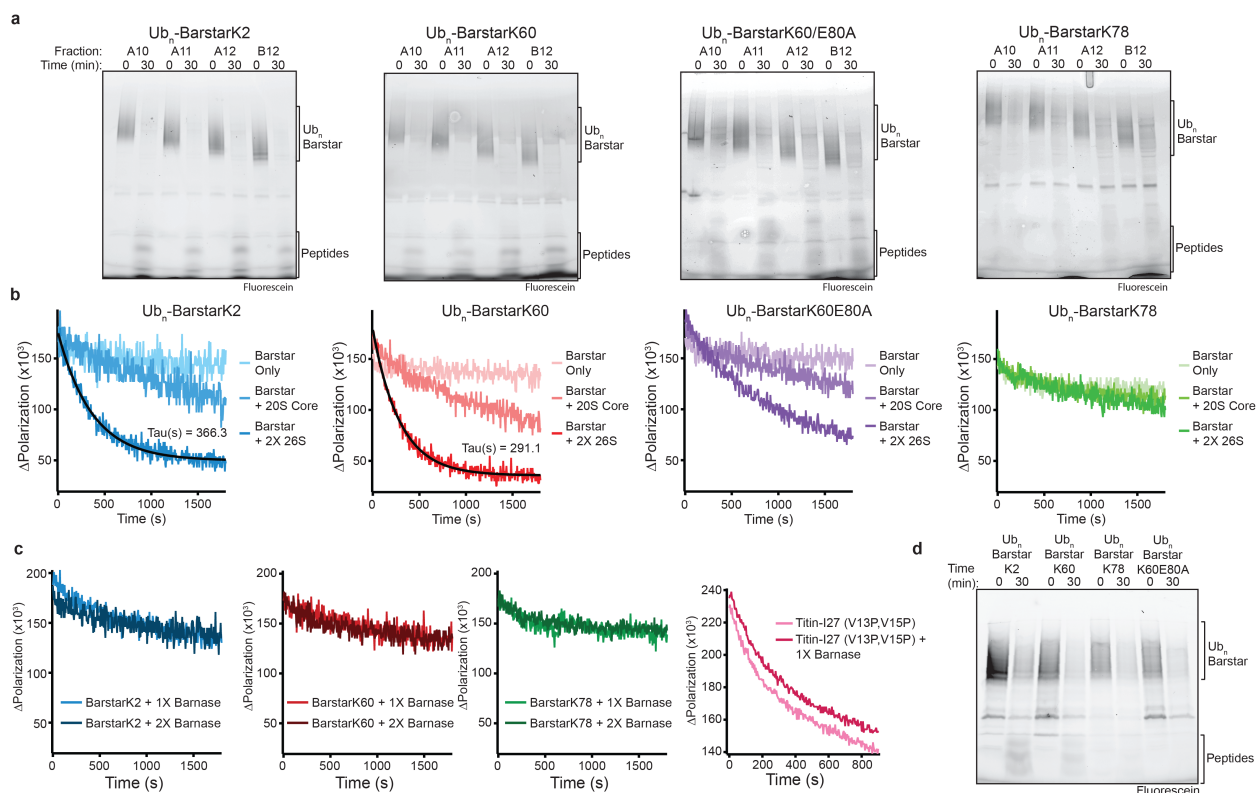


Figure 2.19 | Observed polyUb-barstar degradation is 26S proteasome-dependent. (a) Fluorescein scan of 4-20% TGX (Bio-Rad) SDS-PAGE gels showing the end-point samples from single-turnover degradations of fractions obtained from size exclusion chromatography of Ub_n-barstar variants, with poly-ubiquitinated species and peptides indicated. Fraction A12 from each gel is presented in Figure 2.17 (n=1). (b) Fluorescence polarization of Ub_n-barstar substrates treated with 2X concentration of proteasome (n=1), 900 nM isolated core particle (n=1; see d), or untreated (n=1). Reported time constants were derived from fitting to Equation 3. (c) Changes in fluorescence polarization during single-turnover degradations of Ub_n-barstars in the presence of 20 μ M (1X) or 40 μ M (2X) barnase (Left). Single-turnover degradation of FAM-Titin-I27^{V13PV15P} in the presence or absence of 20 μ M (1X) barnase, monitored by fluorescence polarization (Right). (d) Fluorescence scan of 4-20% TGX (Bio-Rad) SDS-PAGE gels with end-point samples for the incubation of Ub_n-barstar variants (5-10 nM) with excess isolated core particle (900 nM). Peptides and Ub_n-barstar species are indicated.

2.6.2 o-phenanthroline inhibition of Rpn11 suggests C-terminal barstar initiation

Unlike our observations with the ubiquitin-independent delivery system, where we saw buildup of a deubiquitinated species for monoUb-barstarK2 (Figure 2.16), Ub_n-barstarK2 did not populate a deubiquitinated species (Figure 2.17c and Figure 2.19b). Because Ub_n-barstarK2 lacks the appended unstructured C-terminal tail, it must engage via a partially-unfolded state, in which the ubiquitin attachment site may no longer be optimally positioned for Rpn11-mediated cleavage prior to unfolding. Moreover, given that this variant is ubiquitinated near the N-terminus,

it must be engaged C-terminal to the ubiquitination site. This is confirmed by our observation that inhibition of Rpn11 deubiquitination by *o*-phenanthroline did not inhibit degradation of Ub_n-barstarK2, but inhibited all other variants (Figure 2.20a). For Ub_n-barstarK2, the polypeptide between the ubiquitin-attachment point, K2, and the fluorescein-labeled Cys82 (80 residues) is long enough to span the minimal distance between the entrance of the AAA+ pore and the proteolytic active sites (approximately 55 residues; Figure 2.20b). Rpn11-inhibited proteasomes can therefore move this substrate far enough into the 20S core for proteolysis near fluorescein, before translocation stalls on the K2-attached ubiquitin chain (De la Peña et al., 2018).

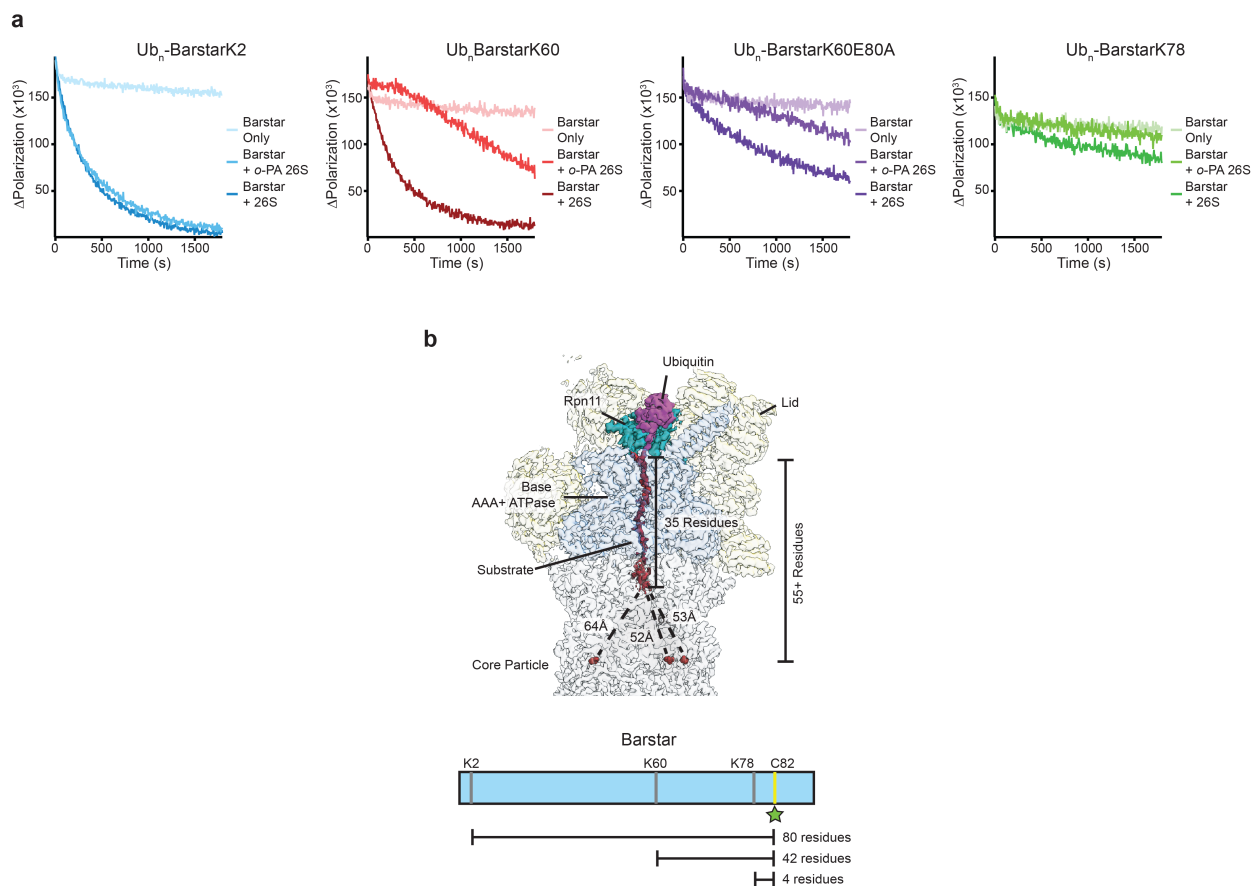


Figure 2.20 | The proteasome engages polyUb-barstarK2 C-terminal to the ubiquitin modification. (a) Single-turnover degradations of Ub_n-barstar substrates in the presence (n=1) and absence (n=6) of an Rpn11 inhibitor *o*-phenanthroline monitored by fluorescence polarization. (b) Density for substrate-bound proteasome (EMD: 9045, PDB: 6FVW) with the lid subunits as well as Rpn1 and Rpn2 in yellow, ubiquitin in magenta, Rpn11 in dark cyan, the base AAA+ ATPase in cornflower blue, substrate polypeptide in red, and the core particle in light grey. Distances were obtained from PDB: 6FVW. Below, cartoon of barstar sequence highlighting single lysine positions and the single, fluorescein-labeled cysteine at position 82.

2.6.3 Engagement is the rate-limiting step in the absence of an intrinsic unstructured region

The proteasomal degradation rates observed for poly-ubiquitinated barstar variants are notably lower than for barstar or other substrates with flexible tails (Bard et al., 2019; Greene et al., 2019; Worden et al., 2017), suggesting that engagement of a spontaneously unfolding region represents the rate-limiting step for degradation. To probe this further, we turned to a proteasome variant, Rpn5-VTENKIF, whose mutations in the RP affect the conformational equilibrium of the proteasome and thereby hinder insertion of flexible segments into the AAA+ pore, making engagement rate-determining even for moderately stable substrates with unstructured tails (Greene et al., 2019). Using Rpn5-VTENKIF proteasome, we see a three-fold (Ub_n-barstarK2) and two-fold (Ub_n-barstarK60) decrease in degradation rates (Figure 2.21), suggesting that their slow degradation kinetics are indeed determined by slow engagement and not unfolding. This leads to the interesting conclusion that for well-folded substrates, exposure of a flexible segment through spontaneous unfolding determines the rate of degradation, providing an alternative means of regulation for proteasomal targeting.

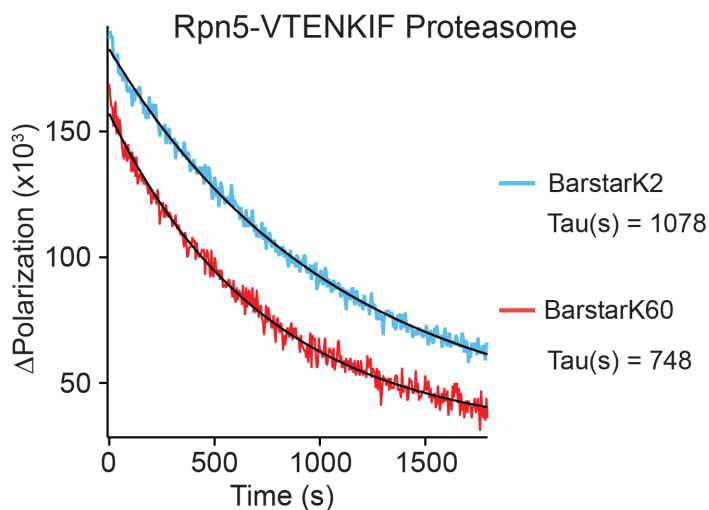


Figure 2.21 | Proteasome engagement can be the rate limiting step for degradation. Single-turnover degradations of Ub_n-barstarK2 and Ub_n-barstarK60 by Rpn5-VTENKIF proteasome and time constants calculated from fitting to Equation 3 (n=1).

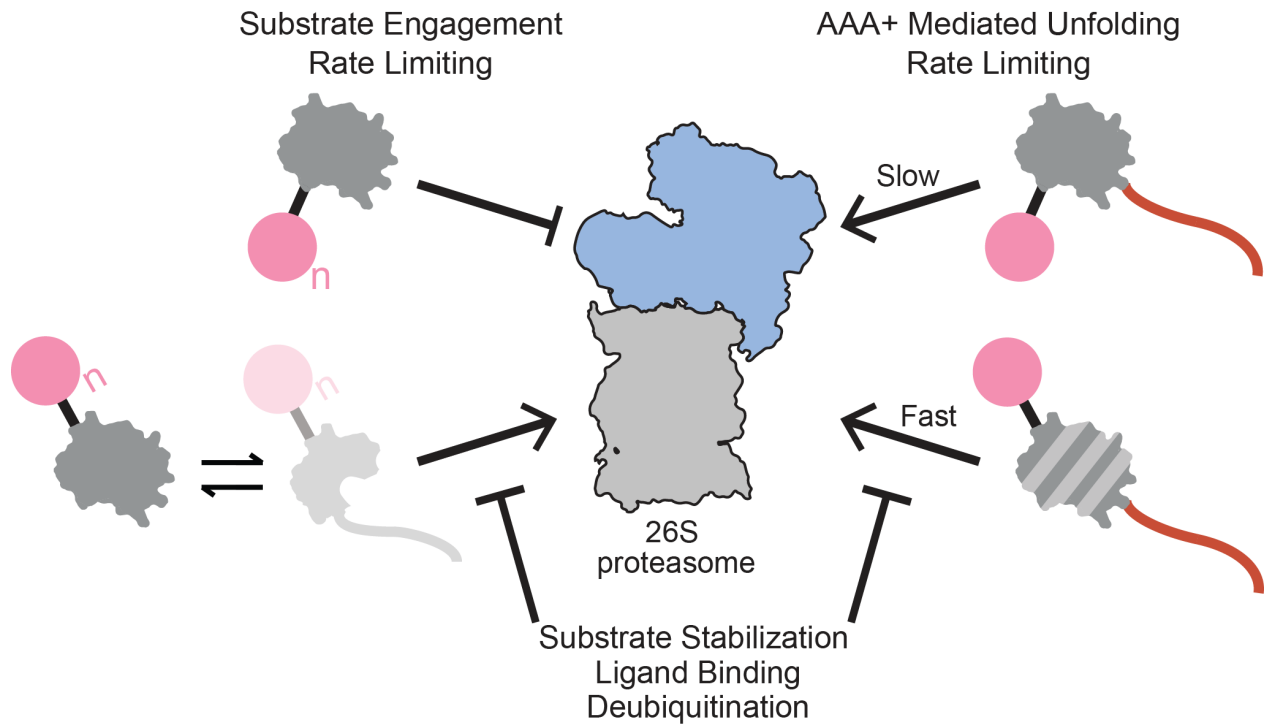


Figure 2.22 | Model for the consequences of site-specific, ubiquitin-induced substrate energy landscape modulation on proteasomal degradation. If ubiquitination occurs on a non-sensitive structured lysine, as in barstarK78, the substrate does not sufficiently populate a partially-unfolded, proteasome-engageable conformation. If ubiquitin-modification occurs on a sensitive lysine, as in barstarK2 and barstarK60, the otherwise well-folded substrate is sufficiently destabilized to populate partially-unfolded, proteasome-engageable conformations and is successfully degraded. The observed degradation kinetics thus appear dependent on the changes to the protein energy landscape upon ubiquitination. When substrates contain an unstructured proteasome-engageable region, ubiquitination at sensitive lysine positions allows for substantially faster degradation kinetics, while degradation kinetics of substrates with non-destabilizing ubiquitinations remain essentially unchanged. Successful proteasome engagement and degradation of ubiquitin-destabilized substrate proteins can be slowed or blocked by a number of energetically stabilizing events, including deubiquitination, ligand binding, or stabilizing mutation.

2.7 Conclusions

Clearance of damaged, misfolded, and regulatory intracellular proteins is paramount for sustaining life and catalyzed largely by the UPS. While substrate energetics critically affect the degradation of various substrates (Bard et al., 2019; Guo et al., 2018; Prakash et al., 2004; Reichard et al., 2016), the influence of the substrate-attached ubiquitin itself has been elusive. Here, we show that ubiquitin

can mediate substrate destabilization with direct consequences for proteasomal degradation. To carry out these studies, we developed a generalizable system to produce ubiquitin-modified single-lysine proteins with native isopeptide bonds (Figure 2.2), achieving efficient ubiquitination for several different single-lysine substrates. We expect that this strategy will be useful to address a number of biological questions that are currently hampered by challenges in producing and purifying proteins with natively attached ubiquitin on structural domains (Faggiano and Pastore, 2014). Using these isopeptide-linked ubiquitinated substrates, we show that ubiquitin-mediated energetic effects can dictate how fast a protein is degraded and, surprisingly, whether a protein is susceptible to proteasomal degradation at all, thus providing an additional regulatory mechanism for clearance of a ubiquitinated substrate based on its conformational and energetic properties.

Consistent with this concept, we found that stabilizing the substrate via ligand binding (as in barstar:barnase) inhibits proteasomal processing. The engagement of these substrates appears to be rate-limiting and modulated directly by the accessibility of partially-unfolded, proteasome-engageable states. Thus, the overall context of the ubiquitinated protein with respect to cellular environment, binding partners, and perhaps other stabilizing or destabilizing PTMs can influence whether a ubiquitinated substrate is actually degraded.

Based on our results, we can build a model for the effect of ubiquitin-mediated, site-specific changes in protein energy landscapes on proteasomal degradation (Figure 2.22), in which: 1) a protein may or may not be engaged by the proteasome based on its altered energetics, and 2), the speed with which ubiquitinated substrates are degraded is related to the extent of ubiquitin-induced destabilization. Both aspects of proteasomal turnover are directly modulated by the increased sampling of partially-unfolded states and further influenced by other factors, such as stabilizing mutations or deubiquitination prior to substrate unfolding, either at the proteasome by Rpn11 or by a host of cellular deubiquitinases (Komander and Rape, 2012).

This model has implications for a number of different processes, including the engineering of substrate degradation via Proteolysis Targeting Chimeras (PROTACs) (Sakamoto et al., 2001). PROTACs are synthetic molecules containing two moieties, a ligand binding the target protein to be degraded and another ligand with affinity for an E3 ubiquitin ligase that facilitates ubiquitination of the target. The linker length between the two ligands has been found to affect whether the target protein is degraded (Nowak et al., 2018), likely because it determines which lysines on the target are ubiquitinated in a manner that facilitates delivery to the downstream processing enzymes (i.e. Cdc48/p97 and the proteasome) (Smith et al., 2019; Twomey et al., 2019), but also possibly depending on whether ubiquitination at these lysines destabilizes the target. Non-specific ligands that promiscuously bind to 50-100 protein kinases were found to facilitate the degradation of only a

small subset of these kinases (Bondeson et al., 2018; Huang et al., 2018), which could also be due to which lysines are ubiquitinated on the different targets and whether these ubiquitinations are sufficiently destabilizing to allow degradation.

While it is clear that ubiquitination has site-specific effects on the energy landscape, the mechanisms for ubiquitin-induced destabilization and the population of partially-unfolded conformers remains unknown. Potential mechanisms include destabilization from reduced conformational entropy in the substrate, a ubiquitin-induced entropic pulling force, direct substrate-ubiquitin interactions, or the ubiquitin-induced population of an intermediate state. There are no clear patterns regarding the region or type of secondary structure within the substrate that is energetically sensitive to the attachment of ubiquitin, nor are the effects correlated with the substrate size, as previously suggested (Morimoto et al., 2016). It is reasonable to expect that the addition of a protein domain, such as ubiquitin, can alter the energetics and dynamics of a target protein in this manner. Biophysical studies of multidomain proteins have demonstrated that the stability of one domain can be modulated by the presence of another (Batey et al., 2008). In differentially-linked polyubiquitin chains, the ubiquitin monomers themselves can have different thermodynamic and mechanical stabilities (Carrion-Vazquez et al., 2003; Morimoto et al., 2015). Studies on N-terminal ubiquitin fusions and disulfide-linked ubiquitin attachments have reported small changes in the midpoints for thermally-induced unfolding depending on the modification (Morimoto et al., 2016).

Computational studies have postulated that ubiquitin-induced destabilization is a result of a decrease in a substrate's overall conformational entropy (Gavrilov et al., 2015). Site-specific effects could be realized through the difference in the potential flexibility at the different sites. The local structure and packing at the three different ubiquitination sites in barstar, however, do not reveal any notable differences in the density of atomic contacts or number of contacting residues (PDB: 1BTA). Detailed calculations or experiments evaluating these potential changes in conformational entropy are needed to explore this hypothesis further.

Our results do not yield specific information about a potential entropic pulling force. NMR studies of the protein FKBP12 with chemically conjugated ubiquitin demonstrated increased backbone flexibility (Morimoto et al., 2016), which could be rationalized by an entropic pulling model whereby a highly stable protein fold, like ubiquitin, attached through a native isopeptide bond with many degrees of translational and rotational freedom, can provide a net pulling force on the substrate from the site of ligation (Sousa and Lafer, 2019).

The energetic modulation may also arise from direct interactions between the ubiquitin and the substrate. Ubiquitin has multiple exposed hydrophobic patches, one near Ile44 and another at Ile36, which could potentially stabilize exposed hydrophobic residues on a partially-unfolded substrate. The Ile44 hydrophobic

patch is known to interact with PCNA when in an N-terminal fusion (Freudenthal et al., 2010) and is responsible for the inter-ubiquitin interactions that give K48-linked ubiquitin chains their compact conformation (Eddins et al., 2007; Varadan et al., 2002). Ubiquitin also contains an acidic patch that electrostatically interacts with some target proteins (Debelouchina et al., 2017). In sum, how exactly ubiquitin destabilizes the substrate protein remains unknown and will require further investigation.

Cellular proteostasis relies upon careful regulation of protein degradation via the UPS, and the consequences of aberrant degradation are severe. We find that ubiquitin directly modulates a protein's conformational energy landscape, and these energetic changes play a pivotal role in regulating both 26S proteasome substrate selection and degradation kinetics. We conclude that ubiquitin signaling and proteasomal degradation overall are dependent on the biological and biophysical contexts of individual ubiquitinated proteins. A full understanding of the energetic effects contributed by a particular ubiquitination event is therefore crucial for building a complete model of how ubiquitin-mediated signals are transduced *in vivo*. We hope the tools and results presented herein can facilitate addressing these questions and be used to expand our model of the biophysical factors governing ubiquitin-mediated signaling.

2.8 Materials and Methods

2.8.1 MATLAB script

First, download fasta file of all sequences in PDB. Then, open the .m file containing the following script and run in MATLAB (written in version 2016b).

```
WT%This code is to read through all pdb files for proteins with a certain
%number of lysine residues
% count for number of sequences to parse
n = 1;

%parse statement
for i=1:341136

    %read each fasta sequence one by one with the blockread function of the
    %fastaread command
    FASTAData = fastaread('pdb_seqres.txt' , 'BlockRead' , n );

    %make a variable for the string that is the sequence
    k = FASTAData.Sequence

    %count the number of lysines in sequence
    numberofk = length(strfind(k , 'K'));
```

```

%If statement that will return the name of each protein with less than
%or equal to two lysine residues
if (numberofk <= 2) && (length(k) >= 100)
    disp(FASTAData.Header);
end

%continue the count through 341136 sequences in the fasta file input
n = n+1;

end

```

2.8.2 Expression and purification of single-lysine substrate proteins

E. coli BL21 Rosetta 2 (DE3) cells were transformed with either pEC072 (single-lysine *srcSH3*), pEC074 (*M. smegmatis* DHFR), pEC076 (barstarK2), pEC062 (barstarK60), pEC081 (barstarK60/E80A), or pEC059 (barstarK78). Cells were then grown in 2 L LB Broth (Fisher) to $0.4 < OD_{600} < 0.8$ and induced with 1 mM IPTG for 3 hours at 37°C. Bacteria were then pelleted and resuspended in 50 mM HEPES pH 7.0, 150 mM NaCl, 0.5 mM TCEP supplemented with 1X Halt™ protease inhibitor cocktail (Thermo) and benzonase (Novagen). Resuspended cells were lysed by sonication and the lysate was clarified by centrifugation at 20,000 rcf, 4°C, 30 minutes. The substrate was first purified by Ni²⁺-NTA affinity chromatography using its N-terminal His₆ tag. Clarified lysate was allowed to batch bind to HisPur™ Ni²⁺-NTA resin (Thermo) washed with 50 mM HEPES pH 7.0, 150 mM NaCl, 25 mM imidazole, 0.5 mM TCEP and eluted with 50 mM HEPES pH 7.0, 150 mM NaCl, 500 mM imidazole, 0.5 mM TCEP. Concentration of protein in the eluate was then measured using UV-Vis absorption at 280 nm. Eluate was then labeled for 2 hours at room temperature with 5X molar excess fluorescein-maleimide dye (Thermo). The labeling reaction was quenched with 10X molar excess DTT and unreacted dye was removed using a S200 16/60 size exclusion column (GE) pre-equilibrated with 25mM HEPES pH 7.5, 150 mM KCl, and 15 mM MgOAc. Peak corresponding to the labeled, full length His-MBP substrate was collected, and quantified by UV-Vis absorption at 280 nm and 495 nm according to the manufacturer's instructions before addition of 10% glycerol and flash freezing to store at -80°C for future use.

2.8.3 Purification of ubiquitination enzymes

Ubiquitination machinery *M. musculus* mE1, *S. cerevisiae* Ubc4, and *S. cerevisiae* Rsp5 were purified as described previously using the same procedure (Bard et al., 2019; Worden et al., 2017). *E. coli* BL21 Rosetta 2 (DE3) pLysS cells were transformed with pAM235 (mE1) or pAM236 (Ubc4) or pAM237 (Rsp5) and grown at 37°C in 6L of terrific broth (Novagen) until $OD_{600} = 0.8$ before expression was induced with 1 mM IPTG and allowed to continue overnight at 18°C. Cells were

resuspended in 50 mM HEPES pH 7.6, 250 mM NaCl supplemented with protease inhibitors (pepstatin A, aprotonin, PMSF, and leupeptin), benzonase, and lysozyme (2 mg/mL) and stored at -80°C. Resuspended cells were thawed and lysed by sonication before lysate was clarified by centrifugation at 20,000 rcf for 30 mins at 4°C. Clarified lysate was batch bound to HisPur™ Ni²⁺-NTA resin (ThermoFisher) equilibrated with 50 mM HEPES pH 7.6, 250 mM NaCl for one hour at 4°C. Resin was washed in a gravity flow column with at least 50 mL of 50 mM HEPES pH 7.6, 250 mM NaCl, 20 mM imidazole before protein was eluted with 50 mM HEPES pH 7.6, 250 mM NaCl, 250 mM imidazole. Eluate was concentrated in an Amicon spin concentrator (Millipore) and loaded onto a Superdex200 16/60 size exclusion column (GE) equilibrated in 20 mM HEPES pH 7.6, 100 mM NaCl, 10% glycerol. Peak corresponding with target protein was collected, concentrated in Amicon spin concentrator (Millipore), quantified by absorbance at 280 nm, and flash frozen in liquid nitrogen for storage at -80°C.

For preparation of AMSH deubiquitinase, *E. coli* BL21 Rosetta 2 (DE3) pLysS cells were transformed with pAM241 and grown in 2 L of terrific broth (Novagen) at 37°C until OD₆₀₀ = 0.6 after which expression was induced with 0.5 mM IPTG overnight at 18°C. Cells were resuspended in 50 mM HEPES pH 7.6, 250 mM NaCl supplemented with protease inhibitors (pepstatin A, aprotonin, PMSF, and leupeptin), benzonase, and lysozyme (2 mg/mL) and stored at -80°C. Resuspended cells were thawed and lysed by sonication before lysate was clarified by centrifugation at 20,000 rcf for 30 mins at 4°C. Clarified lysate was batch bound to HisPur™ Ni²⁺-NTA resin (ThermoFisher) equilibrated with 50 mM HEPES pH 7.6, 250 mM NaCl for one hour at 4°C. Resin was washed with 50 mM HEPES pH 7.6, 250 mM NaCl, 10 mM ATP (to remove contaminating DnaK), 20 mM imidazole. The His₆ tag was cleaved from AMSH by HRV3C-protease overnight at 4°C and AMSH was clarified through an ortho Ni²⁺-NTA step using HisPur Ni²⁺-NTA resin (ThermoFisher). Protein was concentrated in Amicon spin concentrator (Millipore) before being loaded on a S75 16/60 size exclusion column (GE) equilibrated with 20 mM HEPES pH 7.6, 100 mM NaCl, 10% glycerol. Peak corresponding to AMSH was collected, concentrated in an Amicon spin concentrator (Millipore), quantified by absorbance at 280 nm, and flash frozen in liquid nitrogen for storage at -80°C.

2.8.4 Preparation of homogenous mono-ubiquitinated substrate proteins

Substrate proteins, ubiquitin, ubiquitination enzymes, and AMSH were prepared as described above. Ubiquitination reactions were set up in reaction buffer (50 mM HEPES pH 8.0, 150 mM NaCl, 5 mM MgCl₂, and 5% glycerol) in 20 µL aliquots as follows: 5 µM Uba1 (E1), 5 µM Ubc4 (E2), 5 µM Rsp5 (E3), 20 µM substrate, 750 µM wild-type (non-methylated) ubiquitin or methylated ubiquitin, 5 mM ATP and incubated in a thermocycler for 3 hours at 25°C. 48 individual 20 µL reactions were performed for a typical prep. After three hours, reactions were pooled and HRV3C-

protease was added and allowed to cleave overnight at 4°C. If wild-type (non-methylated) ubiquitin was used, reactions were then treated with 0.5 μM AMSH for 30 minutes at room temperature and quenched with 5 mM EDTA. His-tagged ubiquitination machinery and the His-MBP scaffold were then removed via a subtractive Ni²⁺-NTA affinity step using a 1 mL HisTrap HP column (GE) pre-equilibrated with 50 mM HEPES pH 7.0, 150 mM NaCl, 25 mM imidazole. This removed most, but not all, of the His-tagged ubiquitination machinery and ubiquitinated His-MBP substrate scaffold. Flow through was then concentrated and loaded onto an S75i 10/300 size exclusion column (GE) pre-equilibrated with 25 mM HEPES pH 7.5, 150 mM KCl, and 15 mM MgOAc. The peak corresponding to the mono-ubiquitinated substrate was collected, concentrated, and quantified by UV-Vis absorption at 280 nm and 495 nm according to the manufacturer's instructions before addition of 10% glycerol and flash freezing to store at -80°C for future use.

2.8.5 Preparation of mono-ubiquitinated substrate proteins with C-terminal ssrA tag/engageable tail

Substrate proteins and ubiquitination enzymes were prepared as described above. Ubiquitination reactions were set up in reaction buffer (50 mM HEPES pH 8.0, 150 mM NaCl, 5 mM MgCl₂, and 5% glycerol) in 20 μL aliquots as follows: 5 μM Uba1 (E1), 5 μM Ubc4 (E2), 5 μM Rsp5 (E3), 20 μM substrate, 500 μM methylated ubiquitin (Millipore), 5 mM ATP and incubated in a thermocycler for 3 hours at 25°C. 24 individual 20 μL reactions were performed for a typical prep. After three hours, reactions were pooled and HRV3C-protease was added and allowed to cleave for 30 minutes at room temperature. Ubiquitination enzymes and His-MBP were removed by batch binding to MagneHis™ (Promega) magnetic Ni²⁺-NTA resin for 1 hour at 4°C. Resin was pelleted in a magnetic tube rack, and the supernatant was collected for gel based single-turnover ubiquitin-independent degradation assays.

2.8.6 Equilibrium urea denaturation to measure global stability

Two 5 μM protein stocks were prepared: A no denaturant protein stock and a high urea protein stock both in 25 mM HEPES pH 7.5, 150 mM KCl, and 15 mM MgOAc. The exact urea concentration in the high denaturant stock was determined by taking the refractive index. Samples with a range of urea concentrations were prepared by serial dilution of the two stocks and allowed to equilibrate at room temperature overnight. Measurements were then performed at 25°C using a PTI Quantmaster Fluorometer (Horiba). Tryptophan fluorescence was excited at 295 nm and a 10 second kinetic read of fluorescence emission at both 330 nm and 350 nm was performed at each denaturant concentration. Samples were recovered from the cuvette after each measurement and the exact urea concentration was determined by taking the refractive index. The signal was averaged over each 10 second period and reported as a ratio of average signal 330/average signal 350.

Ratios were then normalized using equation 1 and each mono-ubiquitinated and unmodified variant were globally fit with linked baselines to a two state folding model (equation 2) using Igor Pro 7, which allowed determination of the C_m , $\Delta G_{\text{unfolding}}$, and m -value.

$$(1) \frac{y - y_D}{y_N - y_D}$$

$$(2) y = (m1 + m5 * x) * (1 / (1 + (\exp(-(m3 - m4 * x) / RT)))) + (m2 + m6 * x) * (\exp(-(m3 - m4 * x) / RT) / (1 + (\exp(-(m3 - m4 * x) / RT))))$$

Parameter definitions:

m1=folded intercept, m2 = unfolded intercept, m3 = $\Delta G_{\text{unfolding}}$, m4 = m -value, m5= folded baseline slope, m6=unfolded baseline slope

2.8.7 Native-state proteolysis to measure the energetics of partial unfolding

Ubiquitinated substrate sample prep was performed as described above except that AMSH deubiquitinase was allowed sufficient time to leave a mixed population of unmodified and mono-ubiquitinated species. Additionally, the final size exclusion step was omitted. Protein stocks were prepared in a 2 mL volumetric flask with final buffer of 25 mM HEPES pH 7.5, 150 mM KCl, and 15 mM MgOAc. Samples were allowed to equilibrate at room temperature in the dark overnight. Native-state proteolysis experimental protocol was adapted from previous work (Park and Marqusee, 2004). The equilibrated stock was divided into 200 μL aliquots and thermolysin protease (stock concentration 10 mg/mL) was added to a final concentration of 0.04 to 0.4 mg/mL. Time points (15 μL) were taken at (no protease control, 0:15, 0:30, 0:45, 1:00, 1:30, 2:00, 3:00, 5:00, 7:00, and 10:00) from the reactions and quenched in 2.5 μL of 0.5 M EDTA. 2.5 μL of 6X SDS-PAGE loading buffer was added to each sample and time points were run out on a 12% NuPAGE Bis-Tris™ gel (Invitrogen) in 1X MES running buffer (50 mM MES, 50 mM Tris Base, 0.1% SDS, 1 mM EDTA). Gels were imaged using a BioRad ChemiDoc™ and color inverted using the “Invert” command in ImageJ for ease of viewing and analysis. Band intensities of the unmodified and mono-ubiquitinated substrate bands were then quantified using ImageJ. SH3 and mono-ubiquitinated SH3 gels were quantified in ImageQuant (GE Healthcare) with a rolling ball background subtraction because proteolysis products could comigrate near full length protein. Band intensities were normalized to the no protease lane and fit to a first order exponential (equation 3) using IgorPro 7 to calculate the observed proteolysis kinetics (k_{obs}). For a given substrate, k_{obs} was determined at several thermolysin concentrations and plotted against protease concentrations. $\Delta\Delta G_{\text{proteolysis}}$ was calculated from the slope of the linear fit to thermolysin vs. k_{obs} . using equation 4 and equation 5. Individual $\Delta G_{\text{proteolysis}}$ could also be calculated using equation 6 and

the measured $k_{\text{cat}}/K_{\text{M}}$ of thermolysin for a generic protein of $99,000 \text{ M}^{-1}\text{s}^{-1}$ (Park and Marqusee, 2004).

$$(3) y = y_0 + A \cdot \exp(-(x-x_0)/T_{\text{obs}})$$

$$(4) k_{\text{obs}} = K_{\text{op}} (k_{\text{cat}}/K_{\text{M}}) [E] = 1/T_{\text{obs}}$$

slope of k_{obs} vs. $[E]$ linear fit = $K_{\text{op}} (k_{\text{cat}}/K_{\text{M}})$

$$(5) \Delta\Delta G_{\text{proteolysis}} = -RT \cdot \ln(K_{\text{op, mono-ubiquitinated}} (k_{\text{cat}}/K_{\text{M}}) / K_{\text{op, unmodified}} (k_{\text{cat}}/K_{\text{M}}))$$

$$(6) \Delta G_{\text{proteolysis}} = -RT \cdot \ln(K_{\text{op}} (k_{\text{cat}}/K_{\text{M}}) / 99,000 \text{ M}^{-1}\text{s}^{-1})$$

2.8.8 Purification of proteasome lid, base, and core

Lid subcomplex was recombinantly expressed and purified as described previously (Bard et al., 2019). *E. coli* BL21-star(DE3) (Invitrogen) cells were transformed with pAM80, pAM85, and pAM86 for lid. pAM80 encodes for Sem1 and rare tRNA codons, pAM85 encodes Rpn5, MBP-HRV3C-Rpn6, Rpn8, Rpn11, and Rpn9, and pAM86 encodes Rpn3, His₆-HRV3C-Rpn12, and Rpn7. Cells were grown in 2 L of terrific broth (Novagen) at 37°C until $1.0 < \text{OD}_{600} < 1.5$ after which expression was induced with 1 mM IPTG at 16°C for overnight. Bacteria were pelleted and resuspended in 60 mM HEPES pH 7.6, 50 mM NaCl, 50 mM KCl, 10 mM MgCl₂, 5% glycerol and supplemented with protease inhibitors (aprotinin, pepstatinA, leupeptin, and PMSF or AEBSF), benzonase (Novagen), and 2 mg/mL lysozyme and stored at -80°C. Resuspended cells were lysed by sonication and the lysate was clarified by centrifugation at 20,000 rcf, 4°C, 30 minutes. Lid was first purified by Ni²⁺-NTA affinity chromatography via His₆-HRV3C-Rpn12 using a 5mL HisTrap HP (GE) column, washed with 60 mM HEPES pH 7.6, 50 mM NaCl, 50 mM KCl, 10 mM MgCl₂, 5% glycerol, 20 mM imidazole and eluted with 60 mM HEPES pH 7.6, 50 mM NaCl, 50 mM KCl, 10 mM MgCl₂, 5% glycerol, 250 mM imidazole. Eluate was further purified via MBP-HRV3C-Rpn6 and amylose resin (NEB) and eluted with 60 mM HEPES pH 7.6, 50 mM NaCl, 50 mM KCl, 10 mM MgCl₂, 5% glycerol, 10 mM maltose. Amylose eluates were cleaved with HRV3C-protease overnight at 4°C before being loaded onto a Sup6i 10/300 size exclusion column (GE) pre-equilibrated with 60 mM HEPES pH 7.6, 50 mM NaCl, 50 mM KCl, 10 mM MgCl₂, 5% glycerol, 0.5 mM TCEP. Peak corresponding to fully assembled lid was collected, concentrated, and quantified by UV-Vis spectroscopy before being flash frozen and stored at -80°C for future use.

Base subcomplex was recombinantly expressed and purified as described previously (Beckwith et al., 2013). *E. coli* BL21-star(DE3) (Invitrogen) cells were transformed with pAM81, pAM83, and pAM82 for wild-type base or pAM81, pAM83, and pAM210 for SspB₂-Rpt2 base. pAM82 encodes for Rpt1, Rpt2, Rpt3, Rpt4, Rpt5, and Rpt6, pAM210 encodes Rpt1, SspB₂-Rpt2, Rpt3, Rpt4, Rpt5, and Rpt6, pAM81 encodes Rpn1, Rpn2, and Rpn13, and pAM83 encodes rare tRNA

codons and base chaperones (Nas6, Nas2, Rpn14, and Hsm3). Cells were grown in 3 L of terrific broth (Novagen) at 37°C until $0.6 < OD_{600} < 0.8$ after which expression was induced with 1 mM IPTG at 30°C for 5 hours followed by 16°C overnight expression. Bacteria were pelleted and resuspended in 60 mM HEPES pH 7.6, 50 mM NaCl, 50 mM KCl, 10 mM MgCl₂, 5% glycerol, 1 mM ATP and supplemented with protease inhibitors (aprotinin, pepstatinA, leupeptin, and PMSF or AEBSF), benzonase (Novagen), and 2 mg/mL lysozyme and stored at -80°C. Resuspended cells were lysed by sonication and the lysate was clarified by centrifugation at 20,000 rcf, 4°C, 30 minutes. Base was first purified by Ni²⁺-NTA affinity chromatography via His₆-Rpt6 using a 5mL HisTrap HP (GE) column, washed with 60 mM HEPES pH 7.6, 50 mM NaCl, 50 mM KCl, 10 mM MgCl₂, 5% glycerol, 1 mM ATP, 20 mM imidazole and eluted with 60 mM HEPES pH 7.6, 50 mM NaCl, 50 mM KCl, 10 mM MgCl₂, 5% glycerol, 1 mM ATP, 250 mM imidazole. Eluate was further purified via FLAG-Rpt1 and anti-FLAG M2 affinity resin (Sigma) and eluted with 60 mM HEPES pH 7.6, 50 mM NaCl, 50 mM KCl, 10 mM MgCl₂, 5% glycerol, 1 mM ATP, 0.15 mg/mL FLAG peptide (Genscript). FLAG eluates were loaded onto a Sup6i 10/300 size exclusion column (GE) pre-equilibrated with 60 mM HEPES pH 7.6, 50 mM NaCl, 50 mM KCl, 10 mM MgCl₂, 5% glycerol, 1 mM ATP, 0.5 mM TCEP. Peak corresponding to fully assembled base was collected, concentrated, and quantified by Bradford assay (BioRad) using BSA (Sigma) as a standard before being flash frozen and stored at -80°C for future use.

20S core particle from *S. cerevisiae* was purified as described previously (Beckwith et al.) from yeast strain yAM54 bearing 3X-FLAG-Pre1. yAM54 cells were grown in 3 L of YPD at 30°C until saturation (3 days). Cells were pelleted and resuspended in 60 mM HEPES pH 7.6, 500 mM NaCl, 10 mM MgCl₂, 5% glycerol, plunged into liquid nitrogen and subsequently stored at -80°C. Frozen resuspended cells were lysed using a 6875 Freezer Mill Dual Chamber Cryogenic grinder (SPEX Sample Prep). Lysate was diluted in 60 mM HEPES pH 7.6, 500 mM NaCl, 10 mM MgCl₂, 5% glycerol and clarified by centrifugation at 20,000 rcf, 4°C, 45 minutes. Base was first purified by anti-FLAG affinity chromatography using anti-FLAG M2 affinity resin (Sigma), exhaustively washed with 60 mM HEPES pH 7.6, 500 mM NaCl, 10 mM MgCl₂, 5% glycerol, and eluted with 60 mM HEPES pH 7.6, 500 mM NaCl, 10 mM MgCl₂, 5% glycerol, 0.15 mg/mL FLAG peptide (Genscript). Eluate was loaded onto a Sup6i 10/300 size exclusion column (GE) pre-equilibrated with 60 mM HEPES pH 7.6, 50 mM NaCl, 50 mM KCl, 10 mM MgCl₂, 5% glycerol, 0.5 mM TCEP. Peak corresponding to fully assembled core was collected, concentrated, and quantified by UV-Vis spectroscopy before being flash frozen and stored at -80°C for future use.

2.8.9 Preparation of polyubiquitinated barstar variants

Barstar ubiquitination was performed exactly as above except that AMSH removal of K63-linked polyubiquitin chains was omitted. Ortho-Ni²⁺ purified ubiquitinations

were subsequently separated by size-exclusion chromatography on an S200i 10/300 (GE Healthcare) and 0.5 mL fractions were assessed for degradable species by incubating with proteasome under single turnover conditions at 30°C for 30 minutes and analyzing products by SDS-PAGE (Figure 2.19).

2.8.10 Gel-based and fluorescence polarization-based *ssrA/sspB* ubiquitin-independent proteasomal degradations

2X stocks of substrate (300 nM final) were prepared in assay buffer (60 mM HEPES pH 7.6, 50 mM NaCl, 50 mM KCl, 10 mM MgCl₂, 0.5 mM TCEP, 5 mM ATP, 5% glycerol, 1 mg/ml BSA). 2X proteasome stocks were prepared by reconstituting recombinant lid (5 μM final), recombinant SspB₂-Rpt2 base (5 μM final), recombinant Rpn10 (5 μM final), and core particle (2.5 μM final) in assay buffer with an ATP-regeneration system (creatine kinase, creatine phosphate, and 5 mM ATP) and allowed to assemble for 3 minutes at room temperature. Reactions were performed in technical triplicate at 30°C in a thermocycler and initiated by mixing equivolume (12.5 μL) of 2X substrate with 2X proteasome. Time points (1.2 μL) were taken at (0:10, 0:20, 0:30, 0:45, 1:00, 1:30, 2:00, 3:00, 5:00, 10:00, 15:00, 20:00, 30:00 min) from the reactions and quenched in 5 μL of 2X SDS-PAGE loading buffer (125 mM TrisHCl pH 6.8, 20% glycerol, 4% SDS). Gel samples were separated by electrophoresis on 4-20% TGX gels (Bio-Rad) before fluorescence imaging on a typhoon variable mode scanner (GE) with 50 μm per pixel density. Images were quantified in ImageQuant (GE) by normalizing band intensity of each species per total lane intensity to account for loading variation. Quantified species were plotted as percent total signal (Figure 2.13 and Figure 2.14) and fit to a single exponential equation (Equation 3) in IgorPro7. For degradations performed with ATP γ S, proteasomes were assembled in ATP for 3 minutes at room temperature, then ATP γ S was added (5 mM final) for 3 minutes at room temperature prior to substrate addition. For degradations using only the core particle, core particle was added to 900 nM final with substrate and incubated at 30°C for the indicated time points. Time points of 0, 10:00, and 30:00 minutes were quenched in SDS-PAGE loading buffer for trials involving core particle only or ATP γ S inhibited proteasome and separated by SDS-PAGE on 4-20% and assess qualitatively.

For ubiquitin-independent degradations assessed by fluorescence polarization, reactions were initiated with equivolume (2.5 μL) addition of substrate to proteasome directly within a 384-well black bottom plate (Corning) and fluorescence polarization was monitored in a Synergy Neo2 multimode plate reader (BioTek). Decreased fluorescence polarization over time as substrate was processed into peptides could also be fit to a single exponential model (Equation 3) in IgorPro7.

2.8.11 Fluorescence polarization-based WT proteasomal degradations

Substrates were prepared to 2X concentration (6 nM final) in assay buffer. Proteasome was reconstituted to 2X concentration in assay buffer (2.5 μ M lid, base, and Rpn10 with 0.9 μ M core particle) and allowed to assemble for 3 minutes at room temperature prior to reaction initiation. Reactions were initiated with appropriate dilution of 2X substrate (2.5 μ L) into 2X proteasome (2.5 μ L) in a 384-well black bottom plate (Corning) and the decrease of fluorescence polarization over time was monitored on a Synergy Neo2 multimode plate reader (BioTek). Trials were repeated for $n = 3$. Where exponential decay was observed, curves could be fit to a single exponential model (Equation 3) in IgorPro7. For reactions performed with core particle only, core particle was made to 2X concentration (1.8 μ M) and added equivolume with 2X substrate (5 μ L final) and fluorescence polarization was monitored as above. Single turnover conditions were verified by single reactions with doubled proteasome concentration by reconstituting proteasome to 4X concentration and diluting with equivolume substrate (2.5 μ L each) to 2X proteasome and monitoring fluorescence polarization kinetics as described above. For degradations with *o*-phenanthroline inhibited proteasomes, proteasomes were allowed to assemble at 3X concentration for 3 minutes at room temperature between dilution with *o*-phenanthroline (30 mM stock in assay buffer; 5 mM final) to 2X concentration for 2 minutes before degradation initiation as described above. For degradations using only the core particle, core particle was added to 900 nM final with substrate as described above.

For degradations performed in the presence of barnase, substrates were prepared to 2X concentration (6 nM final) in assay buffer with barnase added in excess (20 μ M final) and allowed to come to equilibrium for greater than 5 minutes at room temperature (Pollard, 2010) prior to degradation initiation. Degradations were performed exactly as described above. Saturation of barnase binding was assessed by doubling barnase concentration (40 μ M final) and comparing fluorescence polarization kinetic differences. FAM-Titin-I27^{V13P,V15P} ubiquitinated as described above was degraded in the presence or absence of 20 μ M barnase with proteasome at the same concentration as described.

3. Site-specific mechanisms for ubiquitin modulation of the protein energy landscape

The work presented in this chapter was performed in collaboration with Naomi Latorraca (molecular dynamics simulations collaborator) and Johanna Lindner (hydrogen-deuterium exchange mass spectrometry collaborator), both postdoctoral researchers in the Marqusee lab. Brendan Maguire (Marqusee lab) helped with preparation of proteins, and Jeff Pelton (Berkeley QB3 NMR facility director) helped with NMR data collection and analysis. At the time of submitting this thesis, we are preparing this work for publication.

3.1 Introduction

As discussed in the previous chapters, ubiquitination proceeds via a complex and highly regulated enzymatic cascade that plays a key role in determining the specific, downstream effects of an individual ubiquitination event. The terminal enzymes in this cascade, the E3 ubiquitin ligases, are believed to principally determine substrate selection. Thus, the large number of E3s (more than 600 in the mammalian proteome) (Nguyen, 2016) is believed to simultaneously give rise to broad proteome coverage of possible ubiquitination sites while also allowing for site-specificity of individual ubiquitination events (Chaugule and Walden, 2016; Zheng and Shabek, 2017). Further, E3s do not have the final say, as a host of ~100 cellular deubiquitinating enzymes (DUBs) can remove a ubiquitin modification (Clague et al., 2019).

Here, we extend our previous studies described in Chapter 2 to interrogate mechanisms of site-specificity of ubiquitin-induced energetic changes for the single-lysine barstar variants. We employed two sets of complementary approaches—NMR and hydrogen-deuterium exchange mass spectrometry (HDX-MS), which reveal changes to the conformational landscape of substrate proteins as an equilibrium distribution, and molecular dynamics (MD) simulations, which track the position of every atom in a protein starting from its native conformation in a very short (microseconds) time window. We find that ubiquitination has only subtle effects on the native conformation of the substrate protein, with only the destabilizing sites increasing exposure of the substrate C terminus. The two destabilizing sites arise in local regions of high conformational flexibility, but the energetic changes at each site appear to be the result of distinct thermodynamic mechanisms. In contrast, simulations suggest that ubiquitination at the non-destabilizing site has a protective effect on the barstar C terminus. Thus, the effects of ubiquitination at each site are highly dependent on each site's local biophysical context. We hope this understanding of ubiquitin's site-specificity for energy landscape modulation will not only aid in developing a predictive understanding of the energetic consequences of individual ubiquitination events but also will help in understanding the ways in

which aberrant lysine targeting leads to disease (Ciechanover and Schwartz, 2004; Senft et al., 2018; Wang et al., 2020b).

3.2 Mono-ubiquitinated and unmodified barstar adopt a similar native-state conformation

3.2.1 $^1\text{H}/^{15}\text{N}$ HSQC barstar spectra reveal native-like chemical shifts with some subtle changes

Previously, we characterized the energetic effects of ubiquitin on three sites of the small protein barstar from *Bacillus amyloliquefaciens* using single lysine barstar variants in which all but one native lysine had been mutated to arginine (with the remaining lysine position denoted). As described in chapter 2, ubiquitination at positions K2 and K60 (Figure 3.1a) destabilizes the native structure of barstar, while ubiquitination at K78 has relatively little effect (Figure 3.1b) (Carroll et al., 2020); these energetic effects appear sufficient to allow for proteasomal engagement and degradation.

To further explore the molecular mechanism of these effects, we first turned to NMR spectroscopy to evaluate general changes to the native state upon ubiquitination. We expressed ^{15}N -isotopically labeled barstarK60 and barstarK78 and acquired HSQC NMR spectra of the unmodified and mono-ubiquitinated species (Figure 3.1). All barstar variants were ubiquitinated with methylated ubiquitin, which increased yield and has previously been shown to induce the same energetic effects on barstar as non-methylated ubiquitin ((Carroll et al., 2020), Figure 2.7).

All spectra show well-dispersed peaks characteristic of well-folded proteins (Figure 3.1). Using previously determined peak assignments for wild-type barstar (Lubienski et al., 1993, 1994) and an HNCA triple-resonance experiment acquired with $^{13}\text{C}/^{15}\text{N}$ double-labeled, unmodified barstarK60, we assigned 58/88 barstar amides to distinct peaks in the HSQC spectrum. Perturbations to the conformation, as measured by the number and extent of chemical shifts, appear to be relatively small despite the significant energetic effects experienced by each of these two variants. These subtle effects are consistent with previous observations that, despite their destabilization and dramatic effects on proteasomal degradation, mono-ubiquitinated barstarK2 and barstarK60 can still bind barstar's binding partner, barnase (Carroll et al., 2020). In fact, for barstarK60, the notable changes in the chemical shifts in the HSQC are largely limited to residues directly surrounding the site of the modification including E57, Q61, L62, and T63 as well as residues near the C-terminus including V76. By contrast, mono-ubiquitinated barstarK78 exhibits fewer significant peak shifts near the site of ubiquitin

modification, suggesting that for the non-destabilizing site, ubiquitin modification has a less disruptive effect on local structure.

Taken together, these data indicate that all three ubiquitinated barstar variants adopt the native barstar-like fold independent of their changes in energetics and proteasomal processing. Each exhibits well-dispersed peaks in the HSQC, which mostly overlap with those from the unmodified protein. Notably, the small subtle changes are more apparent in the two-destabilizing variants (K2 and K60) than the non-destabilizing variant (K78).

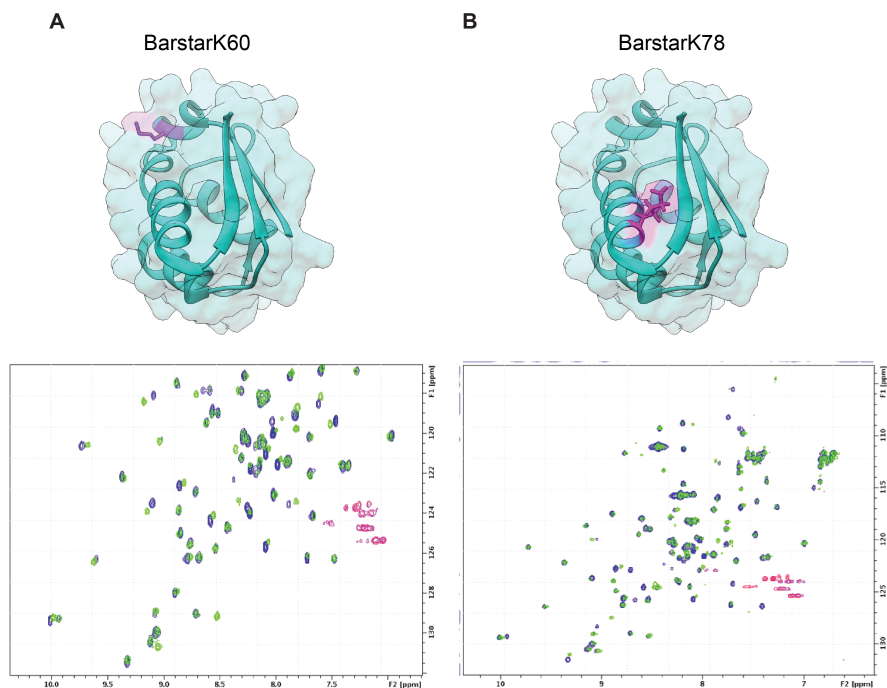


Figure 3.1 | BarstarK60 and BarstarK78 NMR HSQCs show subtle changes to the native conformational upon ubiquitination. (A) Ribbon diagram (PDB ID: 1BTA) depicting the position and surface topology of barstar lysine 60, a ubiquitin-destabilized site located in an α -helix. NMR $^1\text{H}/^{15}\text{N}$ HSQC spectra depict the chemical shifts of amides from each residue in unmodified (blue) and overlaid mono-ubiquitinated (green) barstarK60. **(B)** Ribbon diagram (PDB ID: 1BTA) depicting the position and surface topology of barstar lysine 78, a site located in an α -helix that does not experience substantial destabilization upon ubiquitination. NMR $^1\text{H}/^{15}\text{N}$ HSQC spectra depict the chemical shifts of amides from each residue in unmodified (blue) and overlaid mono-ubiquitinated (green) barstarK78.

3.3 Hydrogen-deuterium exchange/mass spectrometry studies: the effect of ubiquitination

The relatively subtle differences in chemical shifts upon ubiquitination at each site motivated us to map the observed changes in energetics at a structural level using hydrogen exchange. Towards this goal, we first turned to hydrogen-deuterium

exchange mass spectrometry (HDX-MS), monitoring the exchange of labile amide protons for deuterons as a function of time with and without ubiquitination. The extent of deuteration was monitored at the peptide level using MS (see Materials and Methods). We performed these experiments in triplicate for all three unmodified and mono-ubiquitinated single-lysine barstar species and analyzed both the barstar and ubiquitin peptides.

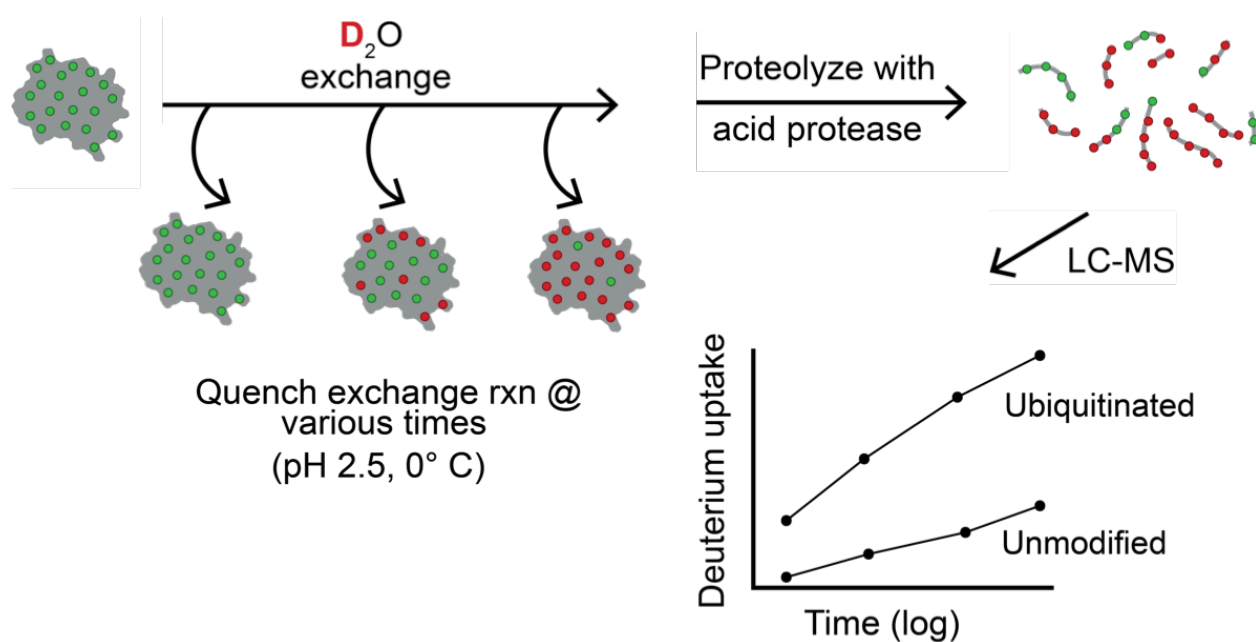


Figure 3.2 | Schematic depicting HDX-MS experimental workflow. Unmodified and mono-ubiquitinated barstarK2, K60, and K78 were diluted into deuterated buffer, and backbone amides exchange with deuterated solvent at rates that are slowed by the presence of stable hydrogen bonding structures. Diagram depicts what example data may look like for deuterium uptake as a function of time in the ubiquitinated and unmodified states.

3.3.1 Uptake plots for non-C-terminal peptides

For all three variants (K2, K60, K78), the majority of peptides analyzed exhibit similar deuterium uptake over time in their ubiquitinated compared to unmodified states (Figure 3.3). Only a small number of these internal peptides exhibit statistically significant differences in deuterium uptake for unmodified barstar compared to mono-ubiquitinated barstar (see peptides covering residue positions 10–16 and 39–52 for mono-ubiquitinated barstarK2).

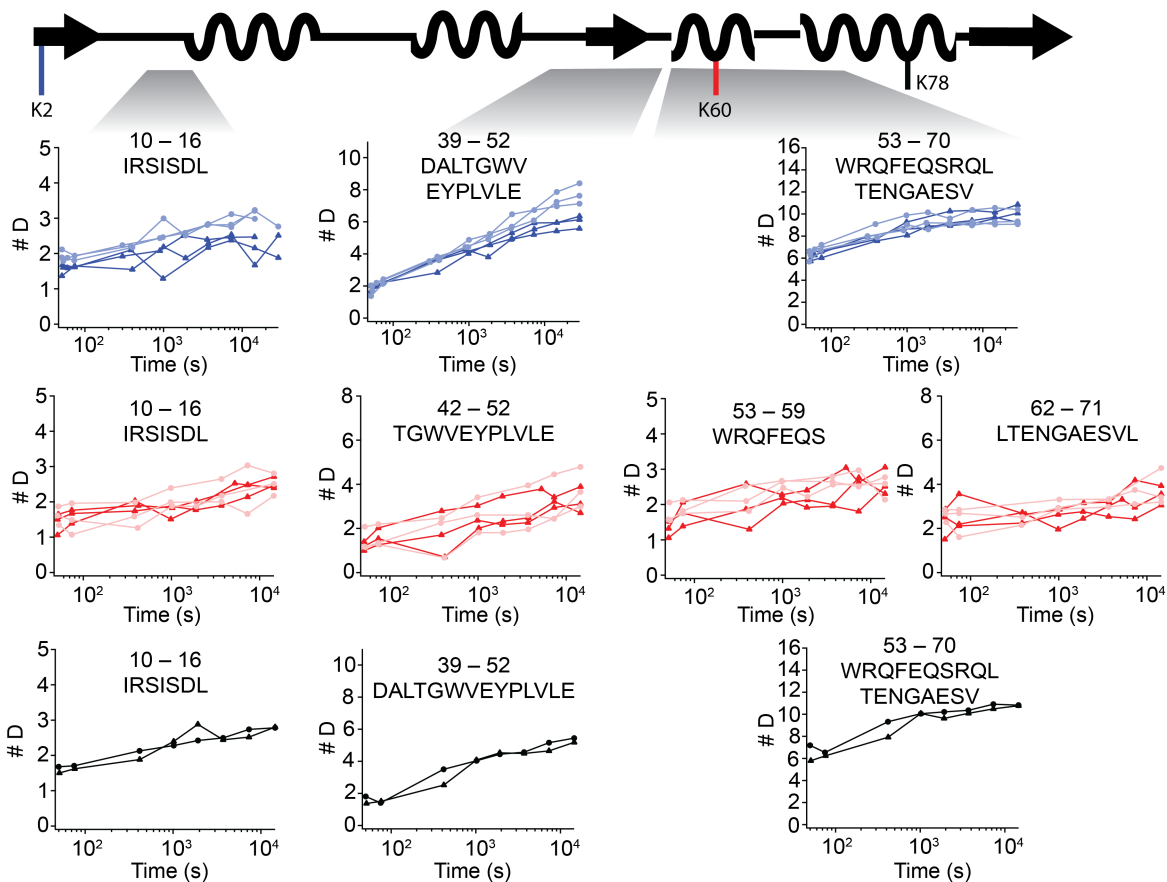


Figure 3.3 | HDX-MS supports hypothesis of subtle structural changes upon ubiquitination at destabilizing sites (cf. dark vs light lines for each peptide).

Deuterium uptake plots from representative peptides from non-terminal regions of unmodified barstarK2 (n = 3, dark blue triangles), barstarK60 (n = 3, dark red triangles), and barstarK78 (n = 1, black triangles) and mono-ubiquitinated barstarK2, (n = 3, light blue circles), barstarK60 (n = 3, light red circles), and bartarK78 (n = 1, black circles).

This HDX-MS approach allows us to also follow the hydrogen exchange behavior of the ubiquitin moiety. Therefore, to evaluate the effect of barstar on ubiquitin, we compared these exchange rates to those of ubiquitin in isolation (See Materials and Methods). Interestingly, these ubiquitin peptides show no discernible change in extent or time course of exchange over the experimental timeframe, indicating that any changes to ubiquitin are not detectable in this time window (data not shown). This is surprising because, due to thermodynamic coupling, destabilization must be reciprocal. Ubiquitin possesses unusually high thermodynamic stability (Jackson, 2006), and our four-hour experiment does not reveal exchange for the most stable sites in ubiquitin; it is conceivable that this high stability serves to protect ubiquitin from unfolding and thus losing signaling recognition and integrity upon conjugation to its myriad of targets *in vivo*.

3.3.2 Uptake plots for C-terminal peptides

Interestingly, barstar ubiquitinated at K2 and K60 (the two destabilizing sites) both exhibit clear changes in exchange behavior for peptides corresponding to the C terminus of the protein. The increased exchange rates and extents of deuteration for five different C-terminal peptides in barstarK2 and barstarK60 (Figure 3.4) indicate increased amide solvent accessibility of the barstarK2 and K60 C termini upon ubiquitination. We could not analyze these C-terminal peptides for barstarK78 (the non-destabilizing site) because the proteolysis scar remaining from the ubiquitin modification at K78 prevented accurate peptide mass analysis/identification. Conversely, barstarK60 N-terminal peptides show nearly identical exchange profiles between unmodified and mono-ubiquitinated samples (Figure 3.4). Again, due to the ubiquitin scar, we could not analyze N-terminal peptides for barstarK2.

These changes at the C termini may be responsible for the observed proteasomal processing of these destabilizing variants. The proteasome frequently engages substrates at either of their termini, and high-energy, partially unfolded states of barstar are stably engaged for proteasome degradation. Our previous biochemical evidence has implicated the C terminus as the probable site of degradation initiation for barstarK2 (Carroll et al., 2020).

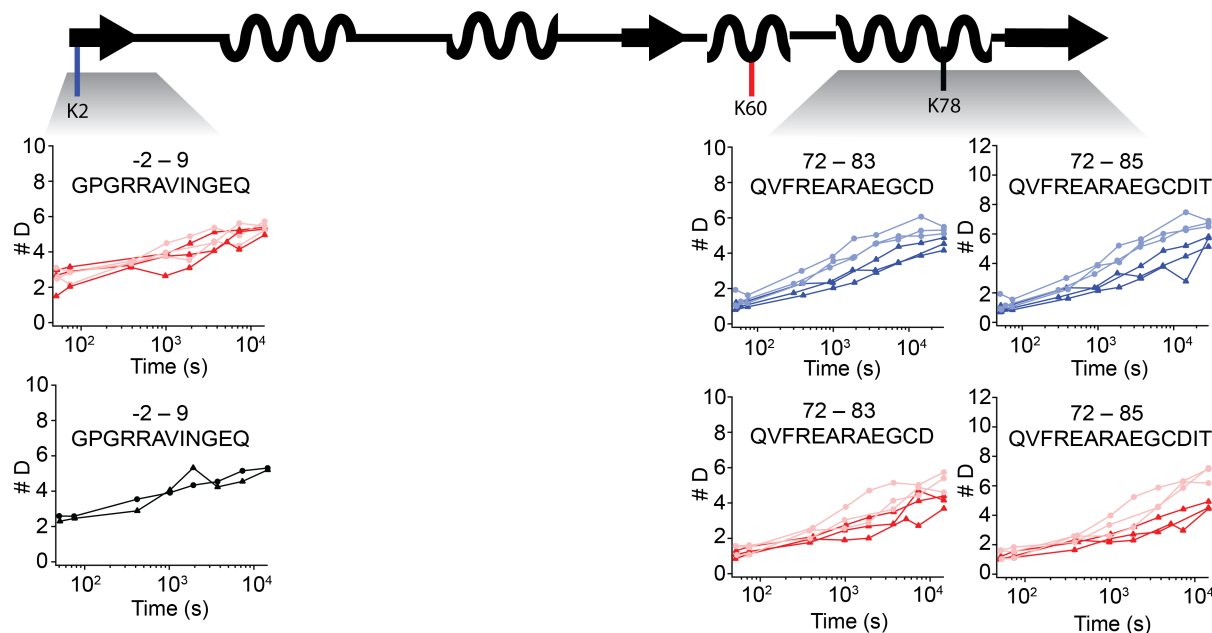


Figure 3.4 | HDX-MS provides evidence for selective increased unfolding of the C terminus in the destabilized/proteasomally processed variants. Deuterium uptake plots from representative peptides from the N-terminal and C-terminal regions for unmodified barstarK2 (n = 3, dark blue triangles), barstarK60 (n = 3, dark red triangles), and barstarK78 (n = 1, black triangles) and mono-ubiquitinated barstarK2, (n = 3, light blue circles), barstarK60 (n = 3, light red circles), and bartarK78 (n = 1, black circles).

Importantly, and perhaps surprisingly, we do not see any notable sites of increased protection due to ubiquitination in any of the above HDX-MS experiments. Thus, there do not appear to be any obvious stabilizing interactions between barstar and ubiquitin. We therefore do not think of the system as a stable protein-protein complex at equilibrium.

3.3.3 NMR-HDX protection factors for unmodified barstarK60

We carried out similar HDX studies, this time monitored by NMR (HDX-NMR) for barstarK60 in order to obtain high-resolution information about the energy landscape of barstar in the absence of ubiquitination (technical challenges prohibited similar experiments in the ubiquitinated form). While these studies do not have the same time resolution as the above mass spectrometry studies, they allow us to assign exchange rates to specific amide protons in the sequence of barstar. Taking advantage of our amide backbone assignments from the HSQC experiments above, we performed HDX-NMR experiments on unmodified and mono-ubiquitinated barstarK60. By following the decrease in the amide proton intensity (peak volume) in the NMR HSQC, we can calculate the observed exchange rate for a given amide (k_{obs}). From these rates, we can determine a protection factor, PF, using the known sequence-dependent exchange rates derived from unstructured peptides, k_{rc} , (Bai et al., 1993; Connelly et al., 1993, Zhang 1995) (SPHERE, <https://protocol.fccc.edu/research/labs/roder/sphere/sphere.html>), where $PF = k_{rc}/k_{obs}$. $\log(PF) = 1$ corresponds to a proton that exchanges at a rate that expected for a unfolded amide, and $\log(PF) > 1$ corresponds to a protected amide. The dead time of these NMR experiments sets a limit of measurable protection factor to $PF > 3$.

Given the limits described above, we successfully determined rates of exchange and PFs for 40 of the 88 amide sites in unmodified barstar (Figure 3.5). In general, regions of secondary structure contain well-protected residues, as expected. The exception is the K60-containing 'helix', which exhibited a notable lack of well-protected amides compared to the other helices in barstar, with resolved amides exhibiting $\log(PF) < 3$. These residue-specific protection factors, which are supported by the simulations described below, suggest that intrinsic dynamics, or flexibility, in different regions of a protein may be important features that govern the energetic effects of ubiquitination events at individual sites within a protein (Figure 3.5).

These NMR and mass-spec experiments raise important mechanistic questions: if ubiquitin-induced destabilization primarily affects the flexibility and/or exposure of the substrate C terminus, how do modifications at sites far from the C terminus induce these effects? Conversely, how can a modification occurring in close proximity to the C terminus, such as the non-destabilizing K78 modification, not

destabilize the protein? To address these questions, we next turned to extensive all-atom molecular dynamics simulations of barstar and each mono-ubiquitinated barstar variant.

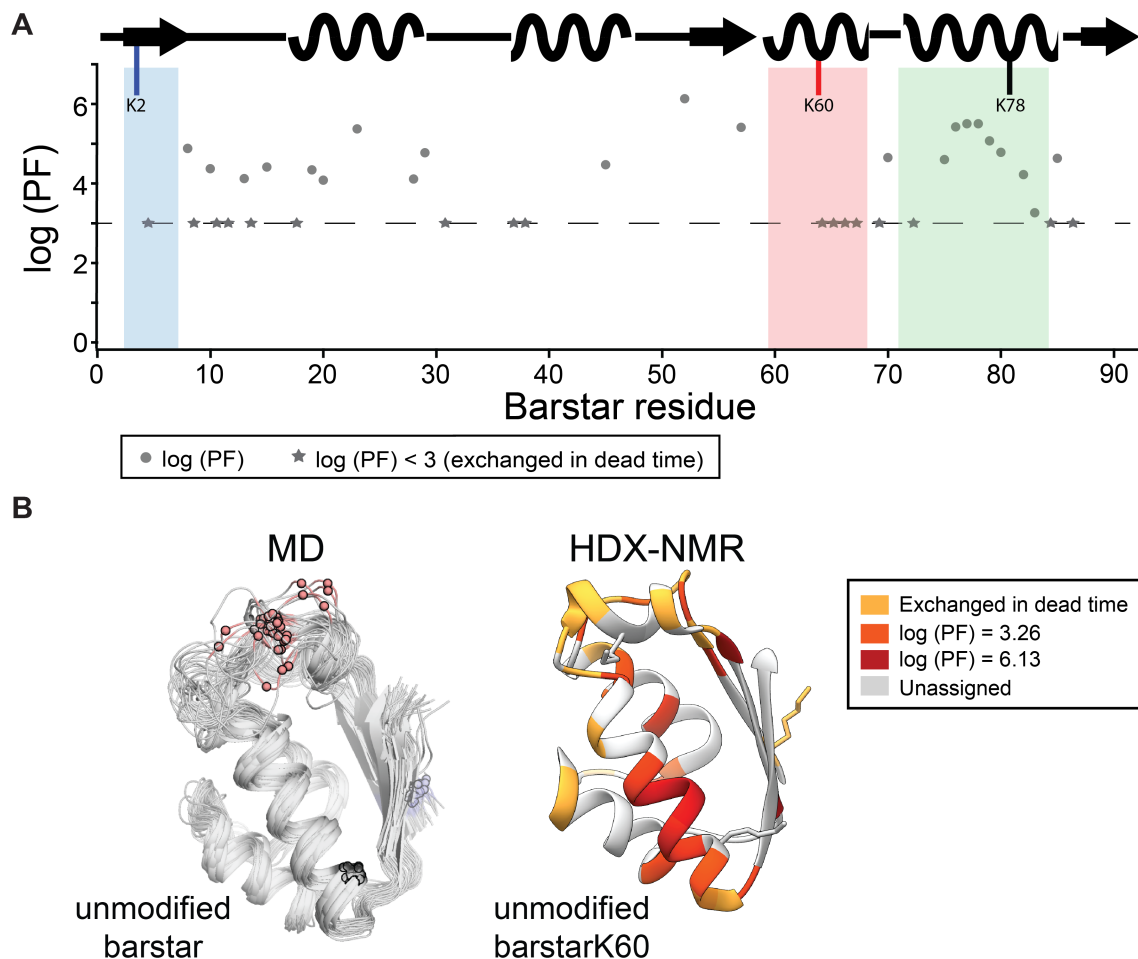


Figure 3.5 | Ubiquitination sites that energetically destabilize barstar exist within regions of high intrinsic conformational flexibility. (A) NMR-HDX unmodified barstarK60 calculated protection factors (grey circles) plotted by barstar residue number. Amide residues that exchange faster than the 20 minute dead time of the experiment are depicted with grey stars along the dotted line showing the lowest protection factor we can detect. The Lys2 β -strand is shaded in blue, the Lys60 α -helix is shaded in red, and the Lys78 α -helix is shaded in grey. **(B)** Sites of backbone flexibility in barstar, as measured through HDX NMR and MD. Left: protection factors from NMR map mapped onto the NMR structure of barstar (PDB ID: 1BTA). Right: overlapping simulation snapshots sampled every 100 ns after removing the first 1.0 μ s (for equilibration) from a representative simulation of barstar. Spheres represent the Ca atom of each ubiquitination site.

3.4 Destabilizing sites occur in regions of high backbone conformational flexibility but destabilize barstar through distinct mechanisms

3.4.1 MD simulation native contacts and C α RMSF plots

Next, we turned to computational approaches to try to uncover any mechanistic principles of the site-specific effects of ubiquitination. We first examined the unmodified native state to look for any differences in the structure and dynamics of barstar at these three sites. Just looking at the structural details of the native conformation at the three sites of modification, we find no obvious trends that could account for the observed differences in the response to ubiquitination. Previous computational studies have suggested that the number of native contacts at the site of modification may determine whether or not ubiquitin is destabilizing (Gavrilov et al., 2015; Hagai and Levy, 2010). Analysis of the static barstar structure (PDB: 1BTA), however, reveals that the number of native contacts—defined as the number of residues within 4 Å of the side chain, at Lys2, Lys60, and Lys78—does not correlate with the destabilizing effect of ubiquitination at each site (Figure 3.6). Interestingly, a different picture emerges when we examine the average number of native contacts analysis over the course of six independent multi- μ s simulations of wild-type unmodified barstar. Here, we see a clear difference in which the two destabilizing sites, K2 and K60, contact far fewer residues per site than non-destabilizing K78 (Figure 3.6), suggesting that the ability to maintain a high density of contacts with adjacent residues could confer resistance to ubiquitin-mediated destabilization.

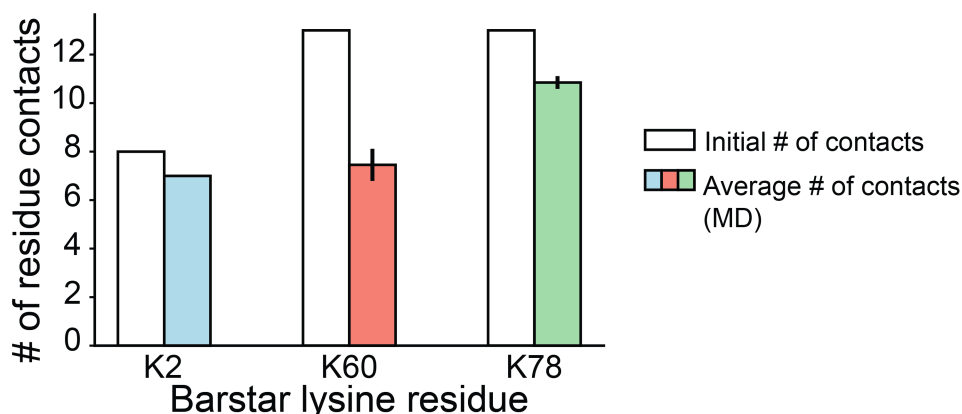


Figure 3.6 | Destabilizing sites form fewer contacts with nearby residues compared to the non-destabilizing site. In an NMR model of barstar (PDB ID: 1BTA), one destabilizing site, Lys2, exhibits far fewer residue contacts compared to the other destabilizing site, Lys60, and the non-destabilizing site, Lys78. By contrast, in all-atom simulations, both destabilizing sites exhibit fewer residue contacts compared to the non-destabilizing site. Residue contacts correspond to the number of residues within 4 Å of non-hydrogen atoms of the native side chain at each site. Error bars represent the standard

error of the mean, computed over six independent, 5.0- μ s simulations of barstar ($P = 2.8 \times 10^{-5}$ for Lys2 vs. Lys78; $P = 3.9 \times 10^{-3}$ for Lys60 vs. Lys78).

We also analyzed the unmodified barstar backbone flexibility by calculating the root-mean-square fluctuation (RMSF) of every C_{α} over the course of the simulation for unmodified barstar and monoubiquitinated barstarK2, K60, and K78 (Figure 3.7). Interestingly, in simulation, the β -strand containing K2 and the α -helix containing K60 have high intrinsic flexibility in unmodified barstar (consistent with the hydrogen exchange results above). Upon mono-ubiquitination, this trend holds, although the K60 helix appears to lose conformational flexibility due to the modification.

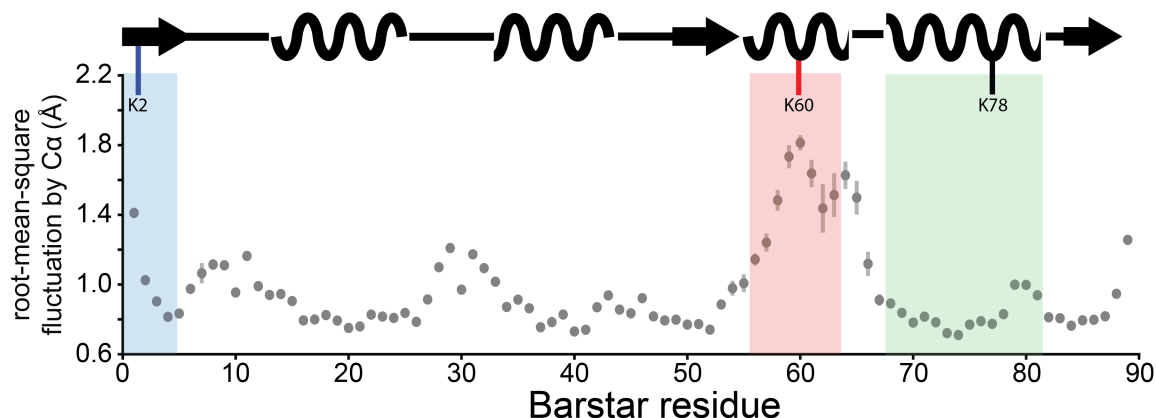


Figure 3.7 | Ubiquitination sites that energetically destabilize barstar occur within regions of predicted high backbone conformational flexibility.

Destabilizing sites occur within flexible regions of barstar, as measured by the root-mean-square fluctuation (\AA) of each C_{α} atom about its average position for each residue in the sequence of barstar, across six independent, 5.0- μ s simulations of barstar alone. Red, blue and gray rectangles indicate the structural motifs containing each ubiquitin modification site.

3.4.2 Disruption of β -strand hydrogen bonds in monoUb-barstarK2, decrease in configurational space in monoUb-barstarK60

To determine the effects of ubiquitination we then ran simulations of ubiquitinated barstar for each of the individual lysine sites and compared the ensembles of each monoubiquitinated protein to the other two monoubiquitinated proteins and barstar alone (see Materials and Methods). Looking first at simulations of mono-ubiquitinated barstar K2 (a destabilizing site), we find fewer hydrogen bonds persist between two beta strands of barstar, residues 1–3 and residues 51–53 over the course of each simulation compared to the simulations of other mono-ubiquitinated variants or to barstar alone (Figure 3.8a). In particular, a greater fraction of those simulation frames exhibited only a single backbone–backbone hydrogen bond between these two strands in the monoUb-barstarK2 simulations compared to the fraction observed the other simulations. These data suggest that a

reduction in hydrogen bonding might disrupt the overall stability of the main beta sheet of barstar, thereby reducing the system's overall enthalpy in the native state. This result is supported by our HDX-MS results, which also demonstrate that in barstar K2, the peptide 39–52 exhibits a ~33% increase in deuteration for mono-ub barstarK2 compared to unmodified. Both results suggest that the modification at barstarK2 might induce sub-global fluctuations in this region.

By contrast, when we analyzed our simulations to examine the effects of ubiquitination at Lys60, we found that in mono-ubiquitinated barstarK60, this region consistently exhibits fewer fluctuations relative to barstar alone (Figure 3.8b). Moreover, in these simulations, the helix to which Lys60 belongs remains helical, whereas in simulations lacking a ubiquitin modification at this site, the helix rapidly deforms within tens of nanoseconds to adopt other loop-like structures. These data are again consistent with the observations from NMR that amides in the Lys60 helix exchanges rapidly, on timescales faster than those resolved by our NMR-HDX (Figure 3.7). Thus, whereas at Lys2 ubiquitination favored conformational changes away from the native structure, at Lys60, ubiquitination reduced the overall number of configurations adopted by its constituent helix. A reduction in configurational space would lead to a reduction in the overall system entropy, consistent with global destabilization of the substrate at this site.

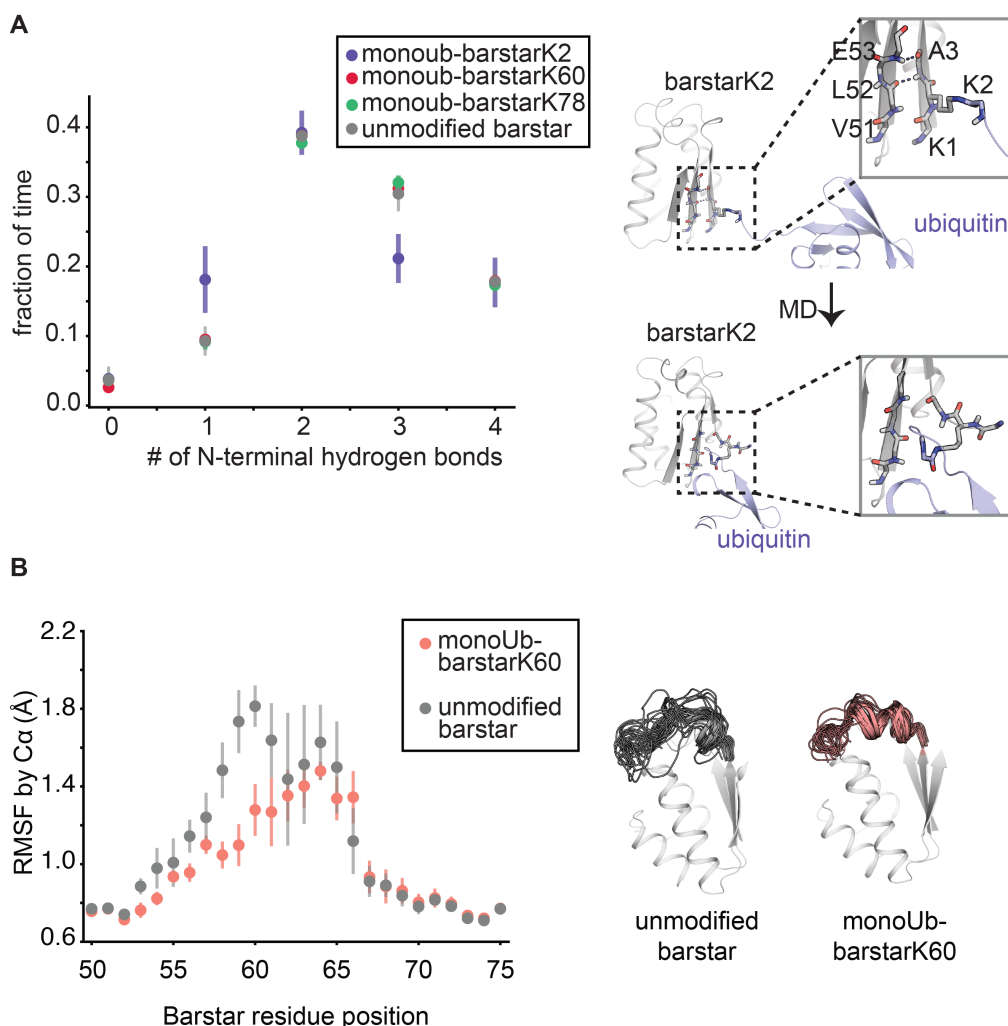


Figure 3.8 | Ubiquitin-mediated destabilization arises through distinct mechanisms at different modification sites, which depend upon the local biophysical context of each site. (A) Ubiquitination at K2 disrupts the N-terminal β -strand of barstar, thereby reducing hydrogen bonding with the neighboring β -strand (residues 50–53). For each simulation, we calculated the fraction of time a given number of hydrogen bonds (between 1 and 4) forms between residues 1–4 and 50–53. Ubiquitination of K2 *increases* the fraction of the time a simulation spends with a single hydrogen bond and *decreases* the fraction of the time a simulation spends with three hydrogen bonds. Ubiquitination at K2 therefore directly disrupts the three-strand β -sheet of barstar. **(B)** Ubiquitination at K60 reduces local conformational heterogeneity in the vicinity of the modification. Modification of K60 substantially reduces backbone fluctuations about the average structure, as measured by computing the root-mean-square fluctuation (RMSF) of each Ca atom. Plots display mean and s.e.m. for six independent simulations of each condition. On right, simulation snapshots representing residues 55–65 of barstar sampled every 100 ns from a representative simulation are overlaid on the simulation starting structure.

These data suggest that while ubiquitin modification sites with destabilizing effects both arose in regions of local conformational flexibility, those modifications likely induce destabilization through different thermodynamic mechanisms, enthalpic in the case of K2 and entropic in the case of K60. Importantly, the properties of the local conformational ensemble, rather than of a single structure alone, appear to determine whether ubiquitin has a destabilizing effect on each particular site.

3.5 Direct, stabilizing ubiquitin-barstar interactions at the non-destabilizing site

3.5.1 Stabilizing hydrogen bonds between flexible ubiquitin C-terminus and barstarK78

We then carried out similar mechanistic analyses of the effects of ubiquitin modification at Lys78, the non-destabilizing site. Intriguingly, in simulations of mono-ubiquitinated barstarK78, we observe the formation of distinct hydrogen bonding networks between ubiquitin's flexible C terminus and the C-terminal barstar β -strand (Figure 3.9a). We can track the dwell time for these interactions over the course of six independent simulations and find that, although the formation of these hydrogen bonds occurs on a timescale of hundreds of ns, the phenomenon consistently appears throughout the course of multiple independent simulations (Figure 3.9a). This interaction is likely stabilizing, perhaps explaining the site specificity of mono-ubiquitinated barstarK78's unique energetic properties. Additionally, by protecting the C terminus, ubiquitination at K78 also could protect mono-ubiquitinated barstarK78 from undergoing proteasomal degradation by preventing C-terminal engagement. Interestingly, this structural motif wherein ubiquitin's C-terminal tail forms hydrogen-bonding interactions with binding-partner β -strands has been frequently observed in ubiquitin-protein recognition by multiple classes of deubiquitinases, and co-crystal structures have been solved in this conformation (Fuchs et al., 2018; Sato et al., 2008; Shrestha et al., 2014; Worden et al., 2017; Ye et al., 2011; Yin et al., 2015) (Figure 3.9b).

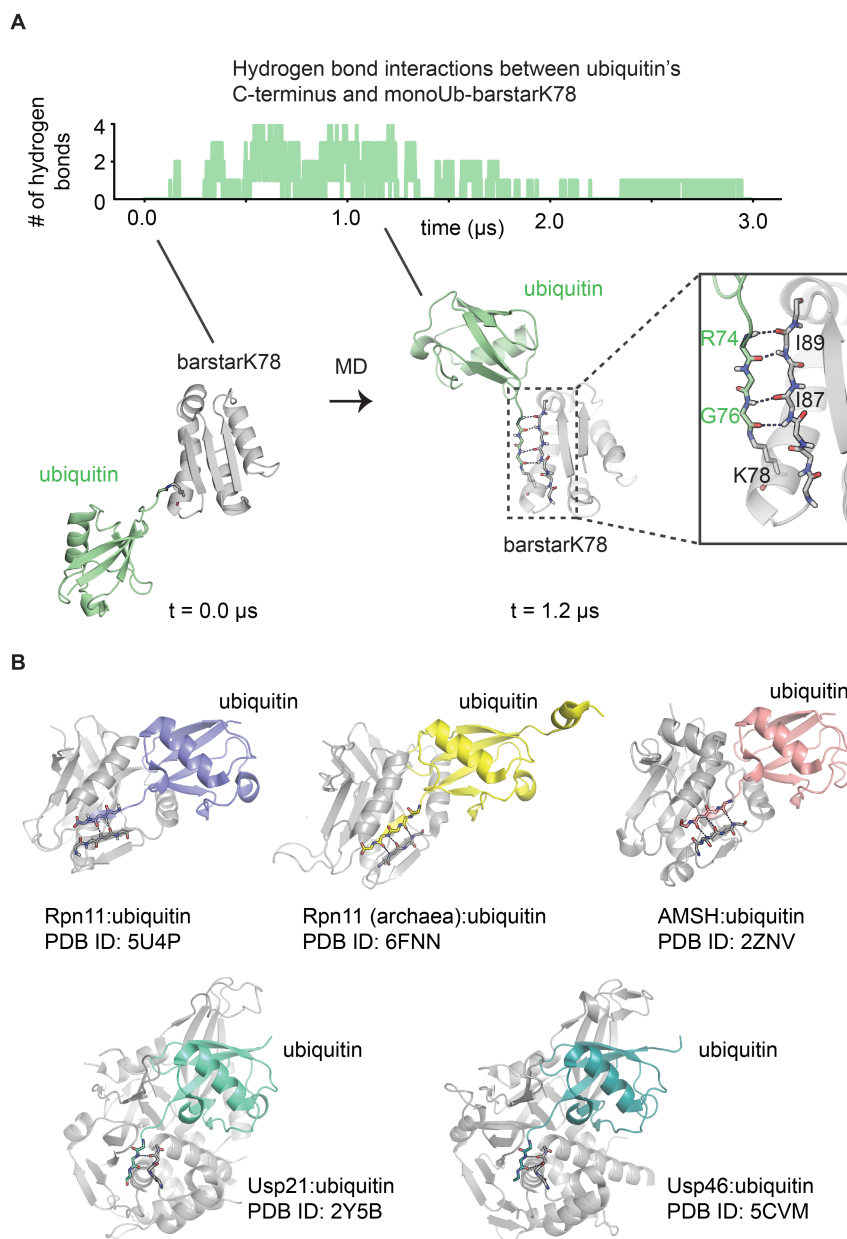


Figure 3.9 | Predicted stabilizing H-bonding networks between ubiquitin and barstarK78. (A) Ubiquitination at K78 protects the C-terminal β -strand of barstar, potentially stabilizing the substrate and protecting it from proteasomal targeting. Over the course of a simulation of barstar monoubiquitinated at K78, the ubiquitin C-terminus forms transient hydrogen bonds with the C-terminus of barstar, effectively adding a fourth β -strand to the existing β -sheet. These hydrogen bonds occur consistently across all six independent simulations of K78-ubiquitinated barstar. (B) The ubiquitin C-terminal tail constitutes a protein recognition and binding site. Crystal structures of other ubiquitin–protein complexes also contain the same interaction motif observed in simulations of K78-ubiquitinated barstar. These include several ubiquitin:deubiquitinase interactions.

Finally, our simulations support our conclusion from the HDX-MS experiments that ubiquitin and barstar do not form a stable protein complex. In our simulations, we do observe intermittent interactions between ubiquitin and substrate. Global analysis of these interactions via ubiquitin–barstar contact maps reveal interresidue interactions are rare. Thus, our data suggest that local perturbations to the substrate in the vicinity of the modification—more than surface–surface interactions between ubiquitin and substrate—lead to the conformational changes associated with global destabilization.

3.6 Conclusions

By using a combination of NMR, HDX-MS and MD simulation we have interrogated the barstar structural ensemble and the effects of ubiquitination on that ensemble. Our results reveal the mechanisms by which a model protein can undergo ubiquitin-mediated changes in a site-specific manner that may underlie regulation of proteasomal degradation. Specifically, we find that modifications promoting degradation favor conformations of barstar that expose its C terminus, while a non-destabilizing ubiquitination site in fact protects the C terminus by creating a novel stabilizing interaction. The atomic-level mechanisms by which each of these effects arise, however, appear specific to the local properties of each modification site, and the effects of such modifications can either be dominated by enthalpic contributions (e.g. by perturbing a substrate hydrogen bonding network) or entropic contributions (e.g. by reducing the configurational entropy of a region of the substrate). Moreover, our data indicate that ubiquitin can destabilize barstar without the formation of specific interactions characteristic of protein–protein complexes. These findings have numerous important implications.

First, we propose that, by favoring only subtle changes in the native ensemble of the substrate protein, ubiquitin modifications avoid the energetically costly process of fully unfolding a protein destined for degradation prior to its engagement with the 26S proteasome. Indeed, the work presented in Chapter 2 demonstrate that ubiquitin-induced modulation of the landscape for barstarK2 and barstarK60 have a sufficiently strong effect to allow population of the partially unfolded, high-energy conformation(s) through which the proteasome can engage the substrate protein. The proteasome typically engages small substrates like barstar at either terminus, and therefore we were particularly interested in understanding potential local destabilization of barstar at its termini upon ubiquitination. HDX-MS mapping of mono-ubiquitinated barstarK2 and barstarK60 conformational dynamics reveals that the C terminus, but not the N terminus, is destabilized for these species, suggesting that this may be the site of proteasome engagement. This is consistent with the biochemical evidence that has implicated the C terminus as the probable site of degradation initiation for barstarK2 (Carroll et al., 2020).

These subtle effects also could reduce the likelihood for ubiquitin-induced unfolding to template protein aggregation in cells, which would require further action by protein quality control machinery and could lead to disease (Balchin et al., 2016; Jahn and Radford, 2008; Kim et al., 2013; Tyedmers et al., 2010). Indeed, previous studies have shown that the proteasome struggles to degrade aggregated proteins (Cliffe et al., 2019; Guo et al., 2018; Ye et al., 2020). Interestingly, recent studies have also shown that binding of a flexible, proteasome-engageable peptide can promote proteasomal degradation of aggregation-prone tau (Chu et al., 2016) and alpha synuclein (Qu et al., 2020) and decrease aggregation-related cytotoxicity. Thus, a better understanding of how ubiquitin modification and other cellular processes affect population of proteasome-engageable states will facilitate therapeutic advances in this area.

Surprisingly we do not observe obvious changes to the landscape of ubiquitin due to attachment of barstar despite expected thermodynamic coupling, with peptides from ubiquitin exhibiting few changes in HDX exchange patterns in our study (which, in our experimental conditions, only probe fluctuations within ~5 kcal/mol of the native state). This is particularly notable because ubiquitin has an unusually high thermodynamic stability (Jackson, 2006) and unusually high sequence conservation across multiple domains of life (Zuin et al., 2014). It is conceivable that this high stability evolved in order to protect ubiquitin from unfolding and thus losing signaling recognition and integrity upon conjugation to its myriad of targets *in vivo*.

Second, our findings imply that, for proteins lacking obviously unstructured regions, multiple molecular mechanisms could allow population of the partially unfolded, proteasome-engageable state on the landscape. Specifically, one destabilizing site, barstarK2, undergoes an enthalpically driven disruption of hydrogen bonding networks at the site of ubiquitination, while the other destabilizing site, barstarK60, undergoes an entropically driven loss of conformational flexibility. Both destabilizing mechanisms serve to alter the energy landscape such that partially unfolded, proteasome-engageable states are populated. Conversely, in our simulations, ubiquitination at K78 protects the substrate C terminus by directly forming hydrogen-bonding contacts with its last three residues. This protection appears to have a dual purpose, both preventing exposure of the C terminus while stabilizing the main beta-pleated sheet on the substrate. We also emphasize the role of ubiquitin's flexible C terminus and the native isopeptide bond in facilitating this beta-stranded interaction, which could be absent in studies of ubiquitin-modified proteins with non-native linkages.

Third, our findings do have certain predictive implications for identifying other ubiquitination sites that also promote destabilization. For example, simulations reveal that both destabilizing sites in barstar occur in areas of low contact density, while the stabilizing site has high contact density. Intriguingly, a previous

simulation study (Hagai and Levy, 2010) found that regions of *high* contact density correlate with destabilizing sites, suggesting that in some cases, ubiquitin modification could directly destabilize the substrate protein by disrupting native contacts. Importantly, we note that an analysis of the static protein structure did not reveal these differences and instead required analysis of the native contacts' dynamics via simulation.

Fourth, that ubiquitin modifications can exert site-specific effects without forming persistent interactions typically characteristic of protein–protein complexes provides a possible explanation for how ubiquitin can have effects on a wide variety of substrate proteins. Ubiquitin is unique as a PTM in its large size (Jackson 2006), and further, ubiquitin's flexible C-terminus allows for a high degree of rotational freedom at the site of attachment, potentially sufficient to allow direct ubiquitin–substrate interactions. One interesting possibility is that the 'bulkiness' of ubiquitin facilitates ubiquitin–substrate interactions, which contribute to the observed site-specific barstar energetic effects. In certain crystal structures, ubiquitin has been observed to form surface–surface interactions with other proteins (Freudenthal et al., 2010). In a subset of cases, the ability to form such interactions might increase the specificity of a particular interaction or allow an E3 ligase to discriminate among nearby lysine residues (Chaugule and Walden, 2016). Nevertheless, evidence from each of the three techniques employed in our study points to an absence of such stable or specific interactions, indicating that ubiquitin can alter substrate energy landscapes by exerting its effects locally, in the vicinity of the modification. These findings might facilitate an 'entropic pulling' effect, whereby transient interactions between the stably-folded ubiquitin modification and substrate protein occur, creating a free energy gradient that generates a destabilizing net pulling force (Rios and Goloubinoff, 2016; Sousa and Lafer, 2019).

Our findings suggest opportunities for aiding in the design of therapeutics that precisely govern ubiquitination. For example, our findings on three sites of ubiquitination in a single protein suggest properties of ubiquitination sites that favor destabilization compared to those that do not. The mechanisms revealed here might help to explain how aberrant ubiquitination occurring at particular sites in the proteome can have severe biological consequences and cause disease (Ciechanover and Schwartz, 2004; Senft et al., 2018). Similarly, the importance of the context of individual ubiquitination sites is consequential for the development of PROTACs, bimodal ligands that contain both a substrate-binding and E3 ligase recruitment moiety to promote degradation of a desired target (Sun et al., 2019). PROTAC efficacy may depend on which lysines are ubiquitinated upon E3 ligase recruitment, and thus a mechanistic understanding of the effect of ubiquitination at these sites will aid in maximizing their therapeutic efficacy.

In this study, we have only examined a handful of modification sites, albeit in great detail, for a single protein. The biophysical approaches we used complement each

other, but each has certain limitations. For example, in simulation, we cannot expect to fully sample the landscape captured by the HDX-MS and NMR data; similarly, the latter two approaches do not reveal smaller fluctuations arising on shorter timescales. Thus, further work is required to fully test the predictions of our study and to expand it to other proteins, particularly those with physiological degradative and non-degradative ubiquitination sites.

Fully understanding how to predict whether a given modification site will have a particular effect on any given substrate will require advances on multiple fronts. While recent advances towards expanding our list of proteins with known ubiquitination sites (Catic et al., 2004; Gendron et al., 2016; Kim et al., 2011b), we are unaware of the consequences of ubiquitinating those sites. Establishing this correlation may facilitate creation of more physiological model substrates to study function. One could develop a predictive understanding of the mechanisms of ubiquitin-mediated destabilization by characterizing ubiquitination site-specificity on a broader range of substrates. Second, we have yet to engineer proteins with particular lysine residues/ubiquitination sites that undergo ubiquitination and degradation in a predictable manner. Such proof-of-principle studies will demonstrate the extent to which mechanisms described generalize across the proteome. Particularly, we hope our work represents a step towards fully understanding how small, well-folded proteins undergo successful, regulated degradation (Shabek et al., 2012) or other ubiquitin-mediated regulatory functions (Ball et al., 2016). Third, we have only examined the mechanistic effects of monoubiquitination, and characterization of the effects of ubiquitin chains with diverse lengths, linkages, and topologies is needed to fully understand the energetic effects conferred by ubiquitination *in vivo*.

Taken together, our work supports the idea that site-specific ubiquitination events induce distinct and consequential mechanisms for modulating a protein energy landscape. This site-specificity allows a single post-translational modification to have a broad range of effects in cells, a phenomenon also associated with phosphorylation and glycosylation (Hagai et al., 2011; Shental-Bechor and Levy, 2008, 2009). Site specificity of ubiquitin attachment is a built-in feature of the enzymatic conjugation and deubiquitination machinery *in vivo*, and the distinct mechanisms of ubiquitin-induced energetic effects represents a new layer of protein quality control and signaling in cells.

3.7 Materials and Methods

3.7.1 $^{13}\text{C}/^{15}\text{N}$ -labeled protein purification for NMR

E. coli BL21 Rosetta 2 (DE3) cells were transformed with either pEC076 (barstarK2), pEC062 (barstarK60), or pEC059 (barstarK78). Cells were then grown in M9 minimal media prepared with ^{15}N -labeled ammonium chloride as the sole nitrogen source. To prepare doubly-labeled samples, ^{13}C glucose was also included as the main carbon source. Cells were grown to $0.4 < \text{OD}_{600} < 0.8$ and induced with 1 mM IPTG overnight at 18°C. Bacteria were then pelleted and resuspended in 50 mM HEPES pH 7.0, 150 mM NaCl, 0.5 mM TCEP supplemented with 1X Halt™ protease inhibitor cocktail (Thermo) and benzonase (Novagen). Resuspended cells were lysed by sonication and the lysate was clarified by centrifugation at 20,000 rcf, 4°C, 30 minutes. The substrate was first purified by Ni^{2+} -NTA affinity chromatography using its N-terminal His₆ tag. Clarified lysate was allowed to batch bind to HisPur™ Ni^{2+} -NTA resin (Thermo) washed with 50 mM HEPES pH 7.0, 150 mM NaCl, 25 mM imidazole, 0.5 mM TCEP and eluted with 50 mM HEPES pH 7.0, 150 mM NaCl, 500 mM imidazole, 0.5 mM TCEP. Eluate was then run over an S200 16/60 size exclusion column (GE) pre-equilibrated with 50 mM HEPES pH 8.0, 150 mM NaCl, and 5 mM MgCl_2 . Peak corresponding to the full length His-MBP substrate was collected, and quantified by UV-Vis absorption at 280 nm before addition of 10% glycerol and flash freezing to store at -80°C for future use.

Before NMR data acquisition, samples were thawed, cleaved with HRV3C protease overnight at 4°C, and then run over an S75 16/60 size exclusion column (GE) equilibrated with 55 mM sodium phosphate pH 6.5 and 55 mM NaCl to collect the pure unmodified barstar peak. Samples were concentrated to 250 μL for data collection in a Shigemi tube. Typical final sample concentrations were in the range of 0.75-2 mM (unmodified barstar) and 75-200 μM (mono-ubiquitinated barstar). Pure, homogeneous, mono-ubiquitinated ^{15}N -labeled barstar samples were purified using methylated ubiquitin as described in section 2.8.4. Samples were diluted with 10% D_2O before NMR data acquisition.

3.7.2 NMR data acquisition and analysis

Data were collected at 25 °C on a Bruker 900 MHz NMR spectrometer equipped with a CP TCI cryoprobe in the Berkeley QB3 NMR Facility. $^{15}\text{N}/^1\text{H}$ HSQC data were analyzed using TopSpin (Bruker) and CARRA NMR software. $^{13}\text{C}/^{15}\text{N}/^1\text{H}$ HNCA data were analyzed in CARRA NMR, and peaks were assigned to individual amide backbone bonds based on previous assignments for wild-type barstar (Lubienski et al., 1994) and experimentally-determined connectivity.

Based on these assignments, we performed hydrogen-deuterium exchange NMR (HDX-NMR) experiments to assign rates of amide-proton exchange to residues

along the sequence of unmodified barstarK60 and mono-ubiquitinated barstarK60. To initiate these experiments, we resuspended lyophilized protein in buffer in D₂O and then began NMR ¹⁵N/¹H HSQC acquisition.. Exchange for a deuteron leads to a disappearance of a given peak at a rate (k_{obs}) we can directly determine from these experiments for assigned peaks. The ratio of k_{obs} in unstructured peptides of matching sequence to k_{obs} in the structured protein corresponds to a protection factor, a measure of how readily each amide proton can exchange. We report a PF as its log, such that $\log(\text{PF}) = 1$ corresponds to a fully exchanging amide and $\log(\text{PF}) > 1$ corresponds to a protected amide. In these experiments, $\log(\text{PF}) < 3$ corresponds to an amide that exchanged within the dead time of the NMR experiment.

3.7.3 Preparation of deuterated buffers and mass spectrometry samples

5 mL of a 50 mM HEPES pH 7.0, 50 mM NaCl, 50 mM KCl, 10 mM MgCl₂ buffer in a 50 mL conical flask was flash frozen in liquid nitrogen and lyophilized overnight. The lyophilized buffer was then resuspended in equivolume D₂O. Exchangeable protons were allowed to exchange for 6 hours at room temperature before flash freezing and lyophilization. This process was repeated for a total of three D₂O resuspension and lyophilization steps. After the final lyophilization step, the lyophilized buffer was parafilm and stored at -80°C for future use.

Unmodified and mono-ubiquitinated barstarK2, barstarK60, and barstarK78 samples were prepared according to the protocols developed in section 2.8.4. Samples were diluted with 50 mM HEPES pH 7.0, 50 mM NaCl, 50 mM KCl, 10 mM MgCl₂ buffer to a final concentration on 10 μ M for mass spectrometry experiments.

3.7.4 Hydrogen-deuterium exchange mass spectrometry experiments

All hydrogen-deuterium exchange mass spectrometry (HDX-MS) experiments were performed using a liquid handling robot (LEAP Technologies) connected to a Q Exactive mass spectrometer (Thermo). The liquid handling robot was programmed to initiate amide proton exchange by diluting barstar or mono-ubiquitinated barstar into deuterated buffer (50 mM HEPES pH 7, 50 mM NaCl, 50 mM, KCl, 10 mM MgCl₂) and then quenching exchange at various timepoints by adding low pH buffer (6 M urea, 200 mM Arginine, 100 mM TCEP, pH 2.5) and cooling to 1° C. Time points collected were 53, 60, 300, 900, 1800, 3600, 7200, 14400, and 28800 seconds. After quenching, the samples are directly subjected to an in-line proteolysis step using a pepsin-packed (to generate barstar peptides) or pepsin and fungal protease-packed (to generate ubiquitin peptides) column before. Proteolysis is followed directly by liquid chromatography using a C4 trap column followed by a C8 analytical column eluted with a 15-100% acetonitrile gradient and identified via

mass spectrometry. Peptide lists were generated from an MS/MS run performed with each replicate using either Proteome Discoverer (Thermo) or Byonic (Protein Metrics). Peptide deuteration states and isotopic distributions were then determined using HD Examiner (Sierra Analytics) with manual adjustment to the HD Examiner peak identifications as needed. Data are reported as absolute mass increases (comparing unmodified and mono-ubiquitinated variants to one another within the same experiment) and are not corrected for back exchange.

3.7.5 All-atom molecular dynamics simulations

We initiated six independent, 5- μ s all-atom molecular dynamics simulations each of wild-type barstar and mono-ubiquitinated barstarK2, barstarK60, and barstarK78 from its NMR structure, PDB entry 1BTA, using the amberff99SB force field with a TIP4P-D water model. To determine the extent to which neighboring side chains pack against each lysine residue, we calculated the average number of side chains whose non-hydrogen atoms fall within 4Å of each lysine side chain over the course of each simulation (next paragraph). To quantify the extent to which the backbone fluctuates along the length of the entire barstar sequence, and in the vicinity of each ubiquitination site, we also calculated the root-mean-square fluctuation of each C α atom about the average, simulated structure for barstar. We also inspected and quantified hydrogen bonding networks between barstar β -sheet 1 (containing K2) and barstar β -sheet 3, which formed spontaneous hydrogen bonding interactions with the flexible C terminus of ubiquitin in the mono-ubiquitinated barstarK78 simulations.

4. References

- Bai, Y., Milne, J.S., Mayne, L., and Englander, S.W. (1993). Primary structure effects on peptide group hydrogen exchange. *Proteins Struct. Funct. Bioinforma.* *17*, 75–86.
- Balchin, D., Hayer-Hartl, M., and Hartl, F.U. (2016). In vivo aspects of protein folding and quality control. *Science (80-)*. *353*.
- Ball, K.A., Johnson, J.R., Lewinski, M.K., Guatelli, J., Verschueren, E., Krogan, N.J., and Jacobson, M.P. (2016). Non-degradative Ubiquitination of Protein Kinases. *PLoS Comput. Biol.* *12*, 1–44.
- Bard, J.A., Goodall, E.A., Greene, E.R., Jonsson, E., Dong, K.C., and Martin, A. (2018). Structure and Function of the 26S Proteasome. *Annu. Rev. Biochem.* *87*, 697–724.
- Bard, J.A.M., Bashore, C., Dong, K.C., and Martin, A. (2019). The 26S Proteasome Utilizes a Kinetic Gateway to Prioritize Substrate Degradation. *Cell* *177*, 286-298.e15.
- Bashore, C., Dambacher, C.M., Goodall, E. a, Matyskiela, M.E., Lander, G.C., and Martin, A. (2015). Ubp6 deubiquitinase controls conformational dynamics and substrate degradation of the 26S proteasome. *Nat. Struct. Mol. Biol.* *22*, 1–10.
- Batey, S., Nickson, A.A., and Clarke, J. (2008). Studying the folding of multidomain proteins. *HFSP J.* *2*, 365–377.
- Beckwith, R., Estrin, E., Worden, E.J., and Martin, A. (2013). Reconstitution of the 26S proteasome reveals functional asymmetries in its AAA+ unfoldase. *Nat. Struct. Mol. Biol.* *20*, 1164–1172.
- Berko, D., Tabachnick-cherny, S., Shental-bechor, D., Cascio, P., Mioletti, S., Levy, Y., Admon, A., Ziv, T., Tirosh, B., Goldberg, A.L., et al. (2012). Article The Direction of Protein Entry into the Proteasome Determines the Variety of Products and Depends on the Force Needed to Unfold Its Two Termini. *Mol. Cell* *48*, 601–611.
- Bondeson, D.P., Smith, B.E., Burslem, G.M., Buhimschi, A.D., Hines, J., Jaime-Figueroa, S., Wang, J., Hamman, B.D., Ishchenko, A., and Crews, C.M. (2018). Lessons in PROTAC Design from Selective Degradation with a Promiscuous Warhead. *Cell Chem. Biol.* *25*, 78-87.e5.

Carrion-Vazquez, M., Li, H., Lu, H., Marszalek, P.E., Oberhauser, A.F., and Fernandez, J.M. (2003). The mechanical stability of ubiquitin is linkage dependent. *Nat. Struct. Biol.* *10*, 738–743.

Carroll, E.C., Greene, E.R., Martin, A., and Marqusee, S. (2020). Site-specific ubiquitination affects protein energetics and proteasomal degradation. *Nat. Chem. Biol.*

Catic, A., Collins, C., Church, G.M., and Ploegh, H.L. (2004). Preferred in vivo ubiquitination sites. *Bioinformatics* *20*, 3302–3307.

Chaugule, V.K., and Walden, H. (2016). Specificity and disease in the ubiquitin system. *44*, 212–227.

Chojnacki, M., Mansour, W., Hameed, D.S., Singh, R.K., El Oualid, F., Rosenzweig, R., Nakasone, M.A., Yu, Z., Glaser, F., Kay, L.E., et al. (2017). Polyubiquitin-Photoactivatable Crosslinking Reagents for Mapping Ubiquitin Interactome Identify Rpn1 as a Proteasome Ubiquitin-Associating Subunit. *Cell Chem. Biol.* *24*, 443-457.e6.

Chu, T.T., Gao, N., Li, Q.Q., Chen, P.G., Yang, X.F., Chen, Y.X., Zhao, Y.F., and Li, Y.M. (2016). Specific Knockdown of Endogenous Tau Protein by Peptide-Directed Ubiquitin-Proteasome Degradation. *Cell Chem. Biol.* *23*, 453–461.

Ciechanover, A., and Schwartz, A.L. (2004). The ubiquitin system: Pathogenesis of human diseases and drug targeting. *Biochim. Biophys. Acta - Mol. Cell Res.* *1695*, 3–17.

Clague, M.J., Urbé, S., and Komander, D. (2019). Breaking the chains: deubiquitylating enzyme specificity begets function. *Nat. Rev. Mol. Cell Biol.* *20*, 338–352.

Cliffe, R., Sang, J.C., Kundel, F., Finley, D., Klenerman, D., and Ye, Y. (2019). Filamentous Aggregates Are Fragmented by the Proteasome Holoenzyme. *Cell Rep.* *26*, 2140-2149.e3.

Coll-Martinez, Bernat; Crosas, B. (2019). How the 26S Proteasome Degrades Ubiquitinated Proteins in the Cell. *Biomolecules* *9*, 1–14.

Connelly, G.P., Bai, Y., Jeng, M. -F, and Englander, S.W. (1993). Isotope effects in peptide group hydrogen exchange. *Proteins Struct. Funct. Bioinforma.* *17*, 87–92.

- Cundiff, M.D., Hurley, C.M., Wong, J.D., Boscia, J.A., Bashyal, A., Rosenberg, J., Reichard, E.L., Nassif, N.D., Brodbelt, J.S., and Kraut, D.A. (2019). Ubiquitin receptors are required for substrate-mediated activation of the proteasome's unfolding ability. *Sci. Rep.* *9*, 14506.
- Debelouchina, G.T., Gerecht, K., and Muir, T.W. (2017). Ubiquitin utilizes an acidic surface patch to alter chromatin structure. *Nat. Chem. Biol.* *13*, 105–110.
- Dill, K.A., Maccallum, J.L., and Folding, P. (2012). The Protein-Folding Problem , 50 Years On. 1042–1047.
- Eddins, M.J., Varadan, R., Fushman, D., Pickart, C.M., and Wolberger, C. (2007). Crystal Structure and Solution NMR Studies of Lys48-linked Tetraubiquitin at Neutral pH. *J. Mol. Biol.* *367*, 204–211.
- Faggiano, S., and Pastore, A. (2014). The Challenge of Producing Ubiquitinated Proteins for Structural Studies. *Cells* *3*, 639–656.
- Freudenthal, B.D., Gakhar, L., Ramaswamy, S., and Washington, M.T. (2010). Structure of monoubiquitinated PCNA and implications for translesion synthesis and DNA polymerase exchange. *Nat. Struct. Mol. Biol.* *17*, 479–484.
- Fuchs, A.C.D., Maldoner, L., Wojtynek, M., Hartmann, M.D., and Martin, J. (2018). Rpn11-mediated ubiquitin processing in an ancestral archaeal ubiquitination system. *Nat. Commun.* *9*, 1–12.
- Gavrilov, Y., Hagai, T., and Levy, Y. (2015). Nonspecific yet decisive: Ubiquitination can affect the native-state dynamics of the modified protein. *Protein Sci.* *24*, 1580–1592.
- Gendron, J.M., Webb, K., Yang, B., Rising, L., Zuzow, N., and Bennett, E.J. (2016). Using the ubiquitin-modified proteome to monitor distinct and spatially restricted protein homeostasis dysfunction. *Mol. Cell. Proteomics* *15*, 2576–2593.
- Godderz, D., Heinen, C., Marchese, F.P., Kurz, T., Acs, K., and Dantuma, N.P. (2015). Cdc48-independent proteasomal degradation coincides with a reduced need for ubiquitylation. *Sci. Rep.* *5*, 1–8.
- Greene, E.R., Goodall, E.A., De La Peña, A.H., Matyskiela, M.E., Lander, G.C., and Martin, A. (2019). Specific lid-base contacts in the 26S proteasome control the conformational switching required for substrate engagement and degradation. *Elife* *1–27*.

Greene, E.R., Dong, K.C., and Martin, A. (2020). Understanding the 26S proteasome molecular machine from a structural and conformational dynamics perspective. *Curr. Opin. Struct. Biol.* *61*, 33–41.

Grice, G.L., and Nathan, J.A. (2016). The recognition of ubiquitinated proteins by the proteasome. *Cell. Mol. Life Sci.* *73*, 3497–3506.

Guinn, E.J., Jagannathan, B., and Marqusee, S. (2015). Single-molecule chemo-mechanical unfolding reveals multiple transition state barriers in a small single-domain protein. *Nat. Commun.* *6*, 1–8.

Guo, Q., Lehmer, C., Martínez-Sánchez, A., Rudack, T., Beck, F., Hartmann, H., Pérez-Berlanga, M., Frottin, F., Hipp, M.S., Hartl, F.U., et al. (2018). In Situ Structure of Neuronal C9orf72 Poly-GA Aggregates Reveals Proteasome Recruitment. *Cell* *172*, 696-705.e12.

Hacker, S.M., Backus, K.M., Lazear, M.R., Forli, S., Correia, B.E., and Cravatt, B.F. (2017). Global profiling of lysine reactivity and ligandability in the human proteome. *Nat. Chem.* *9*, 1181–1190.

Hagai, T., and Levy, Y. (2010). Ubiquitin not only serves as a tag but also assists degradation by inducing protein unfolding. *Proc. Natl. Acad. Sci. U. S. A.* *107*, 2001–2006.

Hagai, T., Azia, A., Tóth-Petróczy, Á., and Levy, Y. (2011). Intrinsic disorder in ubiquitination substrates. *J. Mol. Biol.* *412*, 319–324.

Huang, H.T., Dobrovolsky, D., Paulk, J., Yang, G., Weisberg, E.L., Doctor, Z.M., Buckley, D.L., Cho, J.H., Ko, E., Jang, J., et al. (2018). A Chemoproteomic Approach to Query the Degradable Kinome Using a Multi-kinase Degradator. *Cell Chem. Biol.* *25*, 88-99.e6.

Jackson, S.E. (2006). Ubiquitin: A small protein folding paradigm. *Org. Biomol. Chem.* *4*, 1845–1853.

Jagannathan, B., Elms, P.J., Bustamante, C., and Marqusee, S. (2012). Direct observation of a force-induced switch in the anisotropic mechanical unfolding pathway of a protein. *Proc. Natl. Acad. Sci.* *109*, 17820–17825.

Jahn, T.R., and Radford, S.E. (2008). Folding versus aggregation: Polypeptide conformations on competing pathways. *Arch. Biochem. Biophys.* *469*, 100–117.

- Kamadurai, H.B., Qiu, Y., Deng, A., Harrison, J.S., Macdonald, C., Actis, M., Rodrigues, P., Miller, D.J., Souphron, J., Lewis, S.M., et al. (2013). Mechanism of ubiquitin ligation and lysine prioritization by a HECT E3. *Elife* *2013*, 1–26.
- Kenniston, J.A., Burton, R.E., Siddiqui, S.M., Baker, T.A., and Sauer, R.T. (2004). Effects of local protein stability and the geometric position of the substrate degradation tag on the efficiency of ClpXP denaturation and degradation. *J. Struct. Biol.* *146*, 130–140.
- Khurana, R., Hate, A.T., Nath, U., and Udgaonkar, J.B. (1995). pH dependence of the stability of barstar to chemical and thermal denaturation. *Protein Sci.* *4*, 1133–1144.
- Kim, H.C., and Huibregtse, J.M. (2009). Polyubiquitination by HECT E3s and the determinants of chain type specificity. *Mol. Cell. Biol.* *29*, 3307–3318.
- Kim, H.C., Steffen, A.M., Oldham, M.L., Chen, J., and Huibregtse, J.M. (2011a). Structure and function of a HECT domain ubiquitin-binding site. *EMBO Rep.* *12*, 334–341.
- Kim, W., Bennett, E.J., Huttlin, E.L., Guo, A., Li, J., Possemato, A., Sowa, M.E., Rad, R., Rush, J., Comb, M.J., et al. (2011b). Systematic and quantitative assessment of the ubiquitin-modified proteome. *Mol. Cell* *44*, 325–340.
- Kim, Y.E., Hipp, M.S., Bracher, A., Hayer-Hartl, M., and Ulrich Hartl, F. (2013). Molecular Chaperone Functions in Protein Folding and Proteostasis.
- Komander, D., and Rape, M. (2012). The Ubiquitin Code. *Annu. Rev. Biochem.* *81*, 203–229.
- De la Peña, A.H., Goodall, E.A., Gates, S.N., Lander, G.C., and Martin, A. (2018). Substrate-engaged 26S proteasome structures reveal mechanisms for ATP-hydrolysis-driven translocation. *Science* (80-.). *362*.
- Lee, C., Schwartz, M.P., Prakash, S., Iwakura, M., and Matouschek, A. (2001). ATP-dependent proteases degrade their substrates by processively unraveling them from the degradation signal. *Mol. Cell* *7*, 627–637.
- Liu, T., Whitten, S.T., and Hilser, V.J. (2006). Ensemble-based signatures of energy propagation in proteins: A new view of an old phenomenon. *Proteins Struct. Funct. Genet.* *62*, 728–738.

- Lubienski, M.J., Bycroft, M., Jones, D.N.M., and Fersht, A.R. (1993). Assignment of the backbone ^1H and ^{15}N NMR resonances and secondary structure characterization of barstar. *FEBS Lett.* *332*, 81–87.
- Lubienski, M.J., Bycroft, M., Freund, S.M.V., and Fersht, A.R. (1994). Three-Dimensional Solution Structure and ^{13}C Assignments of Barstar Using Nuclear Magnetic Resonance Spectroscopy. *Biochemistry* *33*, 8866–8877.
- Martin, A., Baker, T.A., and Sauer, R.T. (2008). Protein unfolding by a AAA+ protease is dependent on ATP-hydrolysis rates and substrate energy landscapes. *Nat. Struct. Mol. Biol.* *15*, 139–145.
- Morimoto, D., Walinda, E., Fukada, H., Sou, Y.-S., Kageyama, S., Hoshino, M., Fujii, T., Tsuchiya, H., Saeki, Y., Arita, K., et al. (2015). The unexpected role of polyubiquitin chains in the formation of fibrillar aggregates. *Nat. Commun.* *6*, 6116.
- Morimoto, D., Walinda, E., Fukada, H., Sugase, K., and Shirakawa, M. (2016). Ubiquitylation Directly Induces Fold Destabilization of Proteins. *Sci. Rep.* *6*, 39453.
- Mortensen, F., Schneider, D., Barbic, T., Sladewska-Marquardt, A., Kühnle, S., Marx, A., Scheffner, M., and Ciechanover, A. (2015). Role of ubiquitin and the HPV E6 oncoprotein in E6AP-mediated ubiquitination. *Proc. Natl. Acad. Sci. U. S. A.* *112*, 9872–9877.
- Myers, J.K., Pace, C.N., and Scholtz, J.M. (1995). Denaturant m values and heat capacity changes: Relation to changes in accessible surface areas of protein unfolding. *Protein Sci.* *4*, 2138–2148.
- Na, Y.R., and Park, C. (2009). Investigating protein unfolding kinetics by pulse proteolysis. *Protein Sci.* *18*, 268–276.
- Nguyen, L.K. (2016). Dynamics of ubiquitin-mediated signalling : insights from mathematical modelling and experimental studies. *17*, 479–493.
- Nolting, B., Golbik, R., Neira, J.L., Soler-Gonzalez, A.S., Schreiber, G., and Fersht, A.R. (1997). The folding pathway of a protein at high resolution from microseconds to seconds. *Proc. Natl. Acad. Sci.* *94*, 826–830.
- Nowak, R.P., Deangelo, S.L., Buckley, D., He, Z., Donovan, K.A., An, J., Safaei, N., Jedrychowski, M.P., Ponthier, C.M., Ishoey, M., et al. (2018). Plasticity in binding confers selectivity in ligand-induced protein degradation article. *Nat. Chem. Biol.* *14*, 706–714.

Oh, E., Akopian, D., and Rape, M. (2018). Principles of Ubiquitin- Dependent Signaling. *Annu Rev Cell Dev Biol.* 137–162.

Olszewski, M.M., Williams, C., Dong, K.C., and Martin, A. (2019). The Cdc48 unfoldase prepares well-folded protein substrates for degradation by the 26S proteasome. *Commun. Biol.* 2, 29.

Park, C. (2014). Mini Review P 117-128 Probing Transient Partial Unfolding in Proteins by Native-State Proteolysis. 117–128.

Park, C., and Marqusee, S. (2004). Probing the high energy states in proteins by proteolysis. *J. Mol. Biol.* 343, 1467–1476.

Park, C., and Marqusee, S. (2005). Pulse proteolysis: a simple method for quantitative determination of protein stability and ligand binding. *Nat. Methods* 2, 207–212.

Park, C., and Marqusee, S. (2006). Quantitative determination of protein stability and ligand binding by pulse proteolysis. *Curr. Protoc. Protein Sci. Chapter 20*, Unit 20.11.

Pham, G.H., and Strieter, E.R. (2015). Peeling away the layers of ubiquitin signaling complexities with synthetic ubiquitin-protein conjugates. *Curr. Opin. Chem. Biol.* 28, 57–65.

Pham, G.H., Rana, A.S.J.B., Korkmaz, E.N., Trang, V.H., Cui, Q., and Strieter, E.R. (2016). Comparison of native and non-native ubiquitin oligomers reveals analogous structures and reactivities. *Protein Sci.* 25, 456–471.

Pollard, T.D. (2010). MBOC technical perspective: A guide to simple and informative binding assays. *Mol. Biol. Cell* 21, 4061–4067.

Prakash, S., Tian, L., Ratliff, K.S., Lehotzky, R.E., and Matouschek, A. (2004). An unstructured initiation site is required for efficient proteasome-mediated degradation. *Nat. Struct. Mol. Biol.* 11, 830–837.

Qu, J., Ren, X., Xue, F., Qu, J., Ren, X., Xue, F., He, Y., Zhang, R., Zheng, Y., Huang, H., et al. (2020). Specific Knockdown of a -Synuclein by Peptide- Directed Proteasome Degradation Rescued Its Associated Neurotoxicity Article Specific Knockdown of a -Synuclein by Peptide-Directed Proteasome Degradation Rescued Its Associated Neurotoxicity. 1–12.

Raschke, T.M., Kho, J., and Marqusee, S. (1999). Confirmation of the hierarchical folding of RNase H: A protein engineering study. *Nat. Struct. Biol.* 6, 825–830.

Ravalin, M., Theofilas, P., Basu, K., Opoku-Nsiah, K.A., Assimon, V.A., Medina-Cleghorn, D., Chen, Y.F., Bohn, M.F., Arkin, M., Grinberg, L.T., et al. (2019). Specificity for latent C termini links the E3 ubiquitin ligase CHIP to caspases. *Nat. Chem. Biol.* *15*, 786–794.

Reichard, E.L., Chirico, G.G., Dewey, W.J., Nassif, N.D., Bard, K.E., Millas, N.E., and Kraut, D.A. (2016). Substrate Ubiquitination Controls the Unfolding Ability of the Proteasome. *J. Biol. Chem.* *291*, jbc.M116.720151.

Rios, P.D.L., and Goloubinoff, P. (2016). Hsp70 chaperones use ATP to remodel native protein oligomers and stable aggregates by entropic pulling. *23*, 9–12.

Saeki, Y., Isono, E., and Toh-E, A. (2005). Preparation of ubiquitinated substrates by the PY motif-insertion method for monitoring 26S proteasome activity. *Methods Enzymol.* *399*, 215–227.

Sakamoto, K.M., Kim, K.B., Kumagai, A., Mercurio, F., Crews, C.M., and Deshaies, R.J. (2001). Protacs: Chimeric molecules that target proteins to the Skp1-Cullin-F box complex for ubiquitination and degradation. *Proc. Natl. Acad. Sci.* *98*, 8554–8559.

Sato, Y., Yoshikawa, A., Yamagata, A., Mimura, H., Yamashita, M., Ookata, K., Nureki, O., Iwai, K., Komada, M., and Fukai, S. (2008). Structural basis for specific cleavage of Lys 63-linked polyubiquitin chains. *Nature* *455*, 358–362.

Schreiber, G., Buckle, A.M., and Fersht, A.R. (1994). Stability and function: two constraints in the evolution of barstar and other proteins. *Structure* *2*, 945–951.

Senft, D., Qi, J., and Ronai, Z.A. (2018). Ubiquitin ligases in oncogenic transformation and cancer therapy. *Nat. Rev. Cancer* *18*, 69–88.

Shabek, N., Herman-Bachinsky, Y., Buchsbaum, S., Lewinson, O., Haj-Yahya, M., Hejjaoui, M., Lashuel, H.A., Sommer, T., Brik, A., and Ciechanover, A. (2012). The Size of the Proteasomal Substrate Determines Whether Its Degradation Will Be Mediated by Mono- or Polyubiquitylation. *Mol. Cell* *48*, 87–97.

Shental-Bechor, D., and Levy, Y. (2008). Effect of glycosylation on protein folding: a close look at thermodynamic stabilization. *Proc. Natl. Acad. Sci. U. S. A.* *105*, 8256–8261.

Shental-Bechor, D., and Levy, Y. (2009). Folding of glycoproteins: toward understanding the biophysics of the glycosylation code. *Curr. Opin. Struct. Biol.* *19*, 524–533.

Shrestha, R.K., Ronau, J.A., Davies, C.W., Guenette, R.G., Strieter, E.R., Paul, L.N., and Das, C. (2014). Insights into the mechanism of deubiquitination by jamm deubiquitinases from cocrystal structures of the enzyme with the substrate and product. *Biochemistry* *53*, 3199–3217.

Smith, B.E., Wang, S.L., Jaime-Figueroa, S., Harbin, A., Wang, J., Hamman, B.D., and Crews, C.M. (2019). Differential PROTAC substrate specificity dictated by orientation of recruited E3 ligase. *Nat. Commun.* *10*, 1–13.

Sousa, R., and Lafer, E.M. (2019). The Physics of Entropic Pulling: A Novel Model for the Hsp70 Motor Mechanism. *Int. J. Mol. Sci.* *20*, 2334.

Sun, X., Gao, H., Yang, Y., He, M., Wu, Y., Song, Y., Tong, Y., and Rao, Y. (2019). Protacs: Great opportunities for academia and industry. *Signal Transduct. Target. Ther.* *4*.

Swatek, K.N., and Komander, D. (2016). Ubiquitin modifications. *Cell Res.* *26*, 399–422.

Tomita, T., and Matouschek, A. (2019). Substrate selection by the proteasome through initiation regions. *Protein Sci.* *28*, 1222–1232.

Twomey, E.C., Ji, Z., Wales, T.E., Bodnar, N.O., Ficarro, S.B., Marto, J.A., Engen, J.R., and Rapoport, T.A. (2019). Substrate processing by the Cdc48 ATPase complex is initiated by ubiquitin unfolding. *Science* (80-.). *365*, eaax1033.

Tyedmers, J., Mogk, A., and Bukau, B. (2010). Cellular strategies for controlling protein aggregation. *Nat. Rev. Mol. Cell Biol.* *11*, 777–788.

Varadan, R., Walker, O., Pickart, C., and Fushman, D. (2002). Structural properties of polyubiquitin chains in solution. *J. Mol. Biol.* *324*, 637–647.

Wang, L., Wu, J., Li, J., Yang, H., Tang, T., Liang, H., Zuo, M., Wang, J., Liu, H., Liu, F., et al. (2020a). Host-mediated ubiquitination of a mycobacterial protein suppresses immunity. *Nature* *577*, 682–688.

Wang, Y., Argiles-Castillo, D., Kane, E.I., Zhou, A., and Spratt, D.E. (2020b). HECT E3 ubiquitin ligases - Emerging insights into their biological roles and disease relevance. *J. Cell Sci.* *133*.

Werner, A., Iwasaki, S., McGourty, C.A., Medina-Ruiz, S., Teerikorpi, N., Fedrigo, I., Ingolia, N.T., and Rape, M. (2015). Cell-fate determination by ubiquitin-dependent regulation of translation. *Nature* *525*, 523–527.

- Worden, E.J., Dong, K.C., and Martin, A. (2017). An AAA Motor-Driven Mechanical Switch in Rpn11 Controls Deubiquitination at the 26S Proteasome. *Mol. Cell* **67**, 799-811.e8.
- Xin, F., and Radivojac, P. (2012). Post-translational modifications induce significant yet not extreme changes to protein structure. *Bioinformatics* **28**, 2905–2913.
- Yau, R., and Rape, M. (2016). The increasing complexity of the ubiquitin code. *Nat. Cell Biol.* **18**, 579–586.
- Ye, Y., Akutsu, M., Reyes-Turcu, F., Enchev, R.I., Wilkinson, K.D., and Komander, D. (2011). Polyubiquitin binding and cross-reactivity in the USP domain deubiquitinase USP21. *EMBO Rep.* **12**, 350–357.
- Ye, Y., Klenerman, D., and Finley, D. (2020). N-Terminal Ubiquitination of Amyloidogenic Proteins Triggers Removal of Their Oligomers by the Proteasome Holoenzyme. *J. Mol. Biol.* **432**, 585–596.
- Yin, J., Schoeffler, A.J., Wickliffe, K., Newton, K., Starovasnik, M.A., Dueber, E.C., and Harris, S.F. (2015). Structural Insights into WD-Repeat 48 Activation of Ubiquitin-Specific Protease 46. *Structure* **23**, 2043–2054.
- Yu, H., and Matouschek, A. (2017). Recognition of Client Proteins by the Proteasome. *Annu. Rev. Biophys.* **46**, 149–173.
- Zaidi, F.N., Nath, U., and Udgaonkar, J.B. (1997). Multiple intermediates and transition states during protein unfolding. *Nat. Struct. Biol.* **4**, 1016–1024.
- Zhang, Yu-Zhu, "Protein and peptide structure and interactions studied by hydrogen exchanger and NMR" (1995). *Ph.D. Thesis*, Structural Biology and Molecular Biophysics, University of Pennsylvania, PA, USA.
- Zheng, N., and Shabek, N. (2017). Ubiquitin Ligases: Structure, Function, and Regulation. *Annu. Rev. Biochem.* **86**, 129–157.
- Zuin, A., Isasa, M., and Crosas, B. (2014). Ubiquitin Signaling: Extreme Conservation as a Source of Diversity. *Cells* **3**, 690–701.